II. BRIDGE DESIGN

1 INTRODUCTION TO DESIGN

1.1 Specifications to be applied

This document sets out the basis upon which the detailed design of the Can Tho Bridge is to be developed.

The design is to be based on the AASHTO Specification for Bridge Design with reference to the Vietnamese and Japanese standards, especially for the proof check.

The major references are:

- AASHTO LRFD Bridge Design Specifications, Second Edition 1998 published by AASHTO (American Association of State Highway and Transportation Officials).

- Reference will also be made to the AASHTO Standard Specifications for Highway Bridges, Sixteenth Edition 1996.

- Highway Design Standard (TCVN-4045-85), Vietnam

- Specifications for Bridge Structures (2057/QD-KT4-1979-Vietnam, Highways Bridges Specification)

- Japanese Highway and Bridge Standards

- Other related standards and specifications

1.2 Navigational Clearances

1.2.1 Main Bridge

The central main shipping channel shall provide a vertical clearance of 39m and a horizontal clearance of 110m. The total navigation span shall be 300m wide with a vertical clearance of 30m.

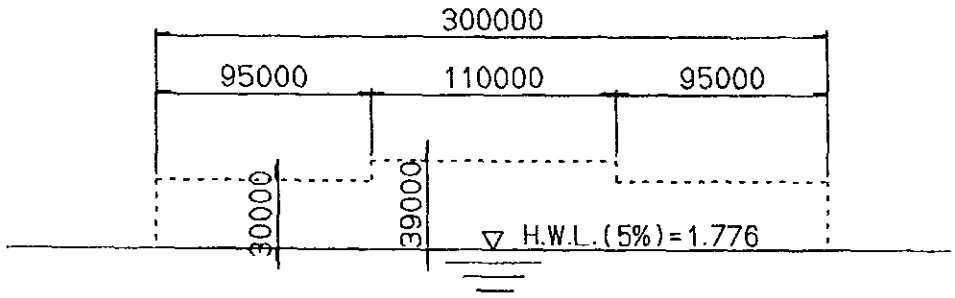

1.2.2 Classification of Waterway

1.2.3 Inland Waterway

Waterways (river and canal) are classified in accordance with Table below.

Water depth and width of water surface shown on Table below are based on low water level of waterway with a frequency of 95% in dry season.

1.2.4 Clearance required

Clearance required for bridge construction are:

- Horizontal clearance : span length, and
- Vertical clearance : height between water level and bottom of girder.

these are provided as shown in Table below for each class of waterway, depending on water level with a frequency of 5%.

Notes : Based on the classification of Inland Waterway TCVN-5664-1992 the Doan Vy Bridge is over a Class III waterway river and the Do Len Bridge is over a Class IV waterway river. For this project, the applicable class is based on the existing structure where appropriate, subject to the approval of the official authority.

Table Classification of Waterway and Navigational Clearance

unit: meters

Class	Waterway size				Curvature	Navigational Clearance		
	Natural River		Canal			Horizontal		Vertical
	Water Depth	Width of Water Surface	Water Depth	Width of Water Surface		River	Canal	
I	> 3	> 90	> 4.0	> 50	> 700	80	50	10
II	2.0 - 3.0	70 - 90	3.0 - 4.0	40 - 50	500 - 700	60	40	9
III	1.5 - 2.0	50 - 70	2.5 - 3.0	30 - 50	300 - 500	50	30	7
IV	1.2 - 1.5	30 - 50	2.0 - 2.5	20 - 30	200 - 300	40	25	6(5)
V	1.0 - 1.2	20 - 30	1.2 - 2.0	10 - 20	100 - 200	25	20	3.5
VI	< 1.0	10 - 20	< 1.2	10	60 - 150	15	10	2.5

'Note : Figure with ( ) can be applied with approval of official agencies.

Table Classification and Clearances Required for mentioned Rivers and Canals

Unit: meters

Station	Class	Name of River	Navigation Clearance		Remarks
			Vertical	Horizontal	
0+800	V	Large Cha Va	3.5	20.0	
1+950	VI	Small Cha Va	2.5	10.0	
3+800	IV	Tra On	6.0	40.0	
7+390	II	Hau	9.0	60.0	
8+475	VI	Not named	2.5	10.0	
8+580	V	Cai Tac Canal	3.5	20.0	
9+590		Cai Tac Canal	1.5	10.0	
10+450	VI	Cai Da Canal	2.5	15.0	
11+170		Ba Mang	1.5	10.0	
12+400	VI	Cai Nai Canal	2.5	15.0	
13+190	V	Ap My Canal	3.5	25.0	
13+900	IV	Cai Rang	5.0	40.0	

1.3 TYPICAL CROSS SECTIONS

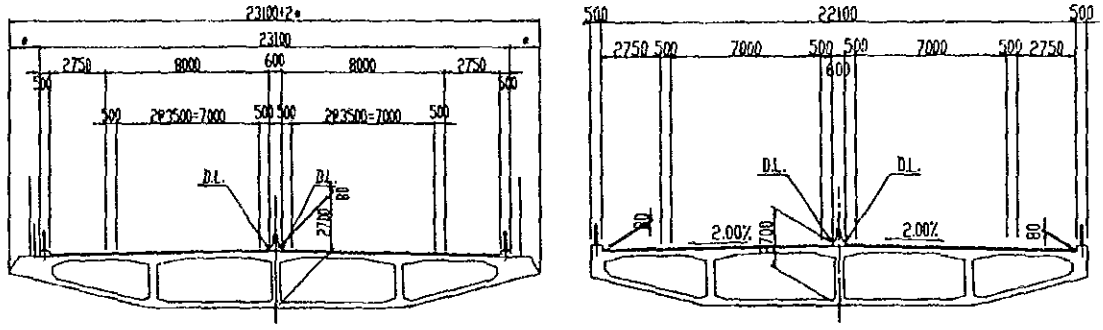

Figure Main Bridge and Approach Span Bridge

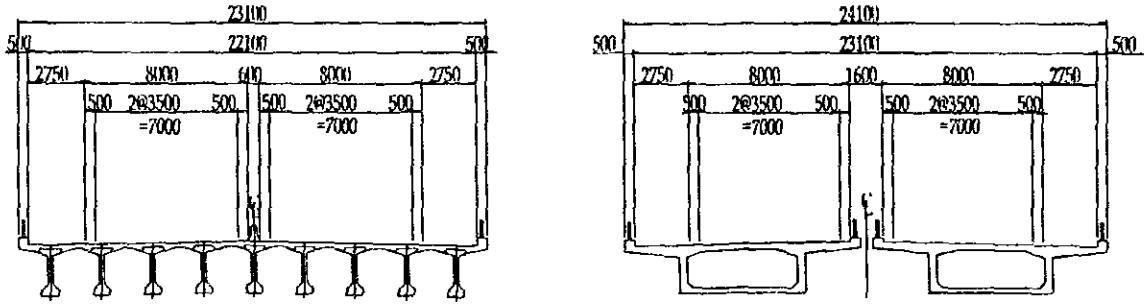

(L ≥ 100m)

Figure Minor Bridge in the Approach Road

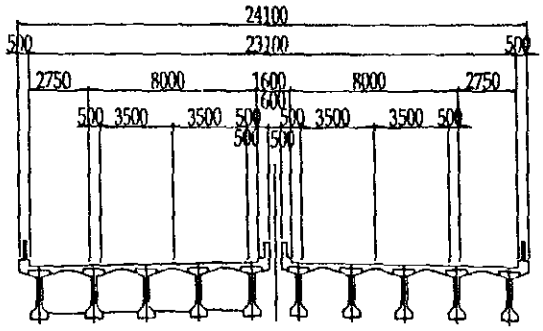

(L < 100m)

Figure Minor Bridge in the Approach Road

2 DESIGN LOADINGS

2.1 Permanent Loads

Permanent loads shall be calculated in accordance with Clause 3.5 of AASHTO LRFD. Dead loads shall include the weight of the concrete, steel reinforcement, prestressing tendons, cable stays, steelworks and any other embedded components, based on the following unit weights.

- Concrete (Reinforced) : 2500 kg/m^3
- Concrete (Unreinforced) : 2300 kg/m^3
- Steel work : 7850 kg/m^3
- Asphalt : 2300 kg/m^3
- Cable Stays

The total superimposed dead load allowance (DW) of 60 kN/m is assumed, with the following breakdown:

- Carriageway asphalt surfacing 39 kN/m
  (thickness 80 mm, no allowance for future overlay)
- Concrete median barrier 7 kN/m
- Steel pedestrian barrier 1 kN/m per side
- Concrete edge barriers 3 kN/m per side
- Possible future services 6 kN/m

2.2 Traffic Loading

Design live loads shall be calculated in accordance with Clause 3.6 of AASHTO Load and Resistance Factor Design (LRFD), and be analyzed under the design philosophy of LRFD bridge specification, refering to the allowable stress design condition.

2.2.1 Design Truck

The design truck shall be the AASHTO HS20-44 and shall have a total weight of 325 kN comprising three axles as shown in AASHTO Cl. 3.6.1.2.2.

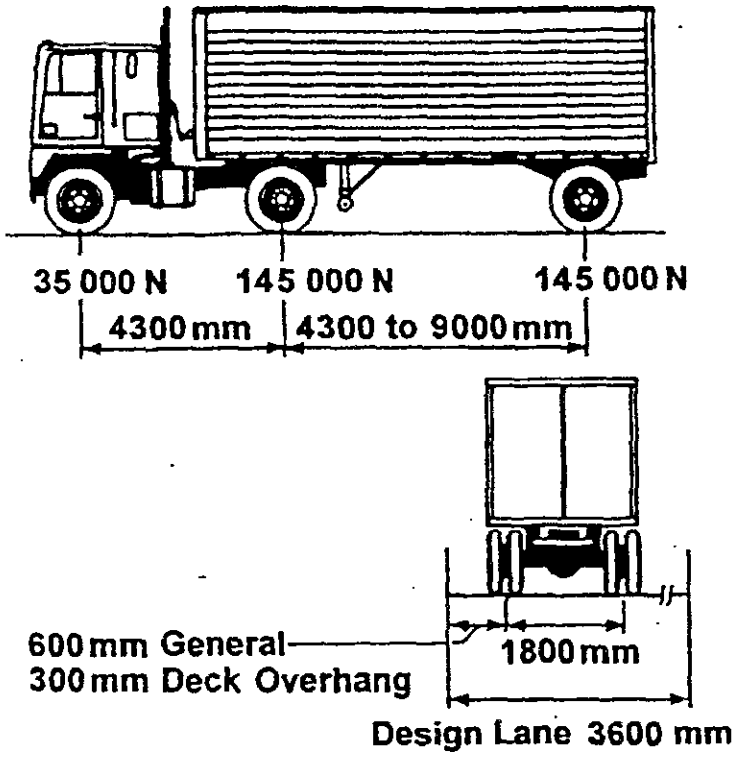

Figure 3.6.1.2.2-1 Characteristics of the Design Truck

2.2.2 Design Lane Loading (W_L)

The design lane load shall be 9.3 kN/m which shall be assumed constant over the full influence length, regardless of span, with no impact effects. (AASHTO Cl. 3.6.1.2.4).

2.2.3 Design Tandem

The design tandem shall comprise a pair of 110 kN axles spaced 1200 mm apart and with a transverse spacing of wheels of 1800 mm. (AASHTO Cl. 3.6.1.2.3)

2.2.4 Multiple Lane loading

The multiple presence factors for truck loading shall be applied in accordance with Clause 3.6.1.1.2 of AASHTO LRFD.

Number of Loaded Lane	Multiple Presence Factor "m"
1	1.20
2	1.00
3	0.85
>3	0.65

2.2.5 Heavy Load Vehicles

It is assumed that only one heavy load vehicle (XB-80) will be transported over the bridge at any time, with no other traffic loading on the bridge at the same time.

2.2.6 Application of Loading

Vehicular live loading on the roadways of bridges or incidental structures, designated HL-93, shall consist of a combination of the:

- Design truck or design tandem, and
- Design lane load

The design Lane Loading shall be applied both as full length and as pattern loading (for maximum load effects), and shall be applied in conjunction with 100% of the design Truck Load or design Tandem Load.

For both negative moment between points of dead load contraflexure and reaction at interior piers only, 90% of the effect of two design trucks shall be applied with minimum axle spacing each truck and 15m between the rear axle of one truck and the lead axle of the other truck. The 90% loading from the two trucks shall be combined with 90% of the design Lane Loading.

Pedestrian loading of 3.6 kPa shall be combined with each of the above Live Load cases.

Impact factors shall be applied only to the Design Truck or Design Tandem component of the above loadings, and not to Lane Loads or Pedestrian Loads.

2.2.7 Local wheel loading W_p

The local wheel load shall comprise a load of 72.5 kN acting over a contact

area of 510 x 300 mm, placed anywhere within the edge barriers.

2.2.8 Dynamic Load Allowance

The dynamic load allowance shall be calculated in accordance with AASHTO Clause 3.6.2.1 for Design Truck or Design Tandem Loads only:

Component	IM
Deck Joint – All Limit States	75%
All Other Components – Fatigue & Fracture	15%
All Other Components – Other Limit States	33%

2.3 Horizontal Forces (Vehicle)

2.3.1 Braking forces

Braking forces shall be calculated in accordance with Clause 3.6.4 of AASHTO LRFD. This requires that a force equivalent to 25% of the axle weights of one design truck (325kN) per lane, acting 1800 mm above the deck surface. Braking effects are not considered for simultaneous lane loading, or for a second design truck per lane.

All design lanes on the Can Tho bridge shall be considered as loaded in the same direction to allow for the possibility of one way operation in the future.

The longitudinal force shall be assumed to be act along the centerline of the bridge.

The design shall also be checked for braking forces calculated in accordance with Article 2.20 of the Vietnamese Bridge design code 2057-QD-KT4-1979. This requires that provision will be made for the effect of a longitudinal force without impact as determined from Table 2.2.6.1 of the standard.

Length of the portion of the loaded span	Longitudinal Force
L= 25m	0.3W = 90 kN
25m<L<50m	0.6W = 180 kN
L>50m	0.9W = 270 kN

In the above table, W = Total Weight of truck = 300 kN for all lanes carrying traffic heading in the same direction.

2.3.2 Shake Forces

Shake forces shall be calculated from Article 2.19 of the Vietnamese Bridge Design Code, which provides for the effect of a transverse force of 4 kN/m without impact. The transverse force is assumed to be located at the road surface level or top of kerb level and is assumed to be generated from design truck loading only.

2.4 Wind load

2.4.1 Static Analysis

In accordance with AASHTO LRFD Clause 3.8.3, aeroelastic force effects must be taken into account in the design as the main spans. The structure is relatively flexible and is therefore deemed to be wind sensitive by the code. Representative wind tunnel tests may be used to satisfy the requirements of AASHTO Clauses 3.8.3.2 and 3.8.3.3.

An analysis of the stability of the structure during construction shall also be performed.

2.4.2 Horizontal Wind Loads

The wind pressures indicated below have been based on a base design wind velocity of 160 km/hr as provided in AASHTO LRFD. An "Open Country" terrain category has been assumed (AASHTO Cl. 3.8.1.1)

The design wind pressures are indicated in the table below assuming PB is 0.0024 Mpa. (Base pressure for beams)

Height above ground	Design Wind Velocity	Design Wind Pressure
(m)	V_{DZ}(km/hr)	PD(MPa)
10	164	0.0025
20	185	0.0033
30	200	0.0037
40	209	0.0041
50	217	0.0044
60	223	0.0047
70	228	0.0049
80	232	0.0051
90	236	0.0052
100	240	0.0054
110	243	0.0055
120	246	0.0057
130	248	0.0058
140	251	0.0059
150	253	0.0060

Bridge deck used pressures in the above table, piers and towers in crease the value by 50%.

2.4.3 Longitudinal Wind Loads on Superstructure

The wind load which is to be assumed for wind directions other than normal to the bridge deck are nominated in Table 3.8.1.2.2 - 1 of AASHTO LRFD.

2.4.4 Forces on Approach Span Piers

The transverse and longitudinal forces to be applied directly to the substructure shall be calculated assuming a uniform wind pressure of 0.002 Mpa. (refer AASHTO Cl. 3.8.1.2.3).

The loads on the main tower shall be calculated using the wind pressures in the table above.

2.4.5 Wind pressure on vehicles

The wind load on live load shall be assumed to be 1.46 kN/m acting 1800 mm above the roadway. (AASHTO Cl. 3.8.1.3)

Wind on live load other than normal to the bridge is defined in Table 3.8.1.3 - 1 of AASHTO LRFD.

2.4.6 Vertical Wind Pressure

A vertical upward wind force of 24 kN/m shall be assumed to act on the underside of the superstructure.

The load shall be applied at the windward quarter-point of the deck width in conjunction with the horizontal loads.

2.4.7 Dynamic Analysis

- The analysis of stability of the bridge for dynamic wind loads will be based on Japanese standards.

- The wind velocity to be used for a dynamic design is the mean velocity over 10 minutes.

- The design wind velocity is determined by height above ground and the local topography

- The design wind velocity is calculated by the formula below:
  Ud = U10 x E1
  Where Ud : design wind velocity
  U10 : basis wind velocity
  E1 : compensating rate. (Altitude, coarseness of and earth surface)

- The design wind velocity is estimated for a return period of 100 years.

- The wind velocity is based on observation records from the Can Tho meteorological observatory and the Soc Trang meteorological observatory and is estimated using combination of the "Iwai", "Gringorten", "Gumbel" methods.

Table Statistical Analysis Results of Wind Data

(Return period calculation of 100 years)

Station	Iwai Method	Gringorten method	Gumbel method
Can Tho (1978 - 1998)	35.6m/s	35.2m/s	37.4m/s
Soc Tran (1949 - 1998)	30.2m/s	24.5m/s	29.8m/s

Calculation of Design Wind Velocity : Ud

Basic Wind Velocity
(10m above the ground level) : U10=40m/s

Compensating Rate

Classification of ground surface : II
(Japanese Standards for Aero-dynamic Stability,1991)
Altitude of target (Deck) = 42.8m(40<z<45m)
Compensating Factor : E1 = 1.26
Design Wind Velocity : Ud = U10:E1 = 50.4m/s

2.5 Earthquake Effects

The structure shall be designed in accordance with AASHTO

LRFD.

- An equivalent static lateral force of 12% of component weight may be assumed for the design of approach and embankment structures. Bearings, movement joints and structural elements shall be designed to accommodate movements resulting from the application of these forces.

- A dynamic analysis of the main structure is required and shall be based on a conservative design spectra to determine forces and displacements for design purposes. This analysis is required due to the complex nature of the main structure and the possible interaction with water and soil.

2.6 Fatigue Load

The fatigue load shall be a single design truck with a 9m trailer axle spacing in accordance with Clause 3.6.1.4 of AASHTO LRFD.

The frequency of the fatigue load shall be taken as 2000 trucks per day, which is based on the AASHTO commentary recommendations for American rural bridges.

2.7 Vessel Collision

2.7.1 Piers in Main River Channel

Loads shall be determined in accordance with Clause 3.14 AASHTO LRFD. The head on ship collision force on the pier is :

$$Ps = 1.2 \times 10^5 V \sqrt{(DWT)}$$

Where:
Ps = equivalent static vessel impact (N)
V = vessel impact velocity
DWT = deadweight tonnage of vessel = 10,000 Mg

The design collision velocity shall be defined in accordance with Clause 3.14.6 of AASHTO.

Note that there will be no reduction in impact speed for piers away from the main channel as the river width is wider than three times the length of the design vessel. The main river channel therefor extends to the location where the river depth is less than 8m.

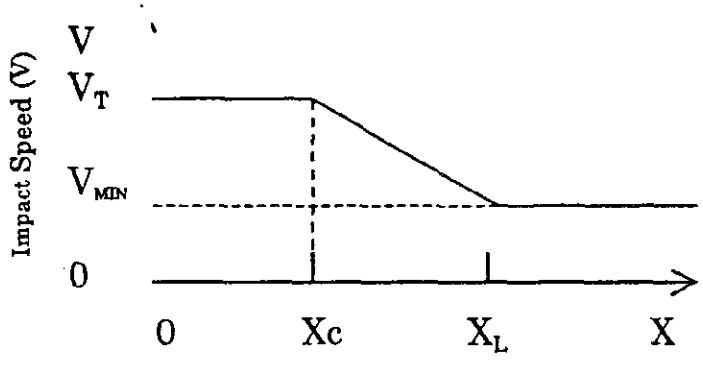

Vt = 5.15 m/s

V/min = 2.0m/s

V = Design Impact Velocity (m/c)

V_T = Typical vessel transit velocity in the channel under normal environmental conditions but not taken to be less than V_{MIN} (m/s)

V_{MIN} = Minimum design impact velocity taken as not less than the yearly mean current velocity for the bridge location (m/s)

X = Distance to face of pier from centerline of channel (mm)

X_C = Distance to edge of channel (mm)

X_L = distance equal to 3.0 times the length overall of the design vessel (mm)

2.7.2 Piers away from Main Shipping Channel

Loads shall be determined in accordance with Clause 3.14 of AASHTO LRFD assuming the standard barge collision force nominated in Cl 3.14.11, unless the piers are adequately protected by fenders, berms, islands or other sacrificial devices.

The properties of the design barge are:

-	Width	10,700	mm
-	Length	60,000	mm
-	Depth	3 700	mm
-	Empty Draft	520	mm
-	Loaded Draft	2,700	mm
-	Mass	1,540	Mg

2.7.3 Application of Impact Force

For substructure design, equivalent static forces parallel and normal to the centerline of the river channel shall be applied separately as follows (Clause 3.14.14):

- 100% of the design impact force in the direction of the river channel.

- 50% of the design impact force perpendicular to the river channel.

The distribution of the load with respect to the structural element being impacted is defined in Clause 3.14.14.1 of AASHTO LRFD.

The vessel in the main shipping channel shall be assumed to overrun the pilecap by 3m during the collision and any piles or caissons within this range will require strengthening to resist the specified loads. Similarly for the barge impact on the piers away from the main shipping channel, it shall be assumed that the overrun of the pilecap is 3.0m during the collision.

2.8 Design Allowances for River Scour

Piers that are located between the northern bank of the main river and the southern bank of the Can Tho channel shall be designed for the effects of river-bed scour as indicated in the table below:

Table Estimation of Maximum Local Scouring Depth around the Foundation at the South Tower

Formula	Local Scouring Depth (m)
Lauren's formula :	23.6
Indian specification (Chezy's)	26.6
Japan railways Formula	21.8

The consequences of this change in riverbed profile shall be checked at the strength and service limit states.

2.9 Other Loads

2.9.1 Friction Forces from Bearings

Friction forces from bearings shall be determined in accordance with article 2.28 of the Vietnamese Bridge Design Code.

2.9.2 Pedestrian loading

A pedestrian load of 3.6 kN/m2 shall be assumed in accordance with Clause

3.6.1.6 of AASHTO LRFD. The pedestrian loading shall be combined with the traffic loading.

2.9.3 Stream Forces

The loads resulting from flowing water on the substructure shall be calculated in accordance with Clause 3.7.3 of AASHTO LRFD.

- Design stream flow velocities V max =3m/sec.(Downstream)

- Design river levels

  High water level (HWL = 5%) : EL = 1.776
  (HWL = 1%) : EL = 1.850

Forces due to possible debris in the river are incidental and not critical compared to ship collision and wind loads.

2.9.4 Buoyancy

Buoyancy shall be considered as an uplift force taken as the sum of the vertical components of static water pressures as outline in Clause 3.7.1 of AASHTO LRFD.

2.9.5 Temperature Effects

Temperatures for the past 20 years in Can Tho Station are indicated in the table below:

	Records : Can Tho Station	Design Thermal Effect
Maximum	36.7 ℃	+10.0 ℃
Minimum	17.7 ℃	-10.0 ℃
Average	26.7 ℃	

The effects of temperature differential shall be in accordance with AASHTO Cl.3.12.3

The temperature difference between the stays and the concrete structure of the main bridge shall be assumed as 15 ℃.

2.9.6 Concrete Creep & Shrinkage Effects

Creep strains for concrete shall be calculated in accordance with AASHTO LRFD Section 5. The effects of load redistribution and time dependence shall also be taken in to account.

2.10 Design for Cable Loss or Replacement

The possibility of accidental loss of a stay cable is extremely low since the cable stays are located behind a vehicle barrier and the pedestrian walkway. The specification for the cable stays should also allow the strands in each stay to be individually inspected and replaced. This means that the bridge should always be supported by a full compliment of cable stays. However the stability of the structure should be checked for the extreme load case of one stay being removed.

This condition shall be checked as an Extreme Event II load case allowing for a maximum of four lanes of live loading. No other loadings are assumed for this load case.

2.11 Settlement of Piers

- The calculated vertical settlements are long term estimated after closure pours. The estimates are at pilecap level and assuming the deepest scour conditions.

- The transverse differential settlement is the estimated settlement across a single pile cap measured at the centerline of the piers.

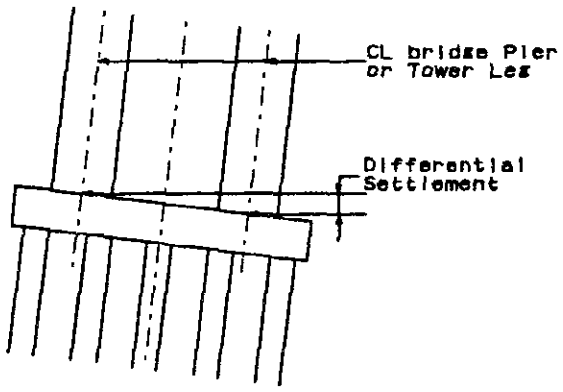

2.12 Construction Loading

The design shall be based upon the following construction loadings:

- Launching Equipment
- Formwork Traveller
- Miscellaneous Live Load

2.13 Earth Pressures on Abutments

The abutments shall be designed to resist the applied earth pressure loads from the embankment as required by Clause 3.11 of AASHTO LRFD.

$P = K_h \gamma_s gz\ (x10^{-9})$

Where:

P = basic earth pressure (Mpa)

Kh = coefficient of lateral earth pressure taken as ka, for walls that deflect or move sufficiently to reach minimum active conditions (refer to table below)

Ys = density of soil (kg/m3)

Z = depth below the surface of earth (mm)

G = gravitational constant (m/s2)

ACTIVE PRESSURE COEFFICIENT, Value of k_a for Log Spiral Failure Surface

δ	I	β	φ (DEG)					
(DEG)	(DEG)	(DEG)	20	25	30	35	40	45
0	-15	-10	0.37	0.30	0.24	0.19	0.14	0.11
		0	0.42	0.35	0.29	0.24	0.19	0.16
		10	0.45	0.39	0.34	0.29	0.24	0.21
	0	-10	0.42	0.34	0.27	0.21	0.16	0.12
		0	0.49	0.41	0.33	0.27	0.22	0.17
		10	0.55	0.47	0.40	0.34	0.28	0.24
	15	-10	0.55	0.41	0.32	0.23	0.17	0.13
		0	0.65	0.51	0.41	0.32	0.25	0.20
		10	0.75	0.60	0.49	0.41	0.34	0.28
ϕ	-15	-10	0.31	0.26	0.21	0.17	0.14	0.11
		0	0.37	0.31	0.26	0.23	0.19	0.17
		10	0.41	0.36	0.31	0.27	0.25	0.23
	0	-10	0.37	0.30	0.24	0.19	0.15	0.12
		0	0.44	0.37	0.30	0.26	0.22	0.19
		10	0.50	0.43	0.38	0.33	0.30	0.26
	15	-10	0.50	0.37	0.29	0.22	0.17	0.14
		0	0.61	0.48	0.37	0.32	0.25	0.21
		10	0.72	0.58	0.46	0.42	0.35	0.31

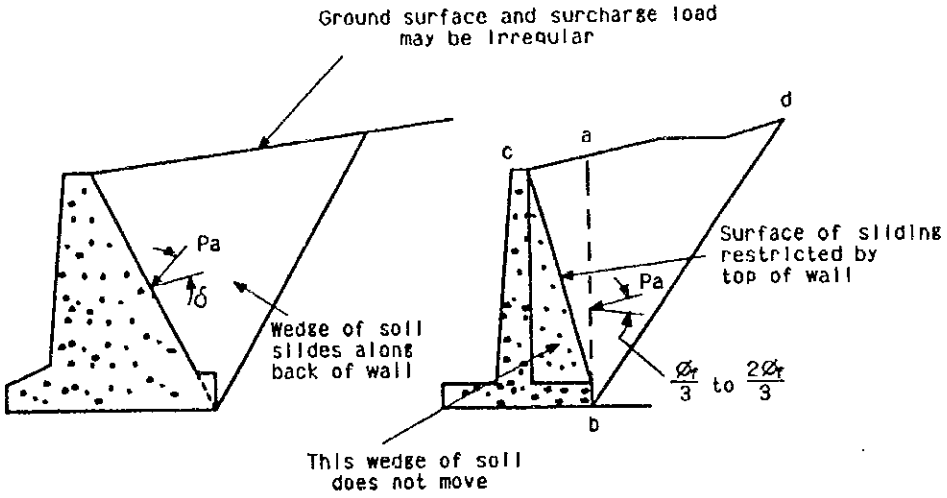

Figure Coulomb wedge theory

$$E_{AB} = 1/2\, g\, \gamma\, H^2 (1 - k_v) K_{AE} \times 10^{-9}$$

Where the seismic active pressure coefficient K_{AE} is

$$K_{AE} = \frac{\cos(\phi - \theta - \beta)}{\cos\theta \cos^2\beta \cos(\delta + \beta + \theta)} \times \left[1 + \sqrt{\frac{\sin(\phi + \delta)\sin(\phi - \theta - i)}{\cos(\delta + \beta + \theta)\cos(i - \beta)}}\right]^2$$

and where

- g = acceleration of Gravity (m/s^2)
- γ = density of soil (kg/m^3)
- H = height of soil face (mm)
- Ø = angle of friction of soil
- θ = arc tan (k_h / (1 – k_v))
- δ = angle of friction between soil and abutment
- kh = horizontal acceleration coefficient
- kv = vertical acceleration coefficient
- i = ackfill slope angle
- β = slope of soil face

2.14 LOAD COMBINATIONS

2.14.1 GENERAL

The load combinations to be considered are nominated in the table below which have been developed from the recommendations outlined in Clause 3.4 of AASHTO LRFD.

2.14.2 Load Designation – Permanent Loads

- DC : Dead load of structural components and nonstructural attachments
- DW : Dead load of wearing surfaces and utilities
- EL : Accumulated locked-in effects resulting from the construction process.

2.14.3 Load Designation – Transient Loads

BR Vehicular braking force and shake force
CL Cable stay loss
CR Creep
CV Vessel collision force
EQ Earthquake
FR Friction
IM Vehicular dynamic load allowance
LL Vehicular live load
PL Pedestrian live load
SE Settlement
SH Shrinkage
TG Temperature gradient
TU uniform temperature
WA water load and stream pressure
WL wind on live load
WS wind load on structure

Load Combination	DC DW EL	LL IM BR PL	WA	WS	WL	FR	TU CR SH	TG	SE	Use One of These at a Time		
										EQ	CV	CL
Strength I	γ_p	1.75	1.00	-	-	1.00	0.5/1.2	-	-	-	-	-
Strength II	γ_p	1.35	1.00	-	-	1.00	0.5/1.2	-	-	-	-	-
Strength III	γ_p	-	1.00	1.40	-	1.00	0.5/1.2	-	-	-	-	-
Strength IV DC.DW	1.50	-	1.00	-	-	1.00	0.5/1.2	-	-	-	-	-
Strength V	γ_p	1.35	1.00	0.40	1.00	1.00	0.5/1.2	-	-	-	-	-
Extreme Event 1	γ_p	0.50	1.00	-	-	1.00	-	-	-	1.00	-	-
Extreme Event 2	γ_p	0.50	1.00	-	-	1.00	-	-	-	-	1.00	1.00
Service I	1.00	1.00	1.00	0.30	1.00	1.00	1.0/1.2	0.50	0.50	-	-	-
Service II	1.00	1.30	1.00	-	-	1.00	1.0/1.2	-	-	-	-	-
Service III	1.00	0.80	1.00	-	-	1.00	1.0/1.2	0.50	0.50	-	-	-
Service IV[2]	1.00	-	1.00	-	-	1.00	1.0/1.2	1.00	1.00	-	-	-
Fatigue LL.IM & CE only	-	0.75	-	-	-	-	-	-	-	-	-	-
Construction - Strength I[3]	γ_p	1.50[1]	-	-	-	-	-	-	-	-	-	-
Construction - Strength II[3]	γ_p	-	-	1.25	-	-	-	-	-	-	-	-
Construction - Service [3]	γ_p	1.00[1]	-	1.00	-	-	-	-	-	-	-	-
Construction-Extreme Event	γ_p	1.00[1]	-	-	-	-	-	-	-	-	1.00[4]	-

(1) Loads from construction equipment

(2) For segmentally constructed bridges

(3) Refer to Notes on load factors for explanation of out of balance calculations. Also refer Cl 5.14.2.3.2 for additional requirements for segmental construction.

(4) Accidental impact of precast segment (refer Cl 5.14.2.3.2)

Strength I Base load combination relating to the normal vehicular use of the bridge without wind.
Strength II Load combination relating to owner specified design vehicle
Strength III Load combination relating to ultimate wind loads
Strength IV Load combination relating to very high dead load to live load ratio.
Strength V Load combination relating to live loads and wind loads
Extreme Event I Load combination relating to earthquake
Extreme Event II Load combination relating to collisions by vessels and vehicles
Service I Load combination relating to normal operational use
Service II Load combination intended to control yielding of steel and slip of connections - Only applicable to steel structures
Service III Load combination intended to control cracking in prestressed concret
Fatigue Load combination for elements susceptible to fatigue or fracture damage.

Load factors for Permanent Loads γ_p

Type of Load	Load Factor	
	Maximum	Minimum
DC : Component and attachments	1.25	0.90
DW: Wearing Surfaces and Utilities	1.50	0.65
EL : Locked-in Erection Stresses	1.00	1.00

2.14.4 Notes on load Factors

Load factors are generally in accordance with those outline in Tables 3.4.1.1 and 3.4.1.2 of AASHTO with the following qualifications:

- Earth pressure loads from abutments have not been included for simplicity.

- Construction load combinations have been included with the load factors taken from Clause 3.4.2 (Refer also to Cl. 5.14.2.3.2 for segmental construction)

- γ_{EQ} is the load factor to be applied to live loads during earthquakes and is defined in Clause 3.4.1 as a load factor to be determined on a project specific bases. The figures suggested by AASHTO are proposed for this project.

- γ_{TG} is the load factor to be applied to load effects resulting from differential temperature gradients which is defined in Clause 3.4.1 as a load factor to be determined on a project specific bases. The AASHTO commentary indicates that there is no general agreement on the factor since there is much discussion on how the effects are distributed in the structure. The figures suggested in AASHTO are proposed for this project since no better information is available.

- γ_{SE} is the load factor to be applied to load effects resulting from differential settlement of foundations. This is defined in Clause 3.4.1 as a load factor to be determined on a project specific basis and the AASHTO code does not provide guidance. The same values as assumed for γ_{t_g} are proposed for this project since no better information is available.

- Vehicular collision forces have not been included, as the substructure elements will be protected in accordance with the requirements of Clause 3.6.5.1 of AASHTO LRFD.

- A load combination for the loss of a cable stay has been added to the extreme event category II.

- The ice load combination has been removed as it is not relevant to Vietnam.

3 STRUCTURAL ANALYSIS

3.1 General

The analysis of the bridge and associated components is fundamental to the design of the structure. The structure is subjected to a wide range of loading effects during normal service and during the cantilever construction process as well as the normal environmental loadings such as wind and stream flow. It is therefore imperative that accurate numerical modes of the structure are created to understand the behavior of the structure under all loading conditions.

3.2 Main Bridge Structure

Cable stayed structures are inherently flexible (with significant second order effects) and therefore accurate modeling is required.

3.2.1 Static Global Analysis

A full superstructure and substructure 3D-beam element model will be required. The major features of this analysis are:

- Linear elastic analysis including second order effects for serviceability and ultimate global loading combinations

- Determination of global permanent effects, transient effects, (excluding HLP) thermal effects, creep and shrinkage effects;

- Investigation of distribution of ship impact forces between substructure and superstructure.

- Generally uncracked section properties calculated in accordance with AASHTO shall be used. A check of the structural performance of the towers shall also be performed using cracked section properties to confirm that concrete stiffness is not critical to the overall performance of the structure.

The effects of the construction staging will be modelled using the same basic model developed for the global analysis with the model being varied to simulate each stage of the construction process.

The main objective of the construction stage analysis is to confirm that the bridge can be constructed using the erection sequence assumed in the design.

3.2.2 Seismic analysis

The design of the structural elements will be carried out assuming the equivalent static force nominated in the design criteria.

The structure will also be modelled numerically using a 3D dynamic analysis of the completed structure to determine elastic structural response.

3.3 Approach Bridge Structure

The approach bridge structures are more conventional in structural form and the complexity of the detailed analysis will therefore not be as significant. However the same basic static structural analysis as for the main bridge will be required.

The following analysis will be form the basis for the major element designs.

3.3.1 Static Global Analysis of Deck

A full superstructure and substructure 3D-beam element model will be required. The major features of this analysis are:

- Linear elastic analysis including second order effects for serviceability and ultimate global loading combinations

- The box girder will be assumed to be a single line element supported by two bearings at each pier. Transverse bending effects in the box section will be investigated separately.

- Determination of global permanent effects, transient effects, (excluding HLP) thermal effects, creep and shrinkage effects:

- Generally uncracked section properties calculated in accordance with AASHTO shall be used. A check of the structural performance of the piers shall also be performed using cracked section properties to confirm that concrete stiffness is not critical to the overall performance of the structure.

The effects of the construction staging will be incorporated into this model.

3.3.2 Static Global Analysis of Substructure

It is proposed that the approach spans will be made continuous and connected to the supporting pier columns. The resulting distribution of longitudinal loads is complex and will required modelling using 3D-frame analysis software. A range of section properties to model the various section stiffnesses will be used as an estimate of the range of values that could be in evidence over the life of the bridge.

4 DESIGN CRITERIA FOR FOUNDATIONS AND EMBANKMENTS

4.1 General

The foundations for the bridges shall be designed in accordance with

AASHTO , Japanese Standard .

4.2 Ground Conditions

Soil properties are reported in the Geotechnical Reports. Results of the site investigations include field measurements and laboratory testing.

5 MATERIALS

5.1 Concrete

The following concrete grades shall be assumed for design purposes (28 days compressive strength f_c).

Location	f_c (Mpa)	Modulus of Elasticity Ec (Mpa)
Blinding	15	-
Walls and abuments: parapets, barriers and kerbs Piers	24	23,500
in-situ deck slab Cast in-place piles, caissons, pilecaps in river	30	26,300
Cast in-situ box girder, Precast girders(I girder), Precast driven piles, tower	40	30,400
Precast box girders for main bridge	50	33,900

Poisons ratio = 0.2

Thermal expansion coefficient 10.8×10^{-6} per °C

5.2 Structural Steel

Structural steels shall conform to the requirements indicate in the table below and the design will be based on the minimum properties indicated.

	Structural Steel	High Strength Low-Alloy Steel	
	A709M Grade 250	A709M Grade 345	A709M Grade 345W
Minimum Tensile Strength, Fu (MPa)	400	450	485
Minimum Yield Point or Minimum Yield Strength F_y (MPa)	250	345	345

The modulus of elasticity is 200,000MPa

Thermal expansion coefficient 11.7×10^{-6} per °C

5.3 Reinforcement

Reinforcement steel ASTM A615 will be assumed in the design. Substitution of this reinforcement with the ASTM A615 grade steel is acceptable.

ASTM A615	Tensile Stress
Yield Point Stress	390 MPa
Breaking Stress	> 440 MPa

5.4 Prestressing Steel

- Uncoated stressed-relieved or low relaxation seven-wire strand or high strength bars to the following standards:

- AASHTO M203 (ASTM A416) - Uncoated seven-wire stress-relieved strand for prestressed concrete

- AASHTO M275 (ASTM A722) - Uncoated High-Strength Bar for Prestressing Concrete

Material	Nom.ld	Area	Elastic Modulus E_p	Min Breaking Load P_B	Min. Tensile Strength	Yield Strength	Yield Stress f_{py}
	Mm	mm^2	MPa	KN	MPa	($\%f_{py}$)	MPa
Strand	15.2	143	197000	265	1860	90%	1675
Bar -	15mm	*	207000	*	1035	85%	880
Plain	36mm						

5.5 Stay Cables

5.5.1 General

The design of the stays shall satisfy the requirements of Post-Tensioning Institute (PTI) Recommendations for Stay Cable Design, Testing and Installation (1993).

The stays will be composed of 7 wire 15.2mm diameter strands with and elastic modulus Es = 195 x 10^3 MPa (adopted for design purposes.)

The effective stay modulus depends on the slope and the force in the stay

according to the Ernst formula.

Stay stresses shall be limited to 0.45 f_p under maximum service loads. This figure may be increased to 0.56 f_p during construction or during stay exchange/removal.

The steel properties are given in the table below (to ASTM standards:)

Material	Nom.Id	Area	Guaranteed Ultimate Tensile Strength	Guaranteed Ultimate Force P_B	Service Limit Force
	Mm	mm^2	MPa	kN	kN
Strand	15.2	140	1862	261	117

The thermal expansion coefficient shall be taken as 12×10^{-6} per °C

5.5.2 Fatigue stress range

Fatigue stress range values for parallel strand stay cables shall be:

No.Cycles	Allowable Stress Range (MPa)
2,000,000	124
500,000	190
100,000	310

5.6 Concrete Cover

The following concrete covers shall be provided, unless otherwise specified.

Location	Concrete Cover(mm)
Retaining walls and abutments	75
Cast-in-situ piles/caissons	75
Precast Piles	50
Pile Caps	50
Deck Slab	35
Piers and Towers	50
Bearing Plinths	50
Precast Girders and parapets	50
In-situ parapets, NJ barriers, kerbs, etc	50

Tolerance on cover is +/- 5mm.

5.7 Stress Limitations for Prestressing Tendons

Stress in prestressing tendons shall be in accordance with Clause 5.9.3 of AASHTO LRFD as indicated below:

	Low Relaxation Strand		Plain High Strength Bars	
Pretensioning				
Immediately prior to transfer	0.75 f_{pu}	1395 (MPa)	0.70 f_{pu}	725 (MPa)
Service Limit State after losses	0.80 f_{py}	1340 (MPa)	0.80 f_{py}	704 (MPa)
Post-tensioning				
Prior to seating (short term)	0.90 f_{py}	1508 (MPa)	0.90 f_{py}	792 (MPa)
At anchorages immediately after anchor set	0.70 f_{pu}	1302 (MPa)	0.70 f_{pu}	725 (MPa)
At end of the seating loss zone immediately after anchor set	0.74 f_{pu}	1376 (MPa)	0.70 f_{pu}	725 (MPa)
Service Limit State after losses	0.80 f_{py}	1340 (MPa)	0.80 f_{py}	704 (MPa)

5.8 Serviceability Stress Limits for Concrete

Stress limits for concrete shall be in accordance with Clause 5.9.4 of AASHTO LRFD.

5.8.1 Match Cast Segmental Construction

The limits indicated in the table below are based on the use of epoxy joints (Type A) between the match cast segmental girders. (Cl 5.5.4.2.2) A summary of the relevant limits is indicated below:

Load Case		Stress Limit (MPa)		
		f_c	40[5]	50[5]
Flexural Tensile Stress	Temporary Condition [1]	No tension	0	0
	In Service [2]	No tension	0	0
Flexural Compressive Stress[4]	Temporary Condition [1]	$0.60f'_{ci}$	19.2	24
	Effective Prestress and Permanent Loads In Service [2] & during shipping and handling	$0.45f'_c$	18.0	22.5
		$0.60f'_c$	24.0	30.0

Temporary stress before lossed – fully prestressed components

Service limit after losses

F'_{ci} assumed as $0.8f'_c$

The web and flange slenderness ratios are assumed to satisfy

$\varphi_w = 1.0$ (refer Cl 5.7.4.7.2)

Table Fully Prestressed In-Situ Construction (post-tensioned)

Load Case		Stress Limit (MPa)		
		F_c	40[5]	50[5]
Flexural Tensile Stress	Temporary Conditions [1]	$0.58\sqrt{f_{ci}}$ [3]	3.28	3.67
	In Service [2]	$0.50\sqrt{f_{ci}}$ [4]	3.16	3.54
Flexural Compressive Stress[6]	Temporary Condition [1]	$0.60\ f_{ci}$	19.2	24.0
	Permanent Loads	$0.45f'_c$	18.0	22.5
	In Service [2]	$0.60f'_c$	24.0	30.0

Temporary stresses before losses – fully prestressed components.

Service limit after losses

Assuming bonded reinforcement sufficient to resist 120% of the tension force in the cracked concrete computed on the basis of uncracked section

Assuming bonded prestressing tendons

f_{ci} assumed as $0.8\ f_c$

The web and flange slenderness ratios are assumed to satisfy φ_w = 1.0 (refer Cl 5.7.4.7.2)

5.9 Strength Limit State Capacity of Concrete

The capacity of concrete sections for the strength limit state shall be calculated using the requirements of Clause 5.5.4 of AASHTO LRFD. The following resistance factors shall be adopted:

	Resistance Factor φ
Flexure and Tension of Reinforced Concrete	0.90
Flexure and Tension of Prestressed Concrete	1.00
Shear and Torsion	0.90
Axial Compression	0.75
Bearing on Concrete	0.70
Compression in strut-and-tie models	0.70
Compression in anchorage zones	0.80
Tension in steel in anchorage zones	1.00
Flexure and Tension of Reinforced Concrete (φ_f)*	0.90
Shear at joints in segmental construction (φ_v)*	0.85

Type a Joints assumed. ie. Cast in place concrete or epoxy joints between precast units

The structural resistance of concrete members for the strength limit state shall be based on the conditions of equilibrium and strain compatibility and the following assumptions:

- Strain in fully bonded reinforcement is directly proportional to the distance from the neutral axis. The stress in bonded prestressing tendonds shall be calculated in accordance with AASHTO Cl. 5.7.3.1.1.

- The difference in strain between the tendons and concrete shall be considered for unbonded or partially bonded tendons. The stress in bonded prestressing tendonds shall be calculated in accordance with AASHTO Cl 5.7.3.1.2.

- A representative stress strain curve shall be assumed for steel reinforcement.

- Unconfined concrete shall have a concrete compressive strain not

greater than 0.003.

- The concrete compressive stress-strain distribution is assumed to be rectangular, parabolic, or generally accepted profile consistent with test results.

Appendix 4

WIND TUNNEL TEST

REPORT ON EVALUATION OF AERODYNAMIC STABILITY OF CAN THO BRIDGE IN THE SOCIALIST REPUBLIC OF VIETNAM

November, 1999

Wind & Structure Laboratory
Dept. of Civil Engineering
Yokohama National University
Yokohama, Japan

CONTENTS

1. INTRODUCTION

This report describes the research on the evaluation of aerodynamic stability of the Can Tho Bridge in the Socialist Republic of Vietnam (Original report was written in Japanese and this report is summarized and translated into English. Detailed descriptions and full references are given in the Original Japanese report.)

The research was contracted between Nippon Koei Co., Ltd. and Wind & Structure Laboratory, Dept. of Civil Engineering of Yokohama National University.

The Can Tho Bridge will be a steel-concrete composite cable-stayed bridge with a center span length of 550 m. The research consists of eigenvalue analysis of the completed bridge, section-model wind-tunnel test of the deck, elastic-model wind-tunnel test of the tower at an erection stage, buffeting analysis of the deck at an erection stage and recommendation for cable vibration.

The research was conducted by the laboratory staff below.

Co-director	Professor	Hitoshi YAMADA, Dr. Eng.
Co-director	Professor	Toshio MIYATA, Dr. Eng.
Leader	Research Associate	Hiroshi KATSUCHI, Dr. Eng.
Staff	Graduate Students	Hiroshi SUGIURA,
		Tomohito SHIMIZU,
		Takeshi SUZUKI,
		Daisuke SONOYAMA
		Hiroaki TANAKA

1.1 General Description of Can Tho Bridge

The Can Tho Bridge is planned to cross the Hau River in the city of Can Tho and to function as a by-pass of the national highway route 1. The bridge will be a steel-concrete composite cable-stayed bridge with a center span length of 550 m and a total length of 1,090 m.

General plans are shown in Figure 1.1.

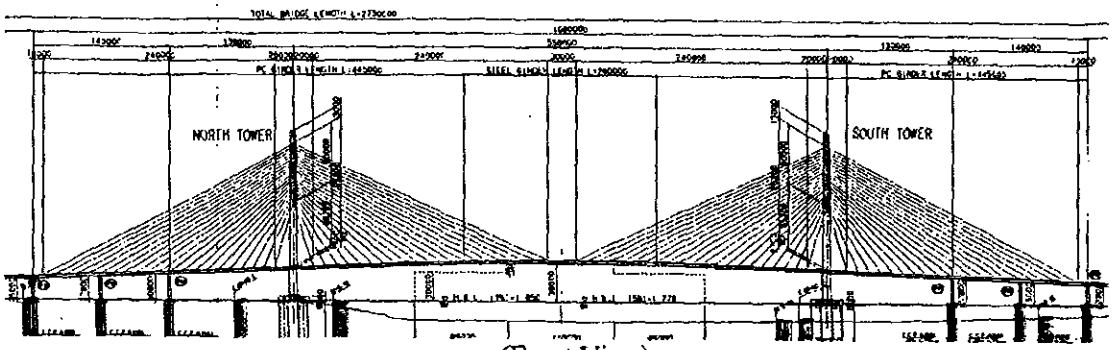

(Front View)

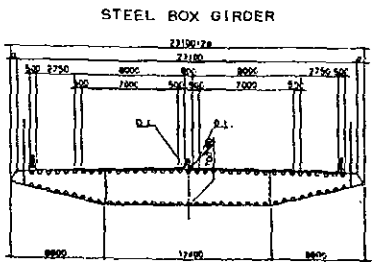

(Steel Section)

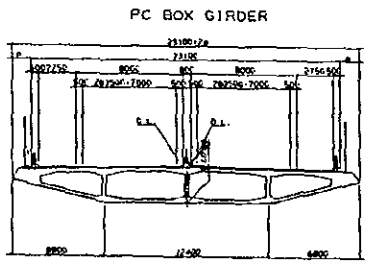

(Concrete Section)

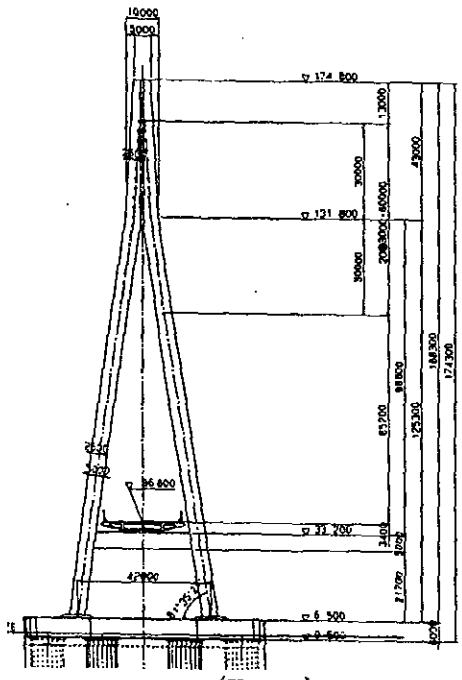

(Tower)

Figure 1.1 General Plan of Can Tho Bridge

The center span length of cable-stayed bridges has extended recently. The longest-span bridge is the Tatara Bridge (890 m) in Japan followed by the Normandie Bridge (856 m) in France. The third group are the Yanpu Bridge (602 m) in China and the Central Meiko Bridge (590 m) in Japan.

The Can Tho Bridge is as same as the third groups in the center span length. Careful investigation on the aerodynamic stability is required.

1.2 Dimensions of Bridge

Dimensions of the bridge are shown below.

Type	3-span continuous cable-stayed bridge
	Deck: steel-concrete composite
	(steel: 200-m-long portion in center span)
	Tower: concrete
Length	1,090 m in total
	550 m in center span
Deck	Box girder
	2.7 m in height
Tower	Inverse Y shape
	168.3 m in height
Cable	Twin cable planes
	$8 \times 21 = 168$ cables

2. METHODOLOGY OF WIND-TUNNEL TESTTING

2.1 Aeroelastic Phenomena of Long-Span Bridge

Aeroelastic phenomena of long-span bridges are classified into some categories considering the convenience in designing. Wind-resistant-design code [2.1] of the Honshu-Shikoku Bridge Authority classifies them as shown in Fig. 2.1.

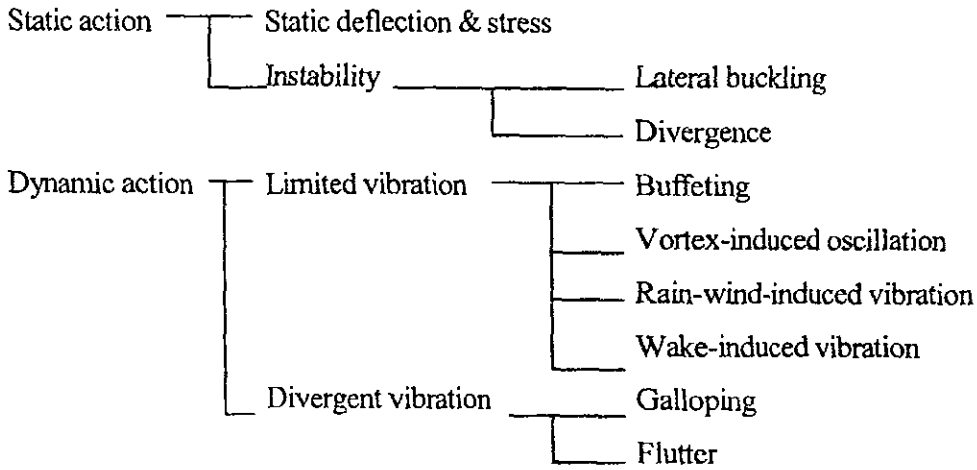

Fig. 2.1 Classification of Aeroelastic Phenomena of Long-Span Bridges [2.1]

Static deflection & stress are stationary phenomena which are independent of time. They are caused by a mean component of time-varying wind speed.

Lateral buckling is typically observed at a very slender deck of a suspension bridge, which suddenly buckles normal to wind axis. The critical wind speed of occurrence is usually higher than that of flutter and galloping. **Divergence** is a phenomenon that a torsionally weak deck suddenly twists at a critical wind speed.

Limited vibrations are defined to be limited in terms of limited amplitude and/or limited wind-speed range. **Buffeting** is a random vibration due to turbulence in wind flow. It is usually estimated by a numerical analysis and is associated with an estimation of the maximum wind load. **Vortex-induce oscillation** is caused by well-known Karman Vortices formed on the leeward of the structure. Since it is not a catastrophic phenomenon, it is viewed as harmful problem to the serviceability such as fatigue and discomfort to users. **Rain-wind-induced vibration** is often observed at stay cables of a cable-stayed bridge with the condition of wind and raining. The cause

of the vibration is due to the formation of a water rivulet on the cable surface and the existence of the axial flow on the leeward surface, both are typical phenomena on an inclined cable. **Wake-induced vibration** is observed at the leeward structure of parallel-aligned structures such as twin cables and twin decks.

Divergent vibrations are defined to be catastrophic once they occur. It must be required that they do not occur in the design wind-speed range. **Galloping**, which is vibration with a vertically dominant component, is typically observed at cables and bluff decks where lift coefficients show a negative slope. **Flutter** is often classified into "torsional flutter" and "bending-torsion flutter (or coupled flutter)" based on the vibration mode. It is well-known incident that flutter destructed the old Tacoma Narrows Bridge.

2.2 Wind-Resistant Design for Long-Span Bridges

Wind-resistant design of bridges is represented by the procedures that a designer estimates how a bridge responds to wind flows and that he judges whether the responses are allowable or not. Furthermore, if the response exceeds a limit, appropriate countermeasures are required such as change of geometry of the bridge and/or attachment of stabilizing devices.

The key to successful and accurate wind-resistant design really depends on the accurate estimation of aerostatic/dynamic forces exerting on the bridge structure and of bridge responses. Since the bridge geometry is too complex to analyze flow patterns around it, wind-tunnel testing is the most reliable and reasonable method to execute wind-resistant design.

2.3 Methodology of Wind-Tunnel Testing

TYPES OF TESTS [2.2]

There are several kinds of wind-tunnel testing, each of which has a different purpose, as shown in Table 2.1.

Aerostatic-force coefficients, which are a function of angle of attack, are used to estimate wind load and buffeting responses. On the other hand, unsteady aerodynamic force coefficients (flutter derivatives), which are motion dependent, are sometimes measured with a section model. The flutter derivatives govern the state (damping & stiffness) of the bridge in wind flow and are used to numerically estimate flutter and/or buffeting.

The spring-mounted model test has widely been carried out to investigate the aerodynamic

characteristics of the bridge deck because the test is relatively easy and inexpensive. The test assumes two dimensions structurally and aeroelastically, that is, the same dimensions of the deck cross section along the bridge span and a small torsional deflection of the deck due to wind loading.

For the purpose of investigating the three dimensional effects, the taut strip model test and/or full-model test are sometimes carried out, which are relatively time-consuming and expensive, however. In particular, the full-model test needs a very careful modeling and preparation. However, once the test is executed, it has a big advantage for one to directly evaluate the aerodynamic responses of the full-scale bridge. Both of the two testing also have an advantage that they can include the effects of the boundary layer turbulence.

Table 2.1 Types of Wind-Tunnel Testing

Name of tests	Quantities measured	Model used	Output	Model scale
Static-force measurement test	Aerostatic force coefficients (C_D,C_L & C_M)	Rigid section model	Coefficients (C_D,C_L & C_M) – angle of attack	1/50 – 1/100
Spring-mounted model test (section model test)	Dynamic & static deflection	Rigid section model	Deflection (amplitude) – wind speed	1/50 – 1/100
Taut strip model test	Aerodynamic damping	3D partial-bridge model	Aerodynamic damping – wind speed	1/100 – 1/300
Full-model test		Elastic full model		1/70 – 1/300

SIMILARITY LAW [2.2 & 2.3]

Executing wind-tunnel testing, several similarity requirements are imposed. They are

(1) Inertia parameter: ρ_s/ρ

(2) Elastic parameter: $E/(\rho U^2)$

(3) Gravity parameter (Froude number): gD/U^2

(4) Viscous parameter (Reynolds number): UD/ν

(5) Damping parameter: δ_s

where ρ: air density, ρ_s: density of the structure, E: Young modulus, U: wind speed, ν: kinematic molecular viscosity of the fluid, D: representative length.

The fourth parameter is difficult to satisfy, so the remaining four parameters are usually

considered.

Since the third parameter (Froude number) affects a gravity-governing structure such as a suspension bridge cable, the testing for a section model of a bridge deck and an elastic tower model can neglect this parameter. After all, three parameters (inertia, elasticity and damping) are required to satisfy in this research.

3. EIGENVALUE ANALYSIS OF CAN THO BRIDGE

3.1 Theory of analysis

Assuming a three dimensional finite element model of the Can Tho Bridge, an equation of motion of non-damped free vibration is given by

$$\mathbf{M}\ddot{\mathbf{u}} + \mathbf{K}\mathbf{u} = \mathbf{0} \tag{3.1}$$

where **M**: mass matrix, **K**: stiffness matrix, **u**: displacement vector and $\ddot{\mathbf{u}}$: acceleration vector.

Assuming a sinusoidal motion of

$$\mathbf{u} = \mathbf{x}\exp(i\omega t) \tag{3.2}$$

with **x**: vibration mode and ω: circular frequency and substituting Eq. (3.2) into Eq. (3.1) give

$$(-\omega^2\mathbf{M} + \mathbf{K})\mathbf{x}\exp(i\omega t) = 0 \tag{3.3}$$

Satisfying Eq. (3.3) requires

$$(-\omega^2\mathbf{M} + \mathbf{K})\mathbf{x} = 0 \tag{3.4}$$

and non-trivial solution of $\mathbf{x} = \mathbf{0}$ for Eq. (3.4) can be obtained if the next condition is satisfied.

$$|\lambda\mathbf{M} + \mathbf{K}| = 0 \tag{3.5}$$

$$\lambda = -\omega^2$$

This equation is called "characteristic equation". Expanding Eq. (3.5) makes n^{th} order polynomial of λ. The roots λ are called eigenvalues and **x** is called eigenvector.

Dividing Eq. (3.4) by ω^2 makes

$$\mathbf{M}\mathbf{x} = \lambda\mathbf{K}\mathbf{x} \tag{3.6}$$

where $\lambda = \dfrac{1}{\omega^2}$.

A generalized eigenvalue problem of Eq. (3.6) is converted into a standardized eigenvalue problem. Assuming that **K** can be expressed by its triangular matrix **U** (upper triangular matrix),

$$\mathbf{K} = \mathbf{U}^t\mathbf{U} \tag{3.7}$$

and substituting Eq. (3.7) into Eq. (3.6) and multiplying by $\mathbf{U}^{-t}$ gives

$$\mathbf{U}^{-t}\mathbf{M}\mathbf{U}^{-1}\mathbf{U}\mathbf{x} = \lambda\mathbf{U}\mathbf{x} \tag{3.8}$$

Eq. (3.8) can be treated as a standardized eigenvalue problem such as

$$\mathbf{A}\mathbf{v} = \lambda\mathbf{v} \tag{3.9}$$

where $\mathbf{A} = \mathbf{U}^{-t}\mathbf{M}\mathbf{U}^{-1}$, $\mathbf{v} = \mathbf{U}\mathbf{x}$.

Solving Eq. (3.9) appropriately yields eigenvalues λ, eigenvectors **v**, and natural frequencies,

etc. are given by

Natural circular frequencies: $\omega_i = \frac{1}{\sqrt{\lambda_i}}$ (rad/sec)

Natural frequencies: $f_i = \frac{\omega_i}{2\pi} = \frac{1}{T_i}$ (Hz)

Period: $T_i = \frac{2\pi}{\omega_i} = \frac{1}{f_i}$ (sec)

Vibration mode: $\mathbf{x}_i = \mathbf{U}^{-1}\mathbf{v}_i$

$(i = 1 \sim n)$

3.2 Analytical conditions

The 3D finite element model used in this research consists of 430 nodes (134 for the deck and 72 for each tower). The deck was modeled as a fish-bone model with a elastic beam at the shear center representing elastic moduli of the deck and masses at the gravity points. A cross section of the deck has 4 nodes (mass, shear center, 2 cable fixing points) connected by rigid bars each other. Three cables were modeled into one cable as a truss element having equivalent elongation stiffness. Mass of the cables is equally divided and each of them was added at cable fixing points of the deck and tower.

Structural properties used in the analysis are summarized in Tables 3.1 and 3.2.

Table 3.1 Masses and stiffness of deck and tower

			Steel deck section	PC deck Section	Tower		
					Section A	Section B	Section C
Weight of deck per unit length		tf/m	15.00	47.37	94.89	42.17	52.53
Weight of pavement per unit length		tf/m	5.00	5.00	-	-	-
Point of vertical centroid	Yu	m	1.18420	1.04384	-	-	-
Section area	A	m^2	1.08888	18.94865	37.95750	16.86775	21.01100
Moment of inertia of area	Iy	m^4	1.22677	18.63102	183.82898	91.85420	79.43178
	Ix	m^4	56.40387	978.15643	76.75493	107.25366	173.44676
Torsional stiffness of section	J	m^4	3.29950	47.06937	192.99409	130.81199	165.65502
Young modulus	E	tf/m^2	2.10E+07	3.30E+06	3.00E+06	3.00E+06	3.00E+06
Shear modulus	G	tf/m^2	8.10E+06	1.40E+06	1.25E+06	1.25E+06	1.25E+06
Flexural rigidity	E・Iy	tf/m^2	1,184,481,270	3,227,916,219	230,264,775	321,760,965	520,340,280
	E・Ix	tf/m^2	25,762,170	61,482,366	551,486,951	275,562,585	238,295,349
Torsional rigidity	G・J	tf/m^2	26,725,950	65,897,118	241,242,606	163,514,988	207,068,775

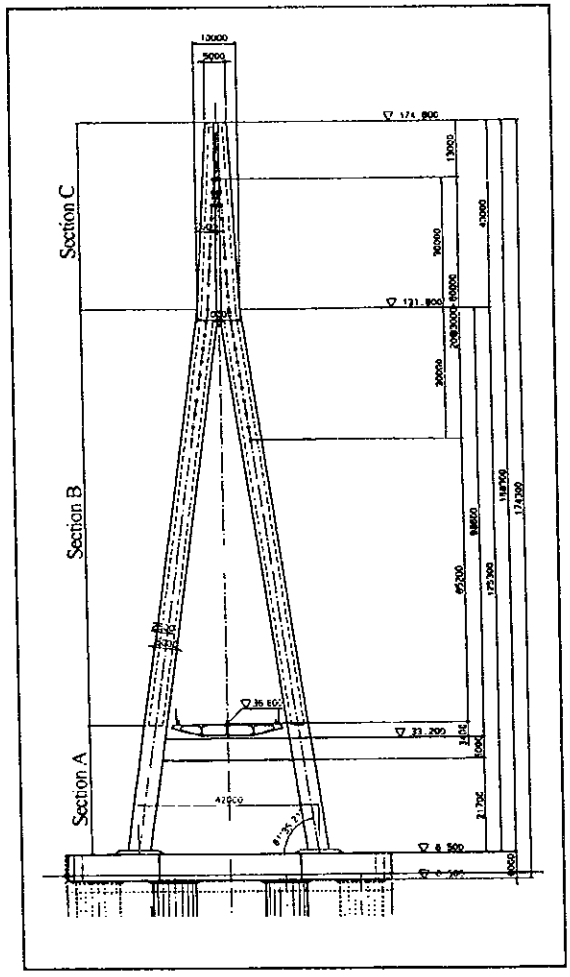

Table 3.2 Dimensions of cables

No.	section area (m^2)	cable tension (tf)	unit weight (kg/m)	type
S1	13.316	828	52.848	2×48H15
S2	13.316	812	52.848	2×48H15
S3	13.316	758	52.848	2×48H15
S4	13.316	741	52.848	2×48H15
S5	13.316	677	52.848	2×48H15
S6	13.316	659	52.848	2×48H15
S7	13.316	598	52.848	2×48H15
S8	16.922	580	67.161	2×61H15
S9	16.922	550	67.161	2×61H15
S10	16.922	608	67.161	2×61H15
S11	16.922	584	67.161	2×61H15
S12	16.922	558	67.161	2×61H15
S13	16.922	616	67.161	2×61H15
S14	13.316	568	52.848	2×48H15
S15	13.316	536	52.848	2×48H15
S16	13.316	503	52.848	2×48H15
S17	13.316	404	52.848	2×48H15
S18	13.316	332	52.848	2×48H15
S19	13.316	309	52.848	2×48H15
S20	13.316	295	52.848	2×48H15
S21	13.316	289	52.848	2×48H15
S22	13.316	443	52.848	2×48H15
S23	13.316	458	52.848	2×48H15
S24	13.316	475	52.848	2×48H15
S25	13.316	511	52.848	2×48H15
S26	13.316	701	52.848	2×48H15
S27	16.922	750	67.161	2×61H15
S28	16.922	823	67.161	2×61H15
S29	16.922	871	67.161	2×61H15
S30	16.922	920	67.161	2×61H15
S31	16.922	965	67.161	2×61H15
S32	16.922	1.009	67.161	2×61H15
S33	16.922	1.041	67.161	2×61H15
S34	16.922	1.080	67.161	2×61H15
S35	13.316	952	52.848	2×48H15
S36	13.316	598	52.848	2×48H15
S37	13.316	616	52.848	2×48H15
S38	13.316	588	52.848	2×48H15
S39	13.316	591	52.848	2×48H15
S40	13.316	605	52.848	2×48H15
S41	13.316	618	52.848	2×48H15
S42	13.316	630	52.848	2×48H15

(per one plane)

Note: cable numbers are shown in the next figure.

CABLE NUMBER

SIDE ELEVATION SCALE 1:2000

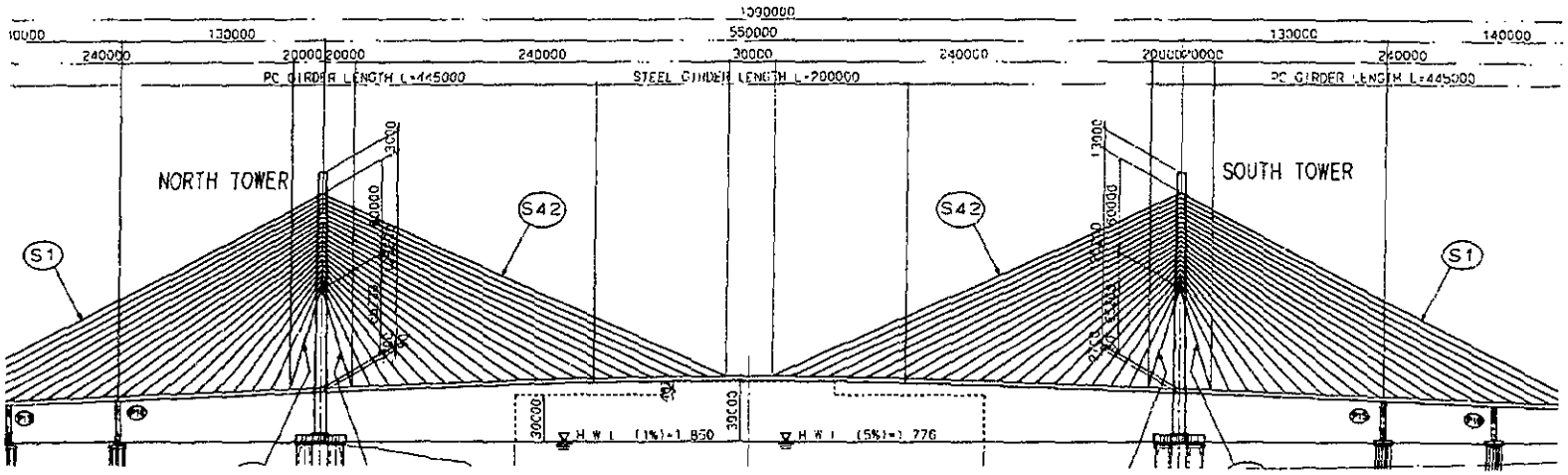

3.3 Analytical results

Natural frequencies and equivalent masses are shown in Table 3.3. Some fundamental vibration modes are shown in Figure 3.1.

Equivalent masses [m] and polar moment of inertias [I] are defined as below.

$$m = \frac{\int_{structure} \varphi^2(s)dw}{\int_{deck} \varphi_h^2(s)} \quad , \quad I_p = \frac{\int_{structure} \varphi^2(s)dw}{\int_{deck} \varphi_\theta^2(s)} \qquad (3.10, 3.11)$$

where $\varphi(s)$: modal value (s: coordinate), $\varphi_h(s)$ and $\varphi_\theta(s)$: vertical and torsional components of mode value, respectively, dw: infinitesimal mass. Integration is carried out for entire structure in numerator and for only deck in denominator.

1st mode is lateral 1st mode, 2nd vertical 1st mode and 14th torsional 1st mode. The natural frequencies of 1st vertical mode and 1st torsional mode are 0.395 Hz and 1.23 Hz, respectively. The ratio of them is 3.1 which is relatively higher than that of other same-length class cable-stayed bridges, as shown in Figure 3.2 [3.1]. The reason may be due to the fact that the Can Tho Bridge is a steel-concrete compound bridge and it has intermediate supports at the side spans.

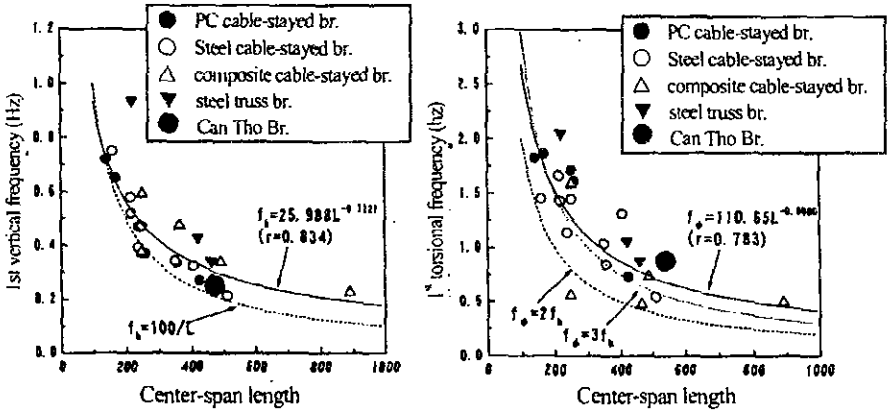

(a) 1st vertical mode (b) 1st torsional mode

Figure 3.2 Relationship of Natural frequencies and span length of 3-span continuous cable-stayed bridges [3.1]

Table 3.3 Natural frequencies and equivalent masses

Natural frequencies & equivalent masses of Can Tho Bridge

No.	Frequency (Hz)	Generalized mass ($tf \cdot sec^2/m$)	Equivalent Mass			Mode
			Lateral	Vertical ($tf \cdot sec^2/m^2$)	Torsion ($tf \cdot m^2 \cdot sec^2/m^2$)	
1	0.270	5.961E+15	3.007E+00	1.499E+14	5.449E+05	1st Lateral (S)
2	0.395	2.140E+03	3.575E+13	3.378E+00	7.613E+12	1st Vertical (S)
3	0.435	1.343E+03	1.516E+13	4.799E+00	3.745E+12	1st Vertical (AS)
4	0.553	7.996E+02	7.876E+13	3.378E+00	4.726E+12	2nd Vertical (S)
5	0.617	9.895E+00	1.006E+11	1.647E+01	6.706E+11	
6	0.649	2.532E+11	4.244E+00	7.562E+10	3.267E+05	1st Lateral (AS)
7	0.691	3.761E+01	1.924E+11	3.859E+00	7.356E+11	2nd Vertical (AS)
8	0.763	1.305E+11	4.670E+04	2.704E+10	3.670E+04	
9	0.764	6.802E+10	2.107E+03	5.496E+10	8.362E+04	
10	0.837	1.941E+03	4.905E+13	3.425E+00	2.790E+12	3rd Vertical (S)
11	0.951	1.572E+03	1.624E+11	7.524E+00	1.909E+10	
12	0.965	1.576E+02	2.698E+11	6.803E+00	3.257E+10	
13	1.127	2.336E+03	9.676E+11	3.586E+00	3.948E+11	
14	1.230	8.957E+07	2.262E+01	5.808E+06	2.277E+02	1st Torsion(1) (S)
15	1.255	1.467E+02	1.334E+07	9.976E+00	2.313E+08	
16	1.260	3.227E+08	4.482E+04	1.666E+07	1.181E+04	
17	1.270	7.687E+08	4.597E+01	1.777E+07	9.348E+02	1st Torsion(2) (S)
18	1.286	1.043E+03	4.039E+11	6.798E+00	2.569E+11	
19	1.299	1.189E+03	4.777E+08	6.745E+00	2.023E+09	
20	1.381	5.412E+02	2.217E+06	4.724E+00	2.166E+08	
21	1.393	1.453E+08	4.516E+00	2.604E+06	8.619E+02	2nd Lateral (S)
22	1.399	9.791E+07	7.954E+02	3.815E+06	2.378E+02	1st Torsion (AS)
23	1.440	4.370E+02	2.255E+09	6.275E+00	1.291E+09	
24	1.474	4.678E+01	2.733E+08	9.364E+00	8.553E+08	
25	1.542	8.247E+01	5.464E+07	6.565E+00	5.302E+08	
26	1.685	7.250E+01	2.856E+08	6.316E+00	4.828E+08	
27	1.769	7.991E+06	1.415E+02	2.551E+05	1.432E+02	2nd Torsion(1) (S)
28	1.797	9.513E+01	8.231E+06	4.905E+00	6.703E+06	
29	1.900	1.999E+05	3.429E+02	3.802E+03	1.628E+03	2nd Torsion(1) (AS)
30	1.902	2.738E+02	2.497E+05	5.238E+00	1.199E+06	
31	1.939	5.667E+05	8.937E+02	3.806E+04	4.657E+02	2nd Torsion(2) (S)
32	1.947	8.543E+01	4.309E+06	6.476E+00	2.998E+06	
33	2.014	2.535E+02	1.604E+08	4.543E+00	1.045E+09	
34	2.162	3.535E+09	3.805E+00	1.413E+09	8.028E+03	2nd Lateral (AS)
35	2.184	1.925E+03	4.345E+09	4.688E+00	1.987E+10	
36	2.245	8.476E+02	3.537E+08	5.167E+00	2.199E+09	
37	2.322	6.045E+01	5.363E+07	4.686E+00	2.571E+08	
38	2.442	8.590E+00	2.764E+07	6.652E+01	1.493E+08	
39	2.446	7.956E+02	2.009E+08	6.176E+02	1.070E+09	
40	2.448	2.516E+01	2.664E+07	8.392E+01	1.396E+08	
41	2.492	1.461E+09	1.768E+02	2.771E+09	1.579E+02	2nd Torsion(2) (AS)
42	2.585	3.534E+03	9.701E+04	3.162E+00	1.114E+06	
43	2.691	1.611E+09	1.246E+02	2.082E+09	2.089E+02	3rd Torsion (S)
44	2.730	1.610E+09	5.931E+03	7.784E+08	2.892E+02	
45	2.734	4.300E+08	3.508E+03	6.530E+08	2.808E+02	
46	2.778	1.967E+03	2.738E+04	5.070E+00	1.142E+05	
47	2.834	8.427E+02	9.990E+03	1.125E+01	7.286E+04	
48	2.865	8.205E+01	3.656E+05	4.243E+01	1.750E+06	
49	2.875	4.872E+02	2.653E+03	8.162E+00	1.869E+04	
50	3.038	5.082E+09	2.215E+04	1.777E+07	4.613E+03	

S: Symmetric
AS: Anti-symmetric

mode1: 1st lateral

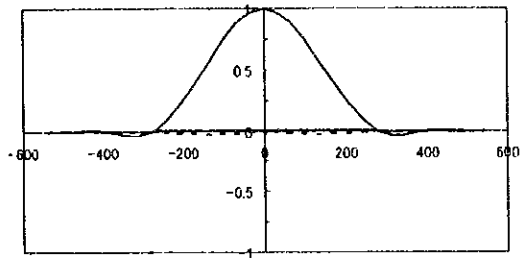

mode2: 1st vertical

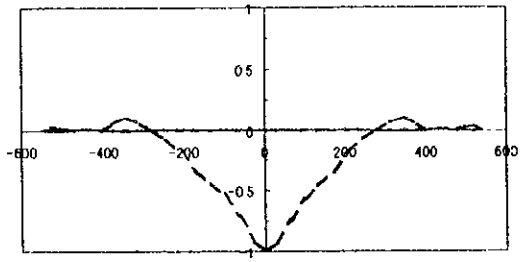

mode3: 1st antisymmetric vertical

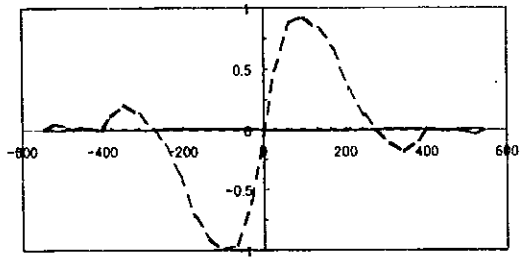

mode4: 2nd vertical

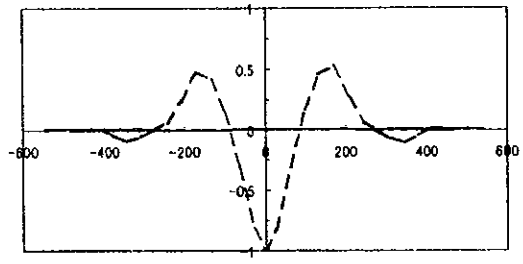

mode 10: 3rd vertical

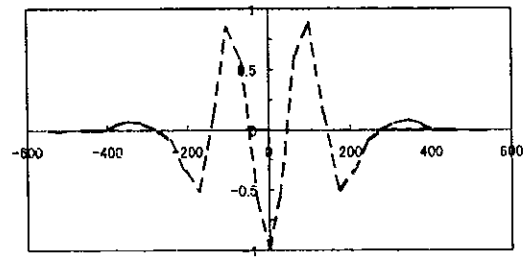

mode 14: 1st torsion(1)

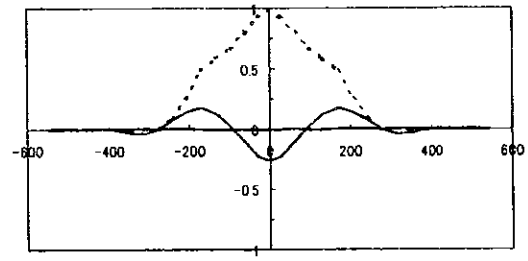

mode 17: 1st torsion(2)

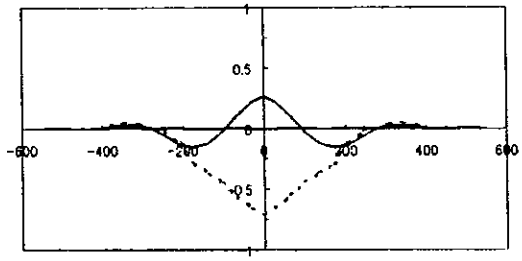

LEGEND

——— : leteral component

— — — — : vertical component

..... : torsional component

4. SECTION MODEL TEST OF DECK

4.1 Description of Test

The aerodynamic stability (characteristics) of the bridge completed was investigated by a section model test, as shown in Figures 4.1 and 4.2. As described in Chapter 2, the section model of the deck is mounted by 4 springs at each side. The model is given 2 degree-of-freedom (vertical and torsion) and the similarity requirements are satisfied.

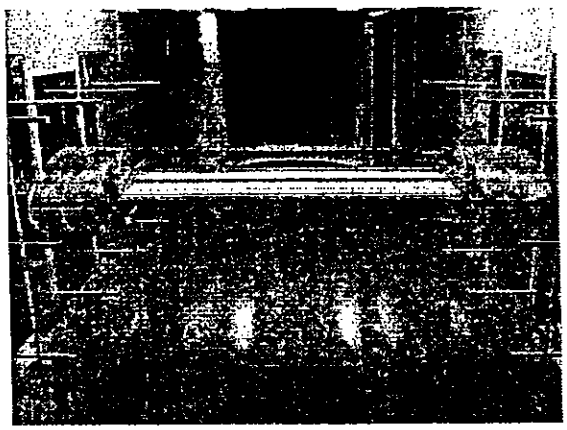

Fig. 4.1 Section model of deck

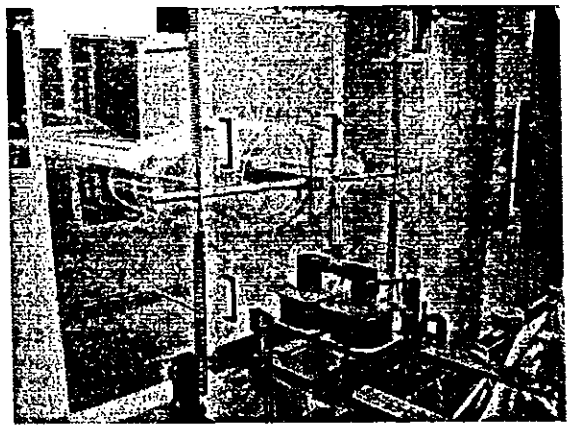

Fig. 4.2 Spring-mount system

The similarity requirements in the section model are

(1) Inertia parameter: $m/(\rho D^2)$, $I_p/(\rho D^4)$,

(2) Elastic parameter: $U/(f_h D)$, $U/(f_\theta D)$

(3) Damping parameter: $\delta_{s,h}$, $\delta_{s,\theta}$,

where m: equivalent mass, I_p: equivalent polar moment of inertia, ρ: air density, D: length, U: wind speed, f: frequency, δ_s: structural damping. The subscripts of h and θ represent vertical and torsion, respectively.

The inertia parameters were adjusted by putting additional masses at appropriate positions so as to satisfy the parameter. The elastic parameters (frequency parameter) were adjusted by spring stiffness and the distance of two springs. The damping parameters were adjusted by using electrical damping devices as shown in Figure 4.2.

In the test, aerodynamic responses were measured with changing wind speed. A smooth flow

was used in the test.

The scale of the section model is 1/60 and its length 1.25 m. Test conditions are shown in Table 4.1. The frequency ratio of vertical and torsion is by 11 % lower than requirement. Since the ratio affects the flutter onset speed, flutter onset speed if measured can be converted with the Selberg formula. In addition, since vertical and torsional vortex-induced oscillation are 1 degree-of-freedom, the difference of the frequency ratio can be dissolved by applying different wind-speed ratio between vertical and torsion.

Table 4.1 Test conditions

	Prototype	Requirement in test	Measured in test	Error (%)
Equivalent mass m (kgf/m)	33.11×10^3	9.197	9.085	- 1.2
Equivalent polar moment of inertia I_p (kgf·m^2/m)	2231.2×10^3	0.1722	0.1697	- 1.5
Vertical frequency f_h (Hz)	0.395	—	1.66	—
Torsional frequency f_θ (Hz)	1.230	—	4.59	—
Frequency ratio (f_θ/f_h)	3.11	3.11	2.77	- 10.9
Structural damping Vertical: $\delta_{s,h}$	—	0.02	0.02	0
Torsion: $\delta_{s,\theta}$	—	0.02	0.02	0

The ratio of wind speed between model and full-scale is given by

$$\frac{f_p B_p}{U_p} = \frac{f_m B_m}{U_m} \tag{4.1}$$

where subscripts of p and m represent full-scale (prototype) and model, respectively. Based on the conditions in Table 4.1, the wind-speed ratios of vertical and torsion are 11.9 and 13.4, respectively.

As for structural damping, it tends to show the trend that damping decreases as the span length increases. Based on previous research, structural damping for vertical and torsion was assumed to be 0.02 in log decrement. Responses with the damping of 0.03 were also investigated, however.

Three angles of attack of wind flow were chosen, that is, -3 degrees, 0 degree and +3 degrees.

4.2 Test Results

The test results (V – A diagrams), which are vertical and torsional responses versus wind speed, are shown in Figures 4.3 – 4.5. The vertical and horizontal axes are converted to the dimensions in the full-scale bridge.

In the case of angle of attack being 0 degree, it was observed that torsional vortex-induced oscillation with amplitude of 0.15 degree would occur at a wind speed of about 20 m/s. However, increasing the structural damping from 0.02 to 0.03 in log decrement suppressed the amplitude to about 0.08 degrees. No vertical vibration was observed. As for flutter, it would not occur until a wind speed of 100 m/s. Coupled flutter was observed to occur at about 311 m/s, however.

In the case of angle of attack being + 3 degree, it was observed that torsional vortex-induced oscillation would occur at a wind speed of about 15 m/s as observed in 0 degree. However, the amplitude was relatively small and about 0.04 degrees. Increasing the structural damping to 0.03 in log decrement completely suppressed the vibration. No vertical vibration was observed. As for flutter, it would not occur until a wind speed of 320 m/s which was the maximum wind speed of the test.

In the case of angle of attack being - 3 degree, relatively small-amplitude (about 0.04 degrees) torsional vortex-induced vibration was observed. On the other hand, vertical vortex-induced vibration with amplitude of about 2.9 cm was observed at a wind speed of 9 m/s. Increasing the structural damping to 0.03 in log decrement completely suppressed the torsional vibration, but slightly suppressed the vertical to about 2.5 cm. As for flutter, coupled flutter was observed at a wind speed of 281 m/s.

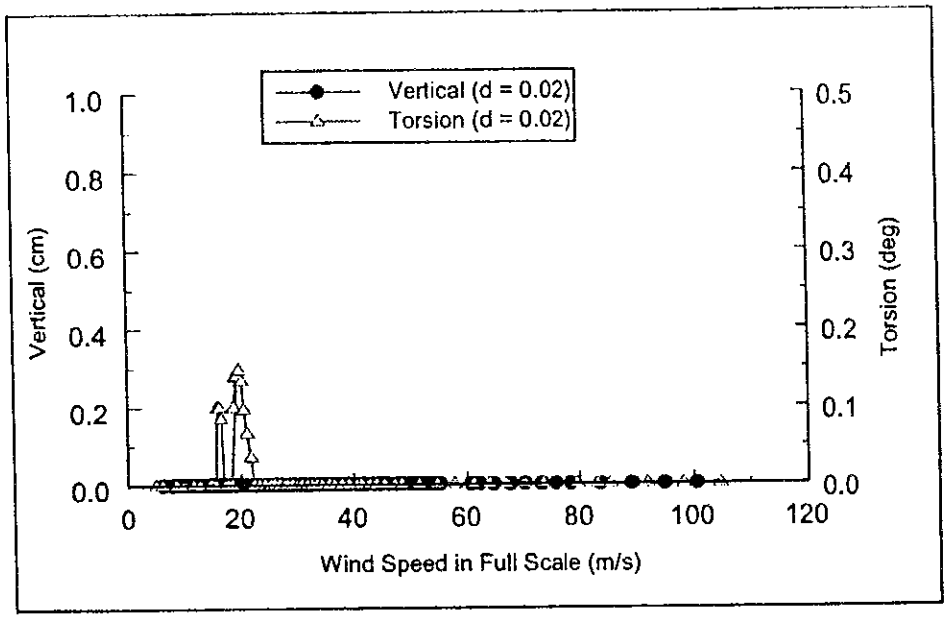

(1) Vertical & Torsion (d = 0.02)

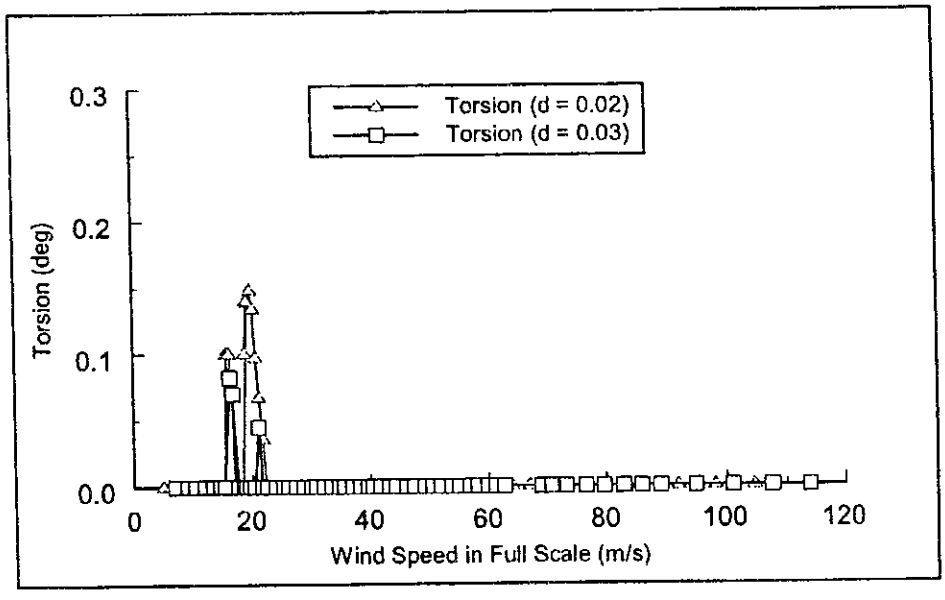

(2) Torsion (d = 0.02 & 0.03)

Relationship between Responses and Wind Speed (a = 0deg)

Figure 4.3 Relationship between vertical & torsional responses and wind speed (angle of attack = 0 degree)

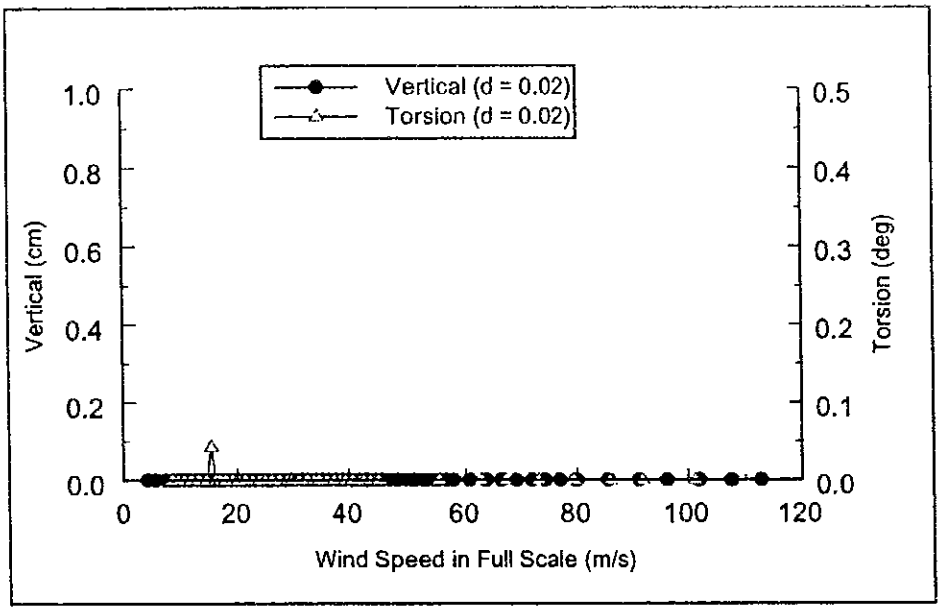

(1) Vertical & Torsion (d = 0.02)

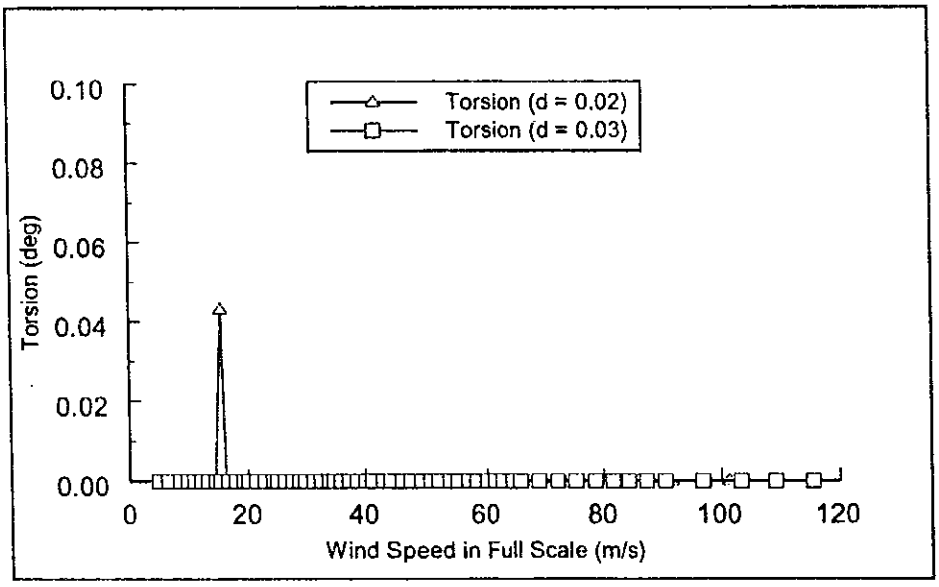

(2) Torsion (d = 0.02 & 0.03)

Relationship between Responses and Wind Speed (d = +3 deg)

Figure 4.4 Relationship between vertical & torsional responses and wind speed (angle of attack = +3 degrees)

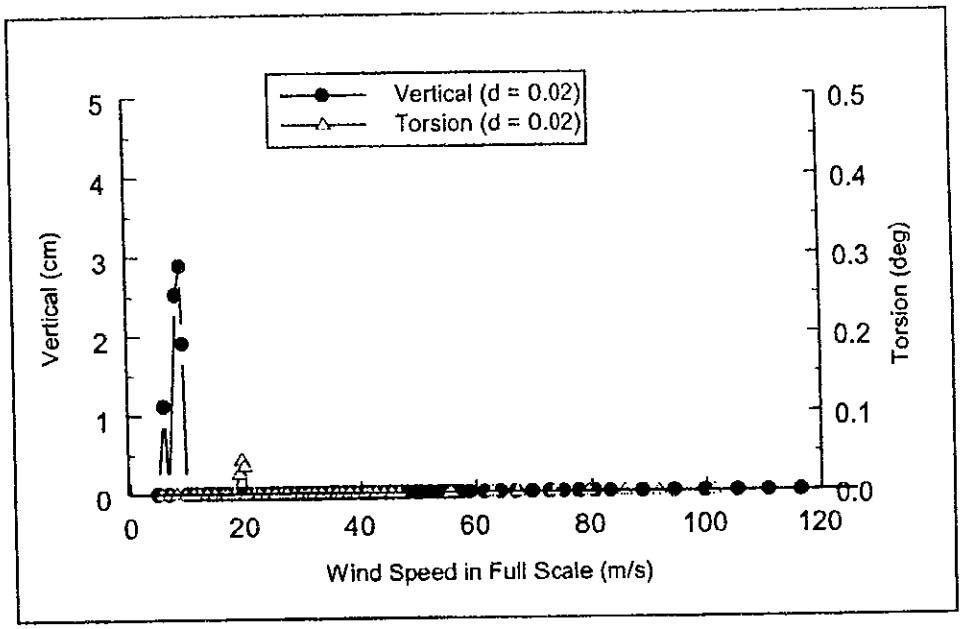

(1) Vertical & Torsion (d = 0.02)

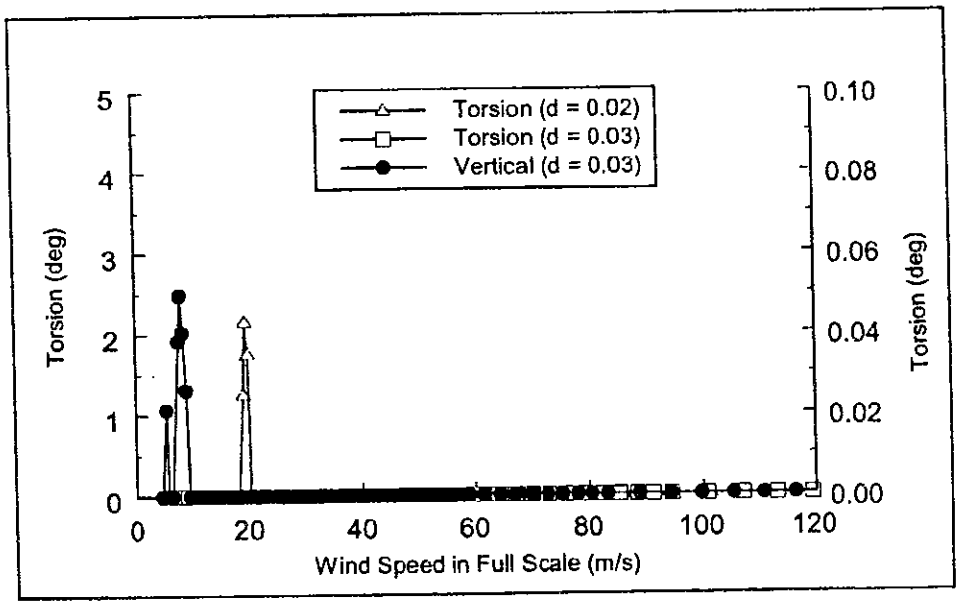

(2) Vertical & Torsion (d = 0.02 & 0.03)

Relationship between Responses and Wind Speed (d = -3 deg)

Figure 4.5 Relationship between vertical & torsional responses and wind speed (angle of attack = - 3 degrees)

4.3 Judgment of Aerodynamic Stability of Deck

The reference wind speed at 10 m, U_{10} is specified as 40 m/s for the Can Tho Bridge. Base on U_{10}, the design wind speed for the deck is calculated as follows [2.1 & 4.1]:

The reference height of the deck is given as the average of shear center height at tower location (36 m) and that at the span center (43 m), that is, 40 m (= [36 + 43] / 2).

Assuming the power law for wind-speed profile and the power of 0.16 (ground roughness category: II), the design wind speed for the deck of the Can Tho Bridge is calculated as

$$U_D = 40 \times \left(\frac{40}{10}\right)^{0.16} = 50 \quad m/s \tag{4.1}$$

The verification wind speed for vortex-induced vibration is defined to be the same as the design wind speed, which is 50 m/s.

The flutter verification wind speed is defined as follows:

$$U_{rf} = 1.2 \times E_{r1} \cdot U_D = 1.2 \times 1.15 \times 50 = 69 \quad m/s \tag{4.2}$$

where E_{r1}: modification factor for wind-speed fluctuations and 1.2: safety factor.

As for vortex-induced vibration, it is primarily required that any vibration would not occur below the verification wind speed. If it occurs, the amplitude of the vibration must be less than an allowable limit. The limit is defined in terms of structural strength, fatigue and discomfort for users.

The wind-resistant design manual for road bridges [4.1] specifies the limit as follows:

[Vertical vortex-induced vibration]

$$h_a = 0.04/f_h = 0.04/0.395 = 0.101 \quad m \tag{4.3}$$

[Torsional vortex-induced vibration]

$$\theta_a = 2.28/(bf_\theta) = 2.28/(9.68 \times 1.23) = 0.19 \quad deg \tag{4.4}$$

where f_h and f_θ : natural frequencies of vertical and torsion, b: distance between deck center and pedestrian lane (= 9.68 m).

Referring to the specified values above, the judgment of the aerodynamic stability of the deck of the Can Tho Bridge is made below and shown in Tables 4.2 and 4.3.

As for flutter, flutter wind speeds measured in all cases are far beyond the verification wind speed. This will lead to the conclusion that the bridge is stable for flutter.

As for vortex-induced vibration, the vibration amplitude even in case of the structural damping

being 0.02 in log decrement is less than the allowable limit. This will conclude that the vortex-induced vibration would not make problem.

Table 4.2 Judgment for Flutter

Angle of attack	Flutter speed measured	Flutter speed modified *)	Flutter verification wind speed
0 degree	311 m/s	354 m/s	69 m/s
+ 3 degree	> 320 m/s	> 365 m/s	
- 3 degree	281 m/s	320.6 m/s	

*) Flutter speed measured was modified by Selberg Formula ($\times 1.14$).

Table 4.3 Judgment for Vortex-Induced Vibration

Angle of attack	Vertical vortex-induced vibration (max. amplitude measured)	(allowance)	Torsional vortex-induced vibration (max. amplitude measured)	(allowance)
0 degree	—	10.1 cm	0.15 deg	0.19 deg
+ 3 degree	—		0.04 deg	
- 3 degree	2.9 cm		0.04 deg	

*) Amplitude measured is based on structural damping of 0.02 in log decrement.

[Selberg Formula]

In this test, the frequency ratio between vertical and torsion, which affects the flutter wind speed, is by 11 % lower than the requirement. Although the flutter wind speeds measured were far greater than the verification, the flutter speeds measured were modified by the Selberg Formula.

$$U_{cf} = 0.44 \times (2\pi f_\theta) \times B \sqrt{\left(1 - \left(\frac{f_h}{f_\theta}\right)^2\right) \frac{\sqrt{\nu}}{\mu}} \qquad (4.5)$$

where $\nu = \dfrac{8I_p}{mB^2}$ and $\mu = \dfrac{\pi\rho B^2}{2m}$.

Based on the values in Table 4.1 and using the Selberg Formula (Eq. (4.5)), the ratio of flutter wind speeds between 3.11 and 2.77 in frequency ratio is calculated as

$$\frac{U_{cf}}{U_{cf}'} = \frac{f_\theta}{f_\theta'}\sqrt{\frac{1-\left(\frac{f_h}{f_\theta}\right)^2}{1-\left(\frac{f_h}{f_\theta}\right)'^2}} = \frac{0.395\times 3.11}{0.395\times 2.77}\sqrt{\frac{1-(1/3.11)^2}{1-(1/2.77)^2}} = 1.14 \qquad (4.6)$$

where (') represent values in the frequency ratio of 2.77.

Eq. (4.6) means that flutter wind speed for the full-scale bridge is estimated by multiplying the measured wind speed with a factor of 1.14.

5 3D ELASTIC MODEL TEST OF TOWER AT ERECTION STAGE

5.1 Description of Test

The aerodynamic stability of the tower at erection stage was investigated by a 3 dimensional elastic model test, as shown in Figures 5.1 and 5.2

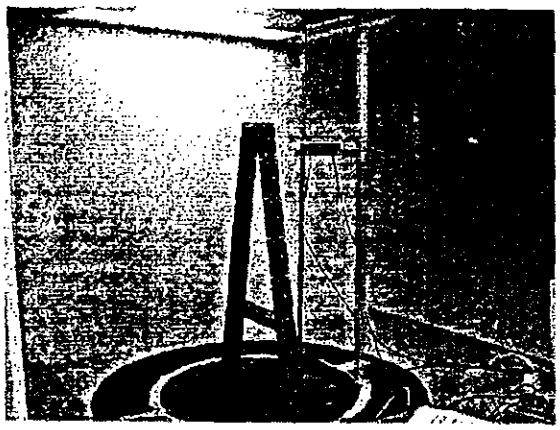

Figure 5.1 3D Elastic Tower Model and Laser Displacement Meters (Wind angle: 90 degrees)

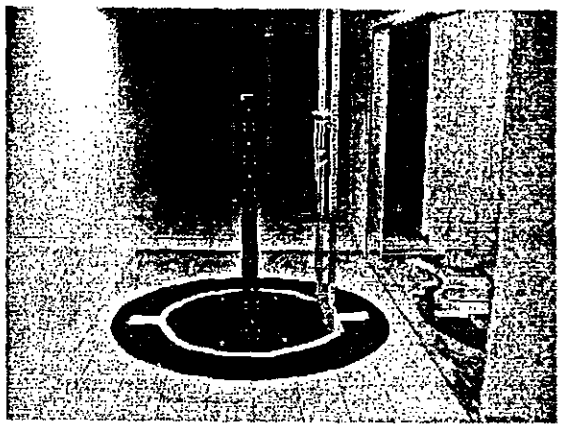

Figure 5.2 3D Elastic Tower Model (Wind angle: 0 degree)

The model consists of steel covers and steel elastic beams inside. The beams represent the stiffness of the full-scale structure based on the similarity requirement. The covers reproduce the physical shape of the full-scale structure. Both of them reproduce the weight distribution.

The tower is inverse Y shape and made by concrete. Since it was feared that an erection-stage tower before two shafts are connected would be most unstable aerodynamically, the wind-tunnel test was carried out with that stage tower model. The scale of the model is 1/95 which is corresponding to 122-m height in the full-scale.

Based on the tower erection plan, the two tower shafts are connected each other at the top during erection period, aerodynamic vibration out of plane of the tower is basically measured with changing wind flow angle (β) (see Figure 5.3) as well as wind speed in the wind tunnel.

Test cases are shown in Table 5.1.

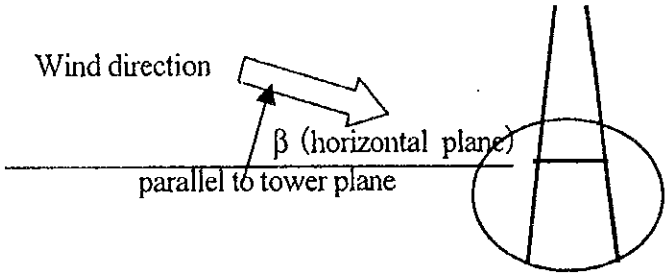

Figure 5.3 Wind Flow Angle: β

Table 5.1 Test Cases of Wind-Tunnel Test of Tower

Wind flow	Flow angle: β (degree)	Connection at tower top	Direction of vibration measured
Smooth flow	0	connected Not connected	Out-of-plane
	10		
	20		
	30		
	45		
	60		
	90		Out-of-plane & In-plane

As for the similarity requirements, the same conditions as those in the case of deck were imposed. That is,

(1) Inertia parameter: $m/(\rho D^2)$

(2) Elastic parameter: $U/(fD)$

(3) Damping parameter: δ_s,

In order to obtain the wind-speed ratio between the test and the full-scale, eigenvalue analysis of the tower at erection stage was executed. Analytical conditions are shown in Table 5.2. The results of natural frequencies and fundamental vibration modes are shown in Table 5.3 and Figure 5.4.

The wind-speed ratio is given by

$$\frac{U_p}{U_m} = 95\frac{f_p}{f_m} \tag{5.1}$$

where U and f are wind speed and frequency, respectively. The subscripts p and m represent the full-scale and test, respectively.

Table 5.2 Analytical Conditions in Eigenvalue Analysis

		Section A	Section B
Unit weight (tf/m)	m	94.89	42.17
Stiffness of cross section (m^4)	I_x	76.75	107.25
	I_y	183.8	91.85
	J	192.99	130.81
Young modulus (tf/m^2)	E	3.30E+06	3.30E+06
Shear modulus (tf/m^2)	G	1.40E+06	1.40E+06
Section area (m^2)	A	37.96	16.87
Height (m) (above basement)		about 122	

Table 5.3 Natural Frequencies of Tower at Erection Stage

mode No.	Frequency (Hz) Real	Model
1	0.4447	0.9426
2	0.5143	0.9690
3	0.5153	1.0040
4	0.5290	1.1100
5	2.3180	4.7690
6	2.6290	5.0450
7	2.7770	5.7540
8	3.4460	6.1580
9	4.8820	9.3000
10	5.3140	11.2000
11	6.3470	13.4400
12	8.6560	16.3500
13	9.1550	18.9200
14	9.4910	20.6400
15	10.3000	21.1200
16	10.7000	24.5500
17	11.7900	29.9400
18	11.9500	34.0900
19	15.6000	34.6000
20	19.4800	41.9000

Note: frequencies (real) and (model) represent natural frequencies analyzed with the full-scale dimensions and model dimensions, respectively.

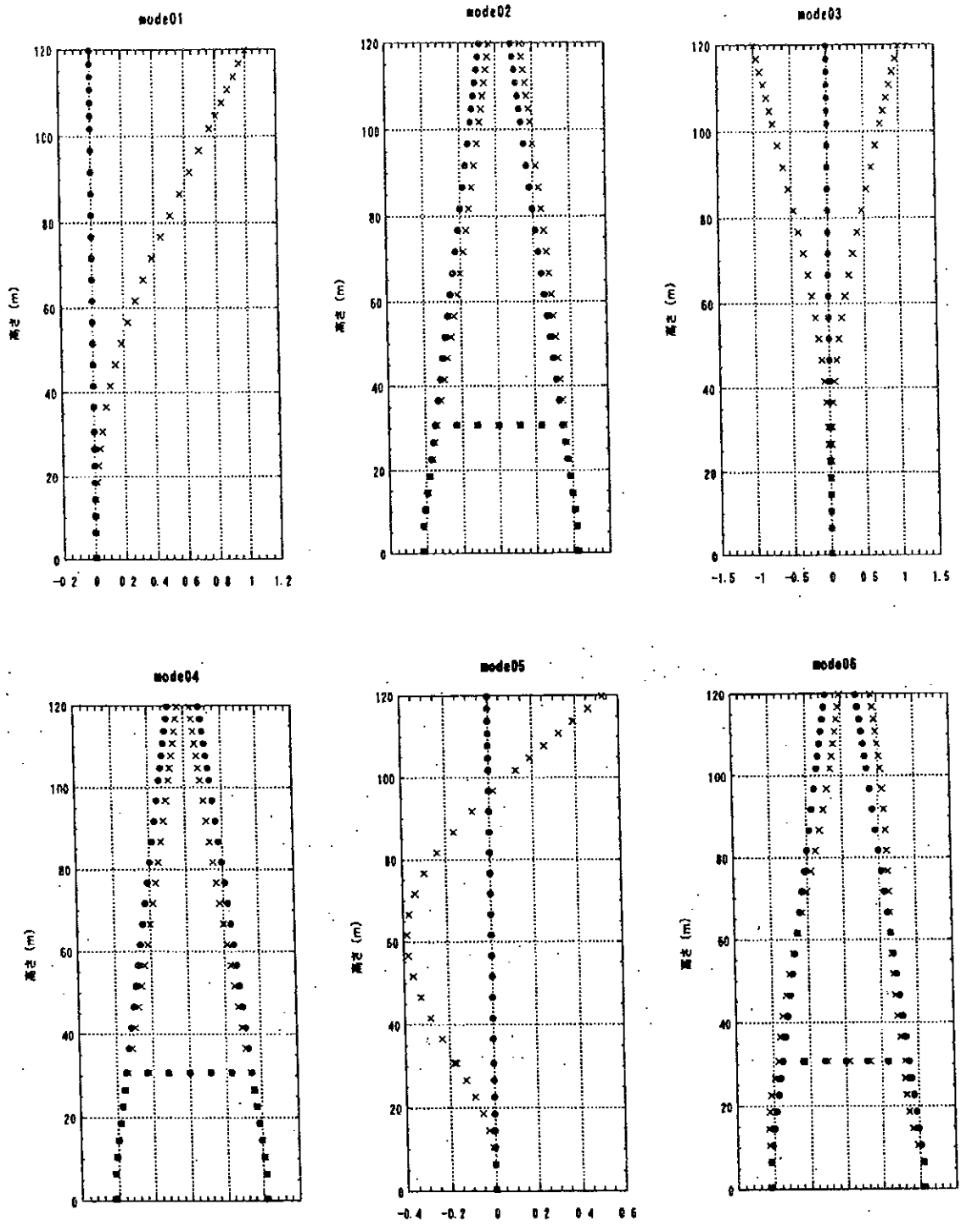

Figure 5.4 Fundamental Vibration Modes of Tower at Erection Stage

5.2 Test Results

Natural frequencies and structural damping measured in test cases are shown in Table 5.4. These frequencies are used calculating the wind-speed ratio.

Table 5.4 Natural frequencies and structural damping

Flow angle (deg.)	Mode 1		Mode 3		Mode 4	
	Natural frequency (Hz)	Structural damping	Natural frequency (Hz)	Structural damping	Natural frequency (Hz)	Structural damping
Connected at tower top						
0	—	—	—	—	—	—
10	—	—				
20	7.54	0.017				
30	7.58	0.012				
45	7.57	0.018				
60	7.54	0.021				
90	7.56	0.024				
Ave.	7.56	0.018	—	—	—	—
Not connected at tower top						
0	7.53	0.012	10.38	0.005	—	—
10	—	—	—	—		
20	7.59	0.017	10.44	0.004		
30	7.55	0.016	10.40	0.005		
45	7.56	0.017	10.31	0.004		
60	7.53	0.015	10.40	0.006		
90	7.57	0.016	10.36	0.004	10.05	0.002
Ave.	7.56	0.016	10.38	0.005	10.05	0.002

Note: Modes 1, 3 and 4 correspond to the mode shapes shown in figure 5.4. Mode 1 is 1st out-of-plane bending, mode 2 1st torsion and mode 4 1st in-plane bending.

Structural damping measured range from 0.012 to 0.024 in log decrement for mode 1, from 0.004 to 0.006 for mode 2 and 0.002 for mode 4. Honshu-Shikoku Bridge Authority specifies structural damping for tower at erection stage as 0.01 in log decrement [2.1]. The values measured are slightly higher than the specification. However, considering many temporary structures such as scaffold are attached on the tower at erection stage and relatively low tower height, it is judged that the damping measured are in allowable range.

Aerodynamic responses of the tower top versus wind flow angle and wind speed are shown in Figures 5.5 (1) – 5.5 (8).

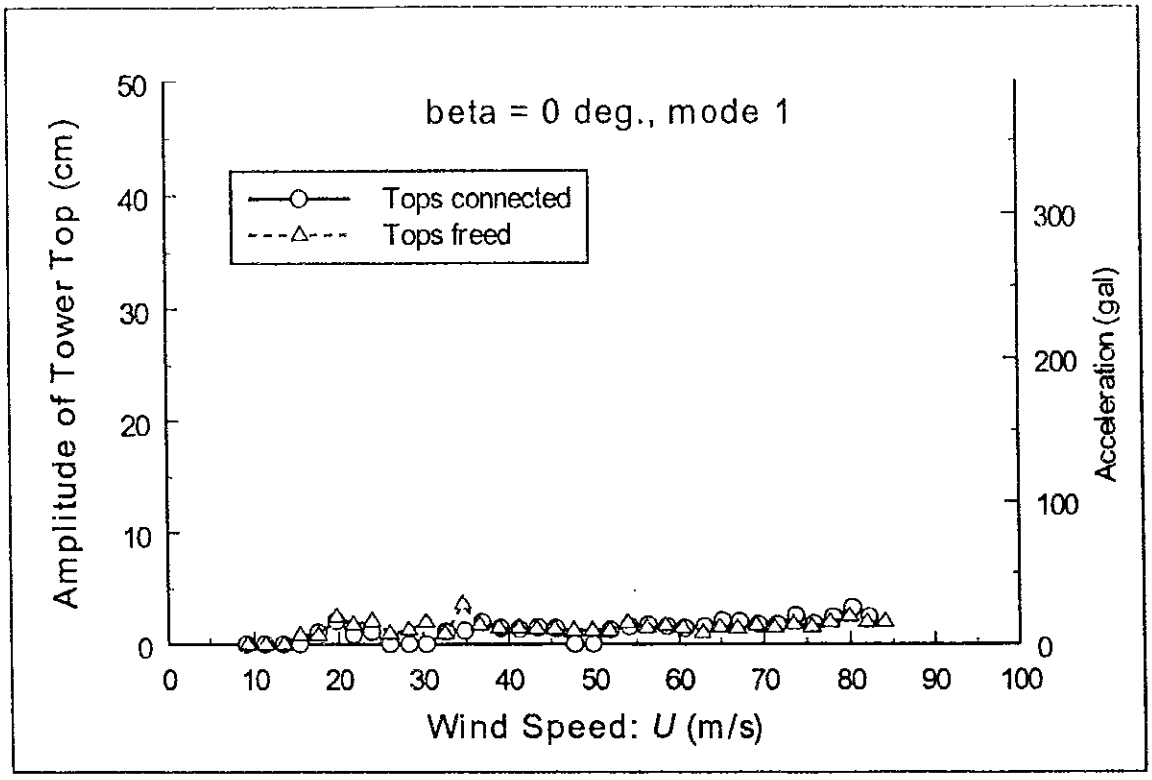

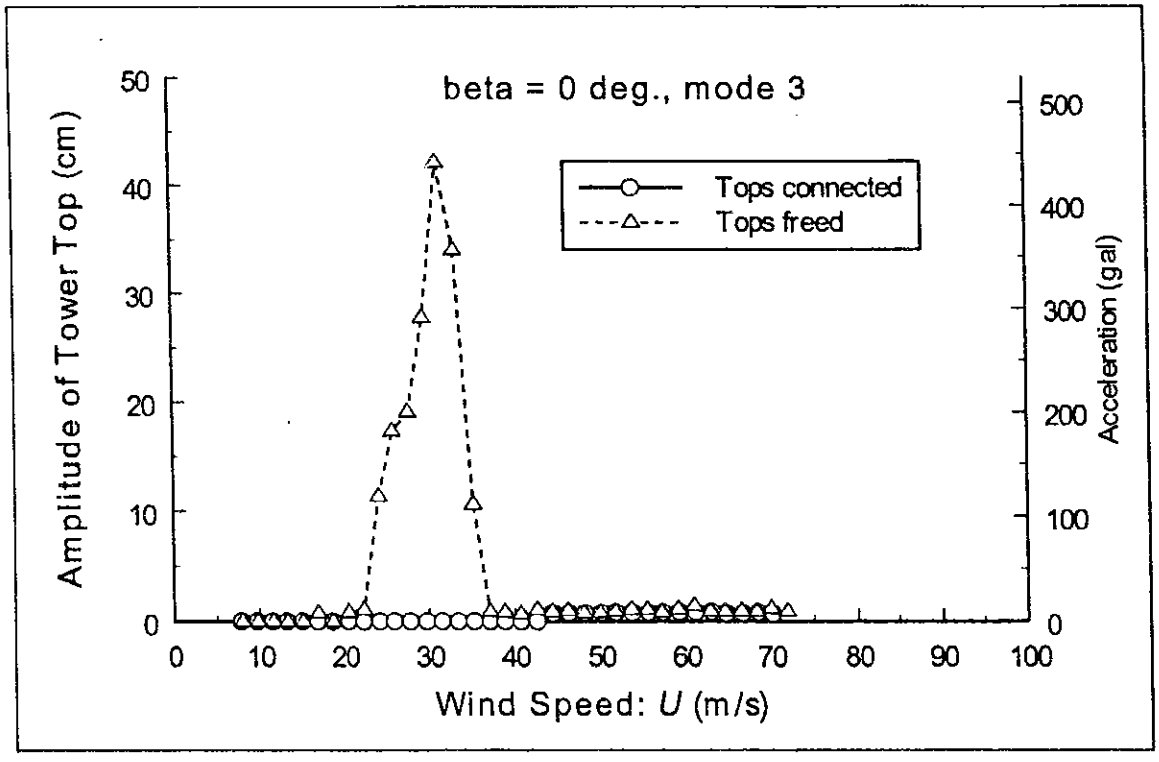

Figure 5.5 (1) Diagram of Tower Top Response versus Wind Speed ($\beta = 0$ deg.)

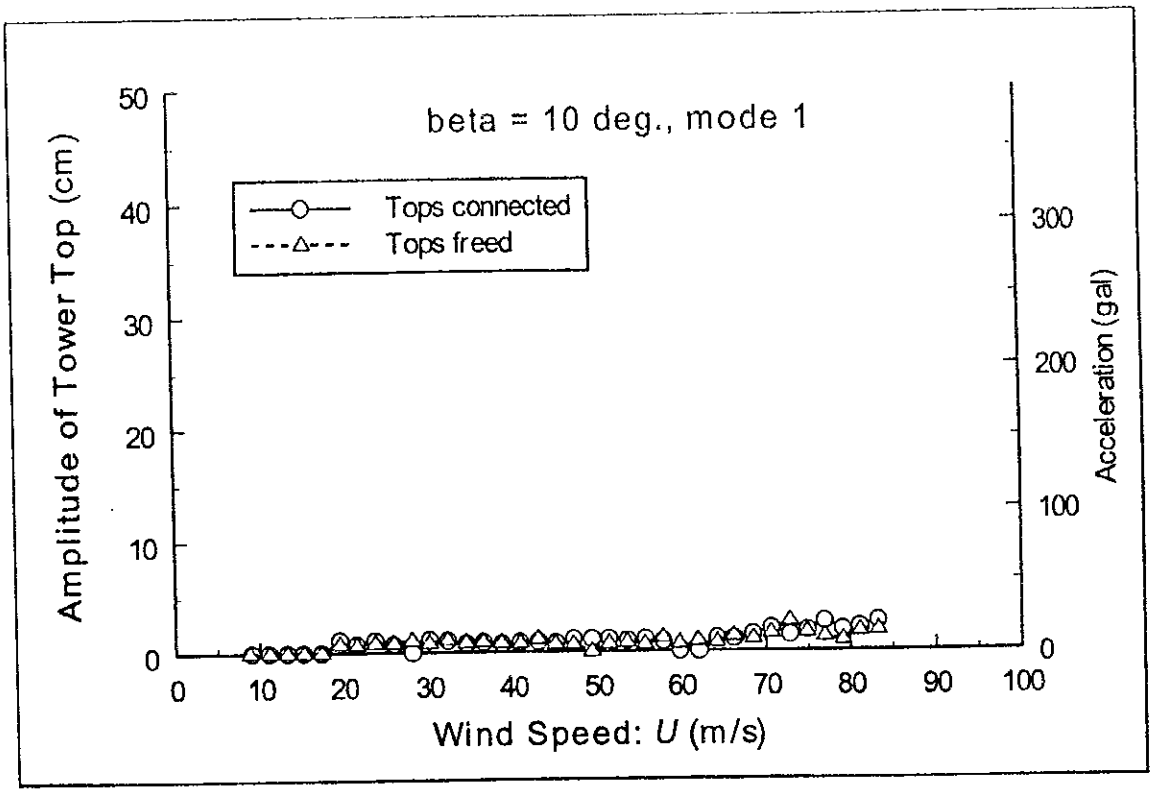

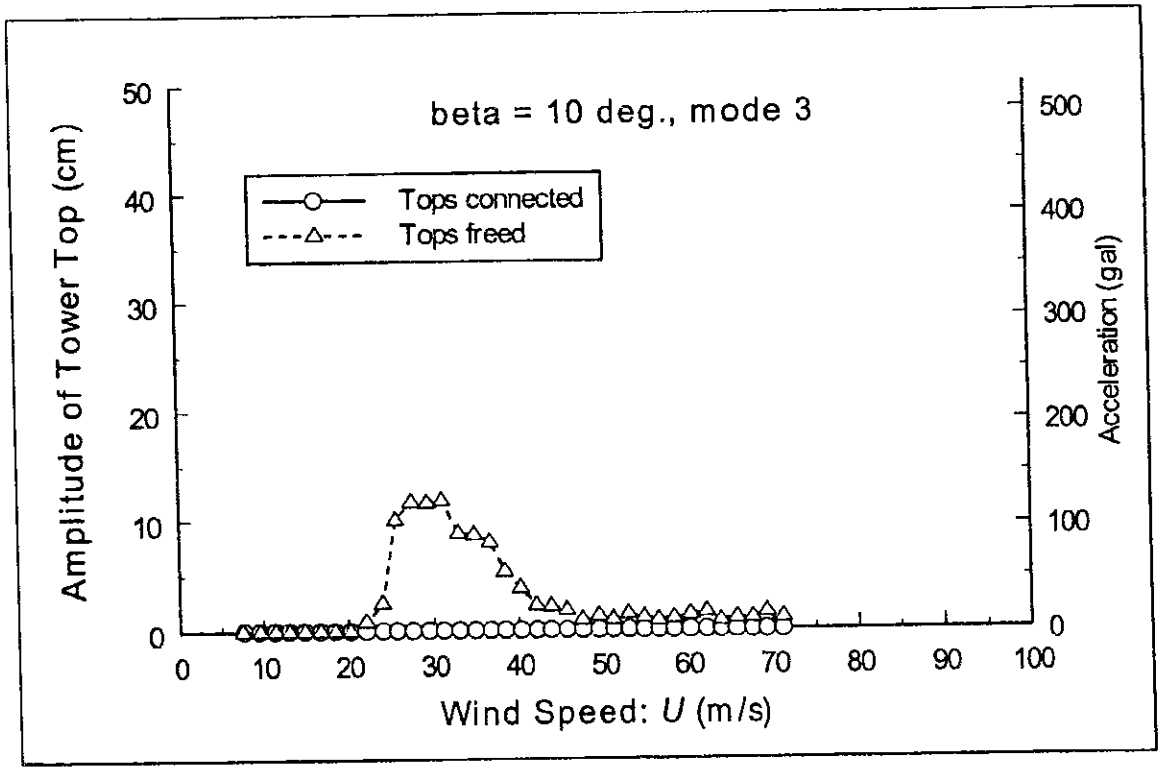

Figure 5.5 (2) Diagram of Tower Top Response versus Wind Speed (β = 10 deg.)

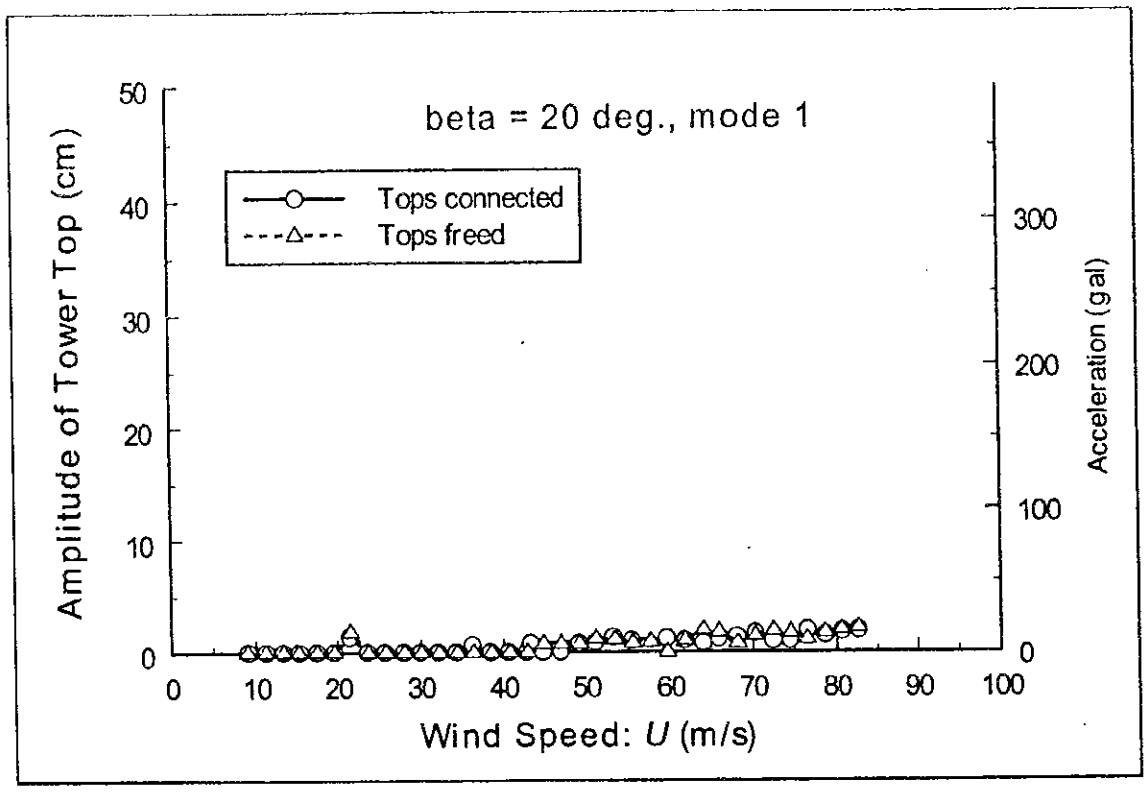

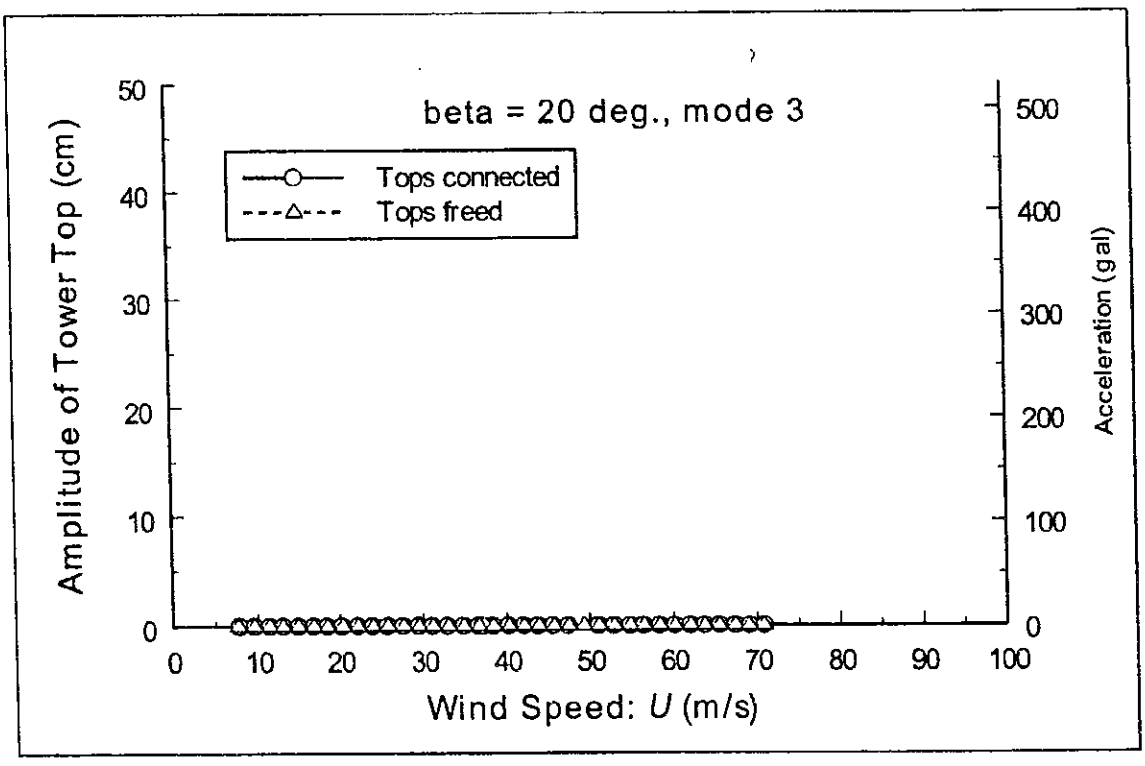

Figure 5.5 (3) Diagram of Tower Top Response versus Wind Speed ($\beta = 20$ deg.)

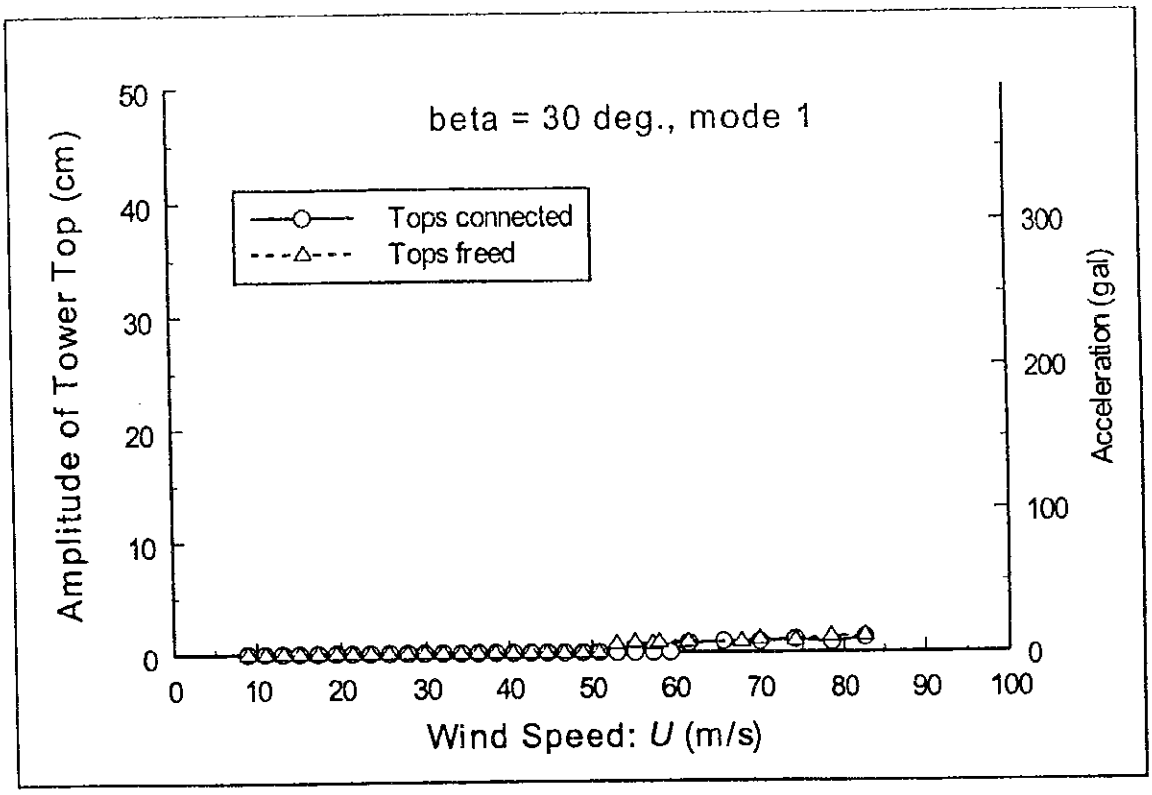

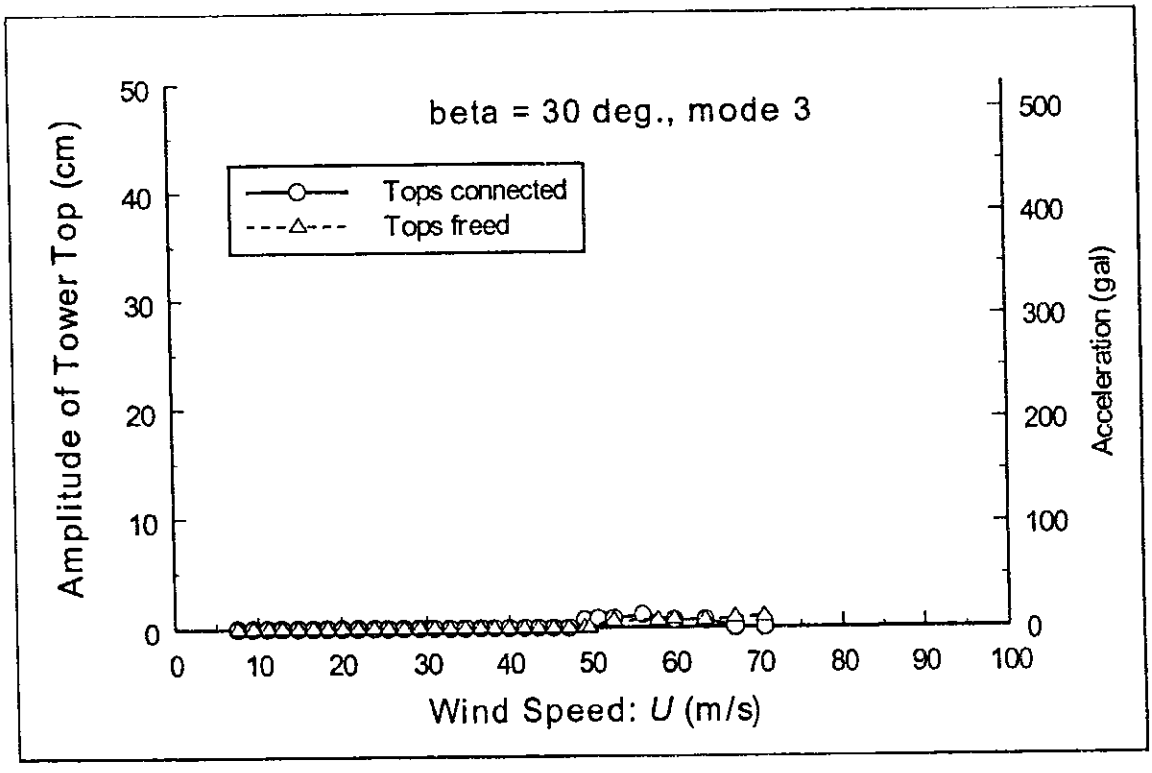

Figure 5.5 (4) Diagram of Tower Top Response versus Wind Speed (β = 30 deg.)

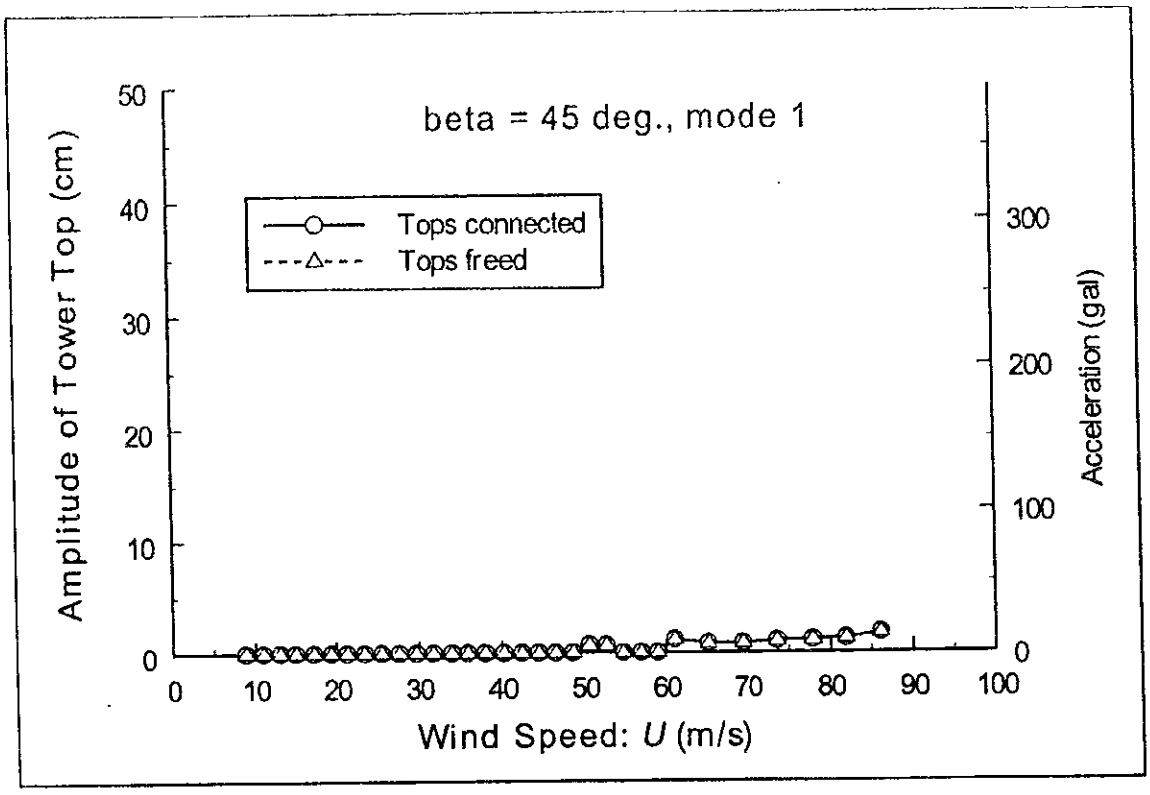

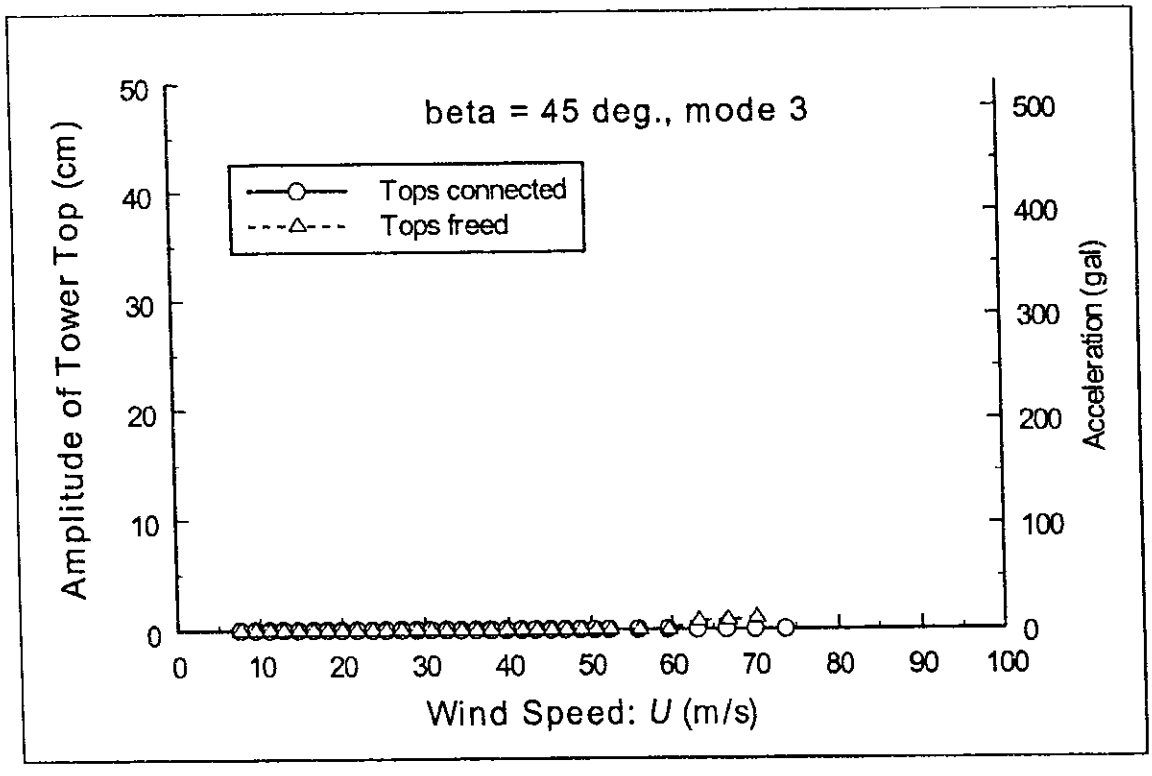

Figure 5.5 (5) Diagram of Tower Top Response versus Wind Speed (β = 45 deg.)

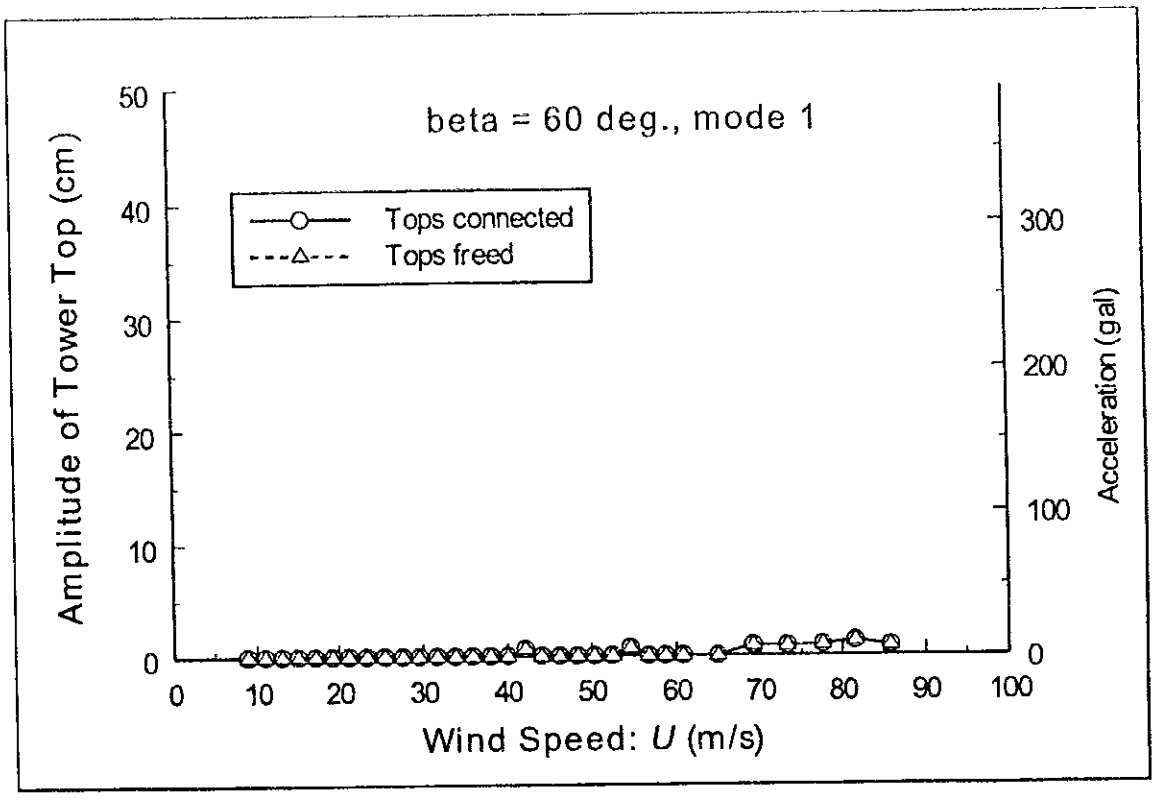

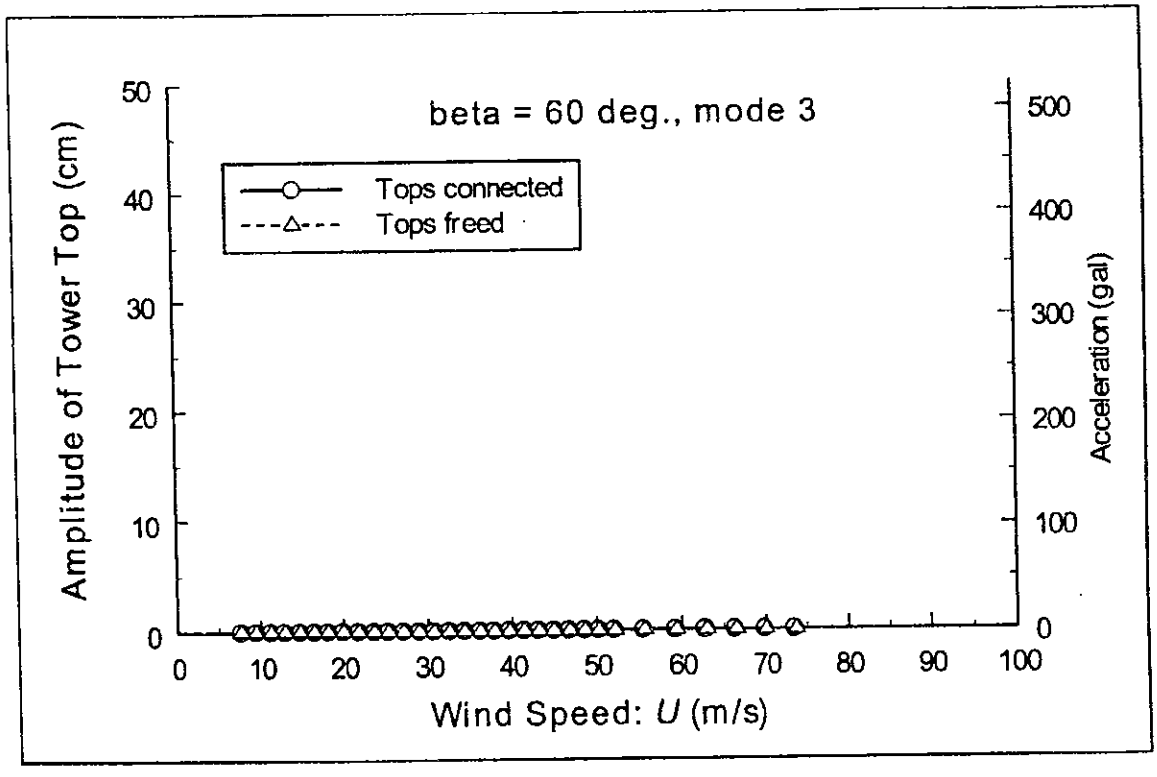

Figure 5.5 (6) Diagram of Tower Top Response versus Wind Speed (β = 60 deg.)

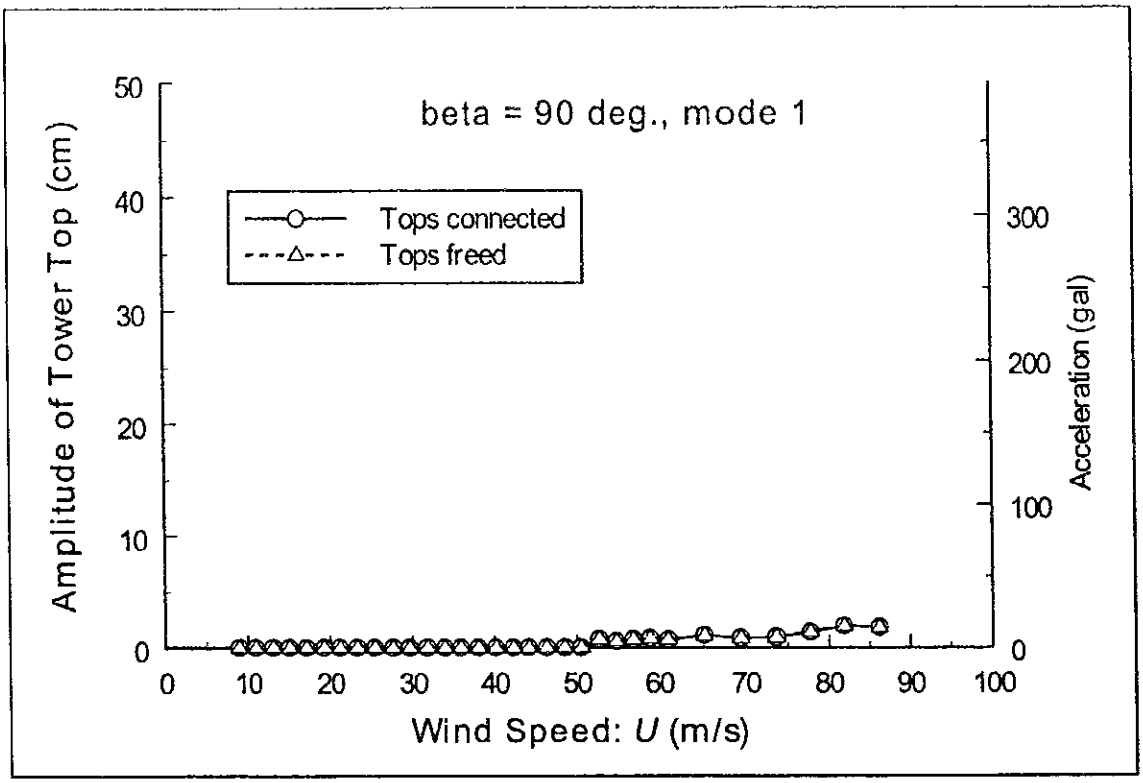

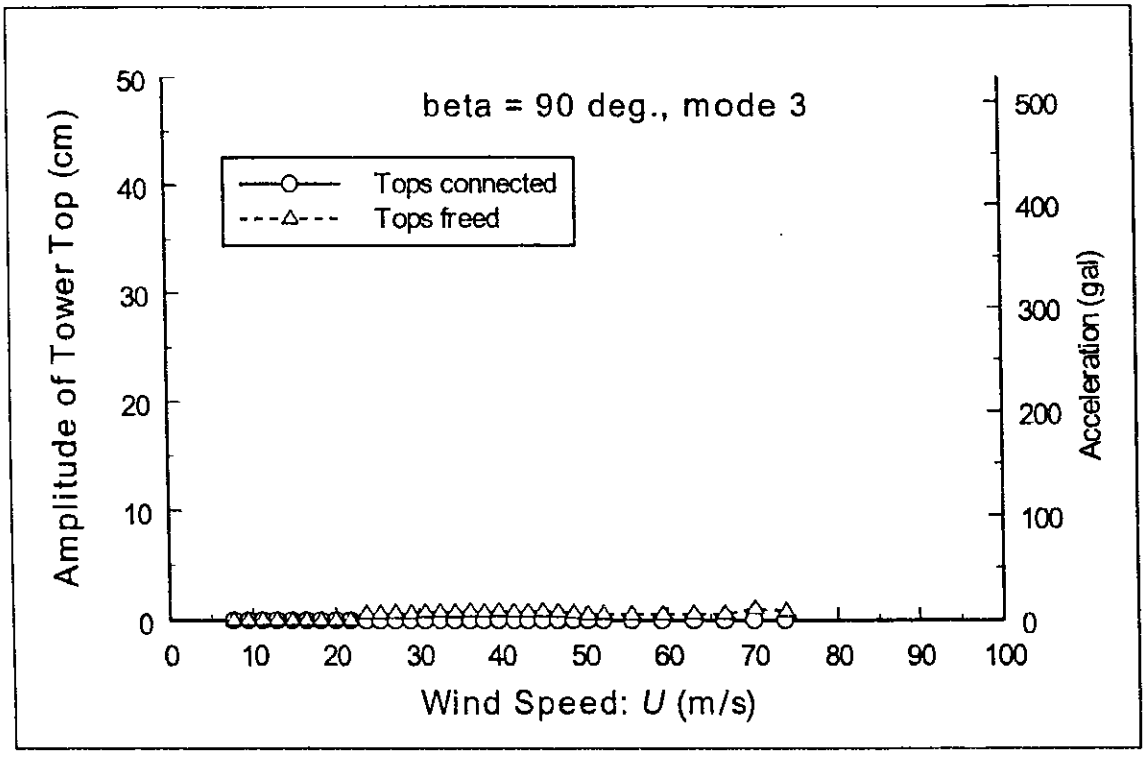

Figure 5.5 (7) Diagram of Tower Top Response versus Wind Speed ($\beta = 90$ deg.)

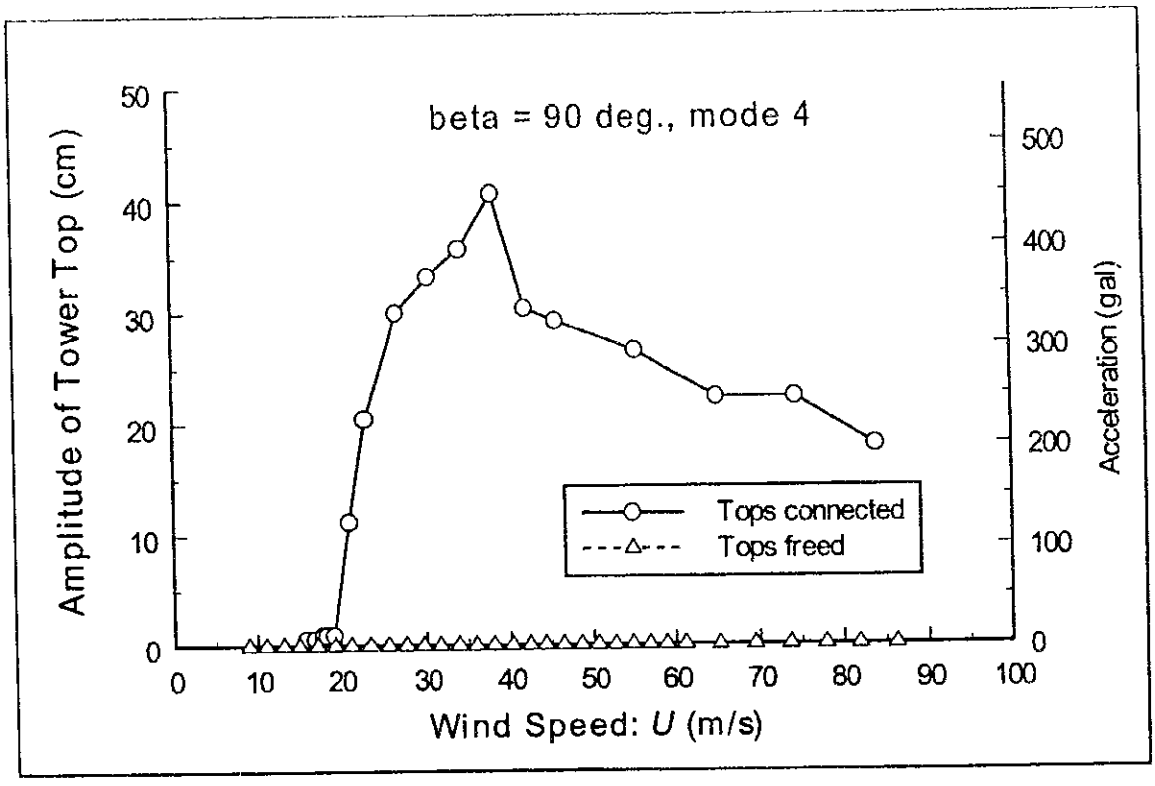

Figure 5.5 (8) Diagram of Tower Top Response versus Wind Speed
($\beta = 90$ deg., in-plane vibration)

5.3 Judgment of Aerodynamic Stability of Tower at Erection Stage

The reference wind speed at 10 m, U_{10} is specified as 40 m/s for the Can Tho Bridge. Base on U_{10}, the design wind speed for the tower at erection stage is calculated as follows [2.1 & 4.1]:

The reference height of the tower is given as the 65 % height of the tower, which is 79 m (= 122 × 0.65). Assuming the power law for wind-speed profile and the power of 0.16 (ground roughness category: II), the design wind speed for the tower at erection stage of the Can Tho Bridge is calculated as

$$U_D = 40 \times \left(\frac{79}{10}\right)^{0.16} = 56 \text{ m/s} \tag{5.2}$$

The verification wind speed for divergent vibration is defined as follows:

$$U_{rf} = 1.2 \times U_D = 1.2 \times 56 = 67 \text{ m/s} \tag{5.3}$$

It is quite natural that design wind speed and verification at an erection period be reduced, because the erection period is short. There are two methods to decide the design wind speeds at erection stage.

One is that an equivalent wind speed giving the wind load half of completed-stage value is defined as an erection-stage value. That is, 0.71 × design wind sped at a completed stage is one at an erection stage. The other one is that a wind speed giving the exceeding probability same as one at a completed stage is defined as an erection-stage value.

Using the second method with an erection period of 2 – 3 years, the factor of an erection stage is calculated as around 0.6, which is smaller than 0.71 from the first method. In this research, in order to give large safety margin, the first method (0.71) is used.

After all, the design wind speed of the tower at erection stage is

$$U_{DE} = 0.71 \times U_D = 0.71 \times 56 = 40 \text{ m/s} \tag{5.4}$$

and the verification wind speed for divergent vibration is

$$U_{rfE} = 0.71 \times U_{rf} = 0.71 \times 67 = 48 \text{ m/s} \tag{5.5}$$

Referring to the specified values above, the judgment of the aerodynamic stability of the tower at erection stage of the Can Tho Bridge is made below.

In the cases of the wind-flow angle being other than 0, 10 and 90 degrees, no harmful vibration was observed.

In the cases of wind-flow angle of 0 and 10 degrees, torsional vibration was observed without the connection at the tower top and its amplitude was 42 cm and 12 cm at a wind speed of 30 m/s,

respectively. Corresponding acceleration reaches 440 gal at 0 degree and 120 gal at 10 degrees. Those vibrations occurred below the design wind speed and its acceleration is not small. However, with connecting the tower top, those vibrations were completely suppressed. Connecting at the tower top will be an effective countermeasure to suppress vibration.

In the case of wind-flow angle of 90 degrees, out-of-plane bending and torsional vibration did not occur with/without the connection at the tower top. However, in-plane bending vibration with amplitude of 41 cm occurred at a wind speed of 39 m/s if not connected at the tower top. Connecting the tower top completely suppressed the vibration.

From the results above, it will be concluded that without the connection at the tower top, large-amplitude vibrations of torsion at 0 & 10 degrees and of in-plane at 90 degrees would occur, however with the connection at the tower top, no vibration would occur. It will also be concluded that there would not occur harmful problem with connecting the tower top during construction.

6 BUFFETING ANALYSIS FOR DECK AT ERECTION STAGE

6.1 Theory of Analysis [2,3, 6.1 & 6.2]

Buffeting analysis used in this study is based on modal analysis in the frequency region. An equation of motion with multi degree-of-freedoms in a matrix form is expressed as

$$\mathbf{M}\ddot{\mathbf{X}} + \mathbf{C}\dot{\mathbf{X}} + \mathbf{K}\mathbf{X} = \mathbf{F} \tag{6.1}$$

where **M**, **C** and **K** are a mass, damping and stiffness matrix, respectively, **X** is a displacement vector, **F** is a forcing vector and (•) represents the differentiation with respect to time.

Dividing **X** and **F** into the time-dependent component and time-independent one, Eq. (6.1) is rewritten as

$$\mathbf{M}\ddot{\mathbf{X}} + \mathbf{C}\dot{\mathbf{X}} + \mathbf{K}(\mathbf{X}_0 + \mathbf{X}) = \mathbf{F}_0 + \mathbf{F}_{ae} + \mathbf{F}_b \tag{6.2}$$

where $\mathbf{X}_0$ and $\mathbf{F}_0$ are time-independent stationary component, **X** time-dependent dynamic displacement, and $\mathbf{F}_{ae}$ and $\mathbf{F}_b$ are aerodynamic forces. $\mathbf{F}_{ae}$ is the unsteady aerodynamic force (flutter derivative) which is motion dependent. $\mathbf{F}_b$ is the buffeting force which is basically dependent on wind-speed fluctuations.

Introducing the modal analysis in which **X** can be expressed by the time-independent mode function Φ and the time-dependent generalized coordinate ξ

$$\mathbf{X} = \Phi \cdot \xi \tag{6.3}$$

and substituting Eq. (6.3) into Eq. (6.2) and premultiplying by Φ^T (transpose matrix of Φ) yield

$$\Phi^T\mathbf{M}\Phi\ddot{\xi} + \Phi^T\mathbf{C}\Phi\dot{\xi} + \Phi^T\mathbf{K}\Phi\xi + \Phi^T\mathbf{K}\Phi\xi_0 = \Phi^T\mathbf{F}_0 + \Phi^T\mathbf{F}_{ae} + \Phi^T\mathbf{F}_b \tag{6.4}$$

In general, assuming the orthogonality of modes makes $\Phi^T\mathbf{M}\Phi$, $\Phi^T\mathbf{C}\Phi$ and $\Phi^T\mathbf{K}\Phi$ a diagonal matrix and Eq. (6.4) is decomposed into multi 1-DOF equation of motion. $\Phi^T\mathbf{M}\Phi$, $\Phi^T\mathbf{C}\Phi$ and $\Phi^T\mathbf{K}\Phi$ are called generalized mass, generalized damping and generalized stiffeness, respectively.

Taking out the stationary components from Eq. (6.4) gives

$$\Phi^T\mathbf{K}\Phi\xi_0 = \Phi^T\mathbf{F}_0 \tag{6.5}$$

Dividing Eq. (6.5) by the generalized inertia I_i (subscript represents ith mode) and decomposing into uncoupled equations give

$$\omega_i^2 \xi_{0,i} = \frac{\left(\Phi^T \mathbf{F}_0\right)_i}{I_i} \tag{6.6}$$

Eq. (6.6) gives the stationary response of ith generalized coordinate and substituting into Eq. (6.3) yields the stationary response of the physical displacement **X**.

As for dynamic response, the deflection components of the bridge deck are represented in terms of the generalized coordinate of the mode $\xi_i(t)$, the deck width B and the dimensionless modal values of the i^{th} mode along the deck $h_i(x)$, $p_i(x)$ and $\alpha_i(x)$ as

$$\text{vertical: } h(x,t) = \sum_i h_i(x) B \xi_i(t) \tag{6.7a}$$

$$\text{lateral: } p(x,t) = \sum_i p_i(x) B \xi_i(t) \tag{6.7b}$$

$$\text{torsion: } \alpha(x,t) = \sum_i \alpha_i(x) \xi_i(t) \tag{6.7c}$$

where x is the coordinate along the deck span and t is time .

For purely sinusoidal motions of frequency ω, the aeroelastic forces can be expressed as

$$L_{ae} = \frac{1}{2}\rho U^2 B\left[KH_1^* \frac{\dot{h}}{U} + KH_2^* \frac{B\dot{\alpha}}{U} + K^2 H_3^* \alpha + K^2 H_4^* \frac{h}{B} + KH_5^* \frac{\dot{p}}{U} + K^2 H_6^* \frac{p}{B} \right] \tag{6.8a}$$

$$D_{ae} = \frac{1}{2}\rho U^2 B\left[KP_1^* \frac{\dot{p}}{U} + KP_2^* \frac{B\dot{\alpha}}{U} + K^2 P_3^* \alpha + K^2 P_4^* \frac{p}{B} + KP_5^* \frac{\dot{h}}{U} + K^2 P_6^* \frac{h}{B} \right] \tag{6.8b}$$

$$M_{ae} = \frac{1}{2}\rho U^2 B\left[KA_1^* \frac{\dot{h}}{U} + KA_2^* \frac{B\dot{\alpha}}{U} + K^2 A_3^* \alpha + K^2 A_4^* \frac{h}{B} + KA_5^* \frac{\dot{p}}{U} + K^2 A_6^* \frac{p}{B} \right] \tag{6.8c}$$

where ρ is the air density, U is the mean wind speed, $K(= B\omega/U)$ is the reduced frequency and H_i^*, P_i^* and A_i^*, i = 1-6 are the flutter derivatives of the deck cross section.

Under assumed slowly varying gust action, the buffeting forces are defined as

$$L_b = \frac{1}{2}\rho U^2 B\left[C_L \chi_L^u (2\frac{u}{U}) + (C_L' + C_D)\chi_L^w \frac{w}{U} \right] \tag{6.9a}$$

$$D_b = \frac{1}{2}\rho U^2 B\left[C_D \chi_D^u (2\frac{u}{U}) + C_D' \chi_D^w \frac{w}{U} \right] \tag{6.9b}$$

$$M_b = \frac{1}{2}\rho U^2 B^2\left[C_M \chi_M^u (2\frac{u}{U}) + C_M' \chi_M^w \frac{w}{U} \right] \tag{6.9c}$$

where C_L, C_D and C_M are the static lift, drag and pitching moment coefficients (referred to deck width B) of a typical deck section, respectively, $C_L' = dC_L/d\alpha$, $C_D' = dC_D/d\alpha$ and $C_M' = dC_M/d\alpha$, and $u = u(t)$, $w = w(t)$ are the along-wind and vertical velocity fluctuations of the wind, respectively. χ is the aerodynamic admittance where super/sub scripts represent

wind-speed-fluctuation component and force component, respectively.

Fourier transformed multi degree-of-freedom equation of motion is expressed in the reduced frequency (K) region as

$$\mathbf{E}\bar{\xi} = \bar{\mathbf{Q}}_b \tag{6.10}$$

where

$$\mathbf{E}_{ij} = -K^2\delta_{ij} + iK\mathbf{A}_{ij}(K) + \mathbf{B}_{ij}(K) \tag{6.11}$$

and $i = \sqrt{-1}$. Subscript i and j in Eq. (6.11) represent ith and jth mode, respectively. $\mathbf{E}$ and $\bar{\mathbf{Q}}_b$ are the impedance matrix and buffeting force vector, respectively.

In order to incorporate the variable section effect, the flutter derivatives should be changed along the span. In this case, $\mathbf{A}$ and $\mathbf{B}$ in Eq. (6.11) are given as

$$\mathbf{A}_{ij}(K) = 2\zeta_i K_i \delta_{ij} - \frac{\rho B^4 l K}{2I_i}[G^{H_1^*}_{h_i h_j} + G^{H_2^*}_{h_i \alpha_j} + G^{H_5^*}_{h_i p_j} + G^{P_1^*}_{p_i p_j}$$

$$+ G^{P_2^*}_{p_i \alpha_j} + G^{P_5^*}_{p_i h_j} + G^{A_1^*}_{\alpha_i h_j} + G^{A_2^*}_{\alpha_i \alpha_j} + G^{A_5^*}_{\alpha_i p_j}] \tag{6.12}$$

$$\mathbf{B}_{ij}(K) = K_i^2\delta_{ij} - \frac{\rho B^4 l K^2}{2I_i}[G^{H_3^*}_{h_i \alpha_j} + G^{H_4^*}_{h_i h_j} + G^{H_6^*}_{h_i p_j} + G^{P_3^*}_{p_i \alpha_j}$$

$$+ G^{P_4^*}_{p_i p_j} + G^{P_6^*}_{p_i h_j} + G^{A_3^*}_{\alpha_i \alpha_j} + G^{A_4^*}_{\alpha_i h_j} + G^{A_6^*}_{\alpha_i p_j}] \tag{6.13}$$

where δ_{ij} is the Kronecker delta function, I_i the generalized inertia and G_*^* represent

$$G^{H_1^*}_{h_i h_j} = \int_0^l H_1^*(x) h_i(x) h_j(x) \frac{dx}{l} \tag{6.14a}$$

$$G^{H_2^*}_{h_i \alpha_i} = \int_0^l H_2^*(x) h_i(x) \alpha_j(x) \frac{dx}{l} \tag{6.14b}$$

$$\vdots$$

$$\vdots$$

The diagonal terms ($i = j$) in Eqs. (6.12) and (6.13) represent the single-degree-of-freedom (and uncoupled) equations. The off-diagonal terms introduce the aeroelastic coupling through the flutter derivatives and the mechanical coupling through the cross-modal integrals among different modes.

The power spectral density matrix for the generalized coordinate ξ is developed from Eq. (6.10)

$$\mathbf{S}_{\xi\xi}(K) = \mathbf{E}^{-1}\mathbf{S}_{Q_b Q_b}[\mathbf{E}^*]^{-1} \tag{6.15}$$

where $\mathbf{E}^*$ is the complex conjugate transpose of matrix $\mathbf{E}$ and $\mathbf{S}_{Q_b Q_b}$ is the PSD of buffeting

force.

Defining the buffeting force vector as

$$\overline{\mathbf{Q}}_{b_i}(K)=\frac{1}{I_i}\left(\frac{B}{U}\right)^2\int_0^l[\mathbf{L}_b(K)h_iB+\mathbf{D}_b(K)p_iB+\mathbf{M}_b(K)\alpha_i]dx \tag{6.16}$$

PSD of buffeting force can be expressed as

$$\begin{aligned}S_{Q_{b_i}Q_{b_j}}(K)=&\left(\rho B^4 l/2U\right)^2\\&\times\frac{1}{I_iI_j}\int_0^l\int_0^l\{\tilde{q}_i(x_A)\tilde{q}_j(x_B)S_{uu}(x_A,x_B,K)\\&+\tilde{r}_i(x_A)\tilde{r}_j(x_B)S_{ww}(x_A,x_B,K)+[\tilde{q}_i(x_A)\tilde{r}_j(x_B)\\&+\tilde{r}_i(x_A)\tilde{q}_j(x_B)]C_{uw}(x_A,x_B,K)+i[\tilde{q}_i(x_A)\tilde{r}_j(x_B)\\&-\tilde{r}_i(x_A)\tilde{q}_j(x_B)]Q_{uw}(x_A,x_B,K)\}\frac{dx_A}{l}\frac{dx_B}{l}\end{aligned} \tag{6.17}$$

where

$$\tilde{q}_i(x)=2[C_L\chi_L^u h_i(x)+C_D\chi_D^u p_i(x)+C_M\chi_M^u\alpha_i(x)] \tag{6.18}$$

$$\tilde{r}_j(x)=(C_L'+C_D)\chi_L^w h_j(x)+C_D'\chi_D^w p_j(x)+C_M'\chi_M^w\alpha_j(x) \tag{6.19}$$

and S_{uu} and S_{ww} are PSD of along- and cross-wind-speed fluctuations, respectively, C_{uw} and Q_{uw} are co-spectrum and quadrature-spectrum density of uw cross spectrum, respectively. In this study, C_{uw} and Q_{uw} are excluded because of small effects.

Expressing the spanwise cross-spectral densities of the wind components in conventional form with the decay factor of $c = 8$ as

$$S_{uu}(x_A,x_B,K)=S_{uu}(K)R_{uu}(x_A,x_B,K)=S_{uu}(K)\exp\left\{-c\frac{f|x_A-x_B|}{U}\right\} \tag{6.20}$$

$$S_{ww}(x_A,x_B,K)=S_{ww}(K)R_{ww}(x_A,x_B,K)=S_{ww}(K)\exp\left\{-c\frac{f|x_A-x_B|}{U}\right\} \tag{6.21}$$

Using

$$H_{r_is_j}(K)=\int_0^l\int_0^l r_i(x_A)s_j(x_B)\exp\left(-\frac{cK}{2\pi B}|x_A-x_B|\right)\frac{dx_A}{l}\frac{dx_B}{l} \tag{6.22}$$

where r_i and $s_i = h_i$, p_i or α_i, the ij^{th} term of the buffeting force matrix can be expressed as

$$\begin{aligned}S_{Q_{b_i}Q_{b_j}}(K)=&\left(\frac{\rho B^4 l}{2U}\right)^2\frac{1}{I_iI_j}[Y_{ij}^{Suu}(K)S_{uu}(K)+Y_{ij}^{Sww}(K)S_{ww}(K)\\&+Y_{ij}^{Cuw}(K)C_{uw}(K)+Y_{ij}^{Quw}(K)Q_{uw}(K)]\end{aligned} \tag{6.23}$$

where

$$Y_{ij}^{S_{uu}}(K) = (2C_L|\chi_L|)^2 H_{h_i h_j}^{S_{uu}} + (2C_D|\chi_D|)^2 H_{p_i p_j}^{S_{uu}} + (2C_M|\chi_M|)^2 H_{\alpha_i \alpha_j}^{S_{uu}} + 4C_L C_D(\chi_L \chi_D^* H_{h_i p_j}^{S_{uu}} + \chi_D \chi_L^* H_{p_i h_j}^{S_{uu}}) + 4C_L C_M(\chi_L \chi_M^* H_{h_i \alpha_j}^{S_{uu}} + \chi_M \chi_L^* H_{\alpha_i h_j}^{S_{uu}}) + 4C_D C_M(\chi_D \chi_M^* H_{p_i \alpha_j}^{S_{uu}} + \chi_M \chi_D^* H_{\alpha_i p_j}^{S_{uu}}) \quad (6.24)$$

$$Y_{ij}^{S_{ww}}(K) = ((C_L' + C_D)|\chi_L|)^2 H_{h_i h_j}^{S_{ww}} + (C_D'|\chi_D|)^2 H_{p_i p_j}^{S_{ww}} + (C_M'|\chi_D|)^2 H_{\alpha_i \alpha_j}^{S_{ww}} + (C_L' + C_D)C_D'(\chi_L \chi_D^* H_{h_i p_j}^{S_{ww}} + \chi_D \chi_L^* H_{p_i h_j}^{S_{ww}}) + (C_L' + C_D)C_M'(\chi_L \chi_M^* H_{h_i \alpha_j}^{S_{ww}} + \chi_M \chi_L^* H_{\alpha_i h_j}^{S_{ww}}) + C_D' C_M'(\chi_D \chi_M^* H_{p_i \alpha_j}^{S_{ww}} + \chi_M \chi_D^* H_{\alpha_i p_j}^{S_{ww}}) \quad (6.25)$$

where * represents complex conjugate.

Aerodynamic admittance functions for drag and lift & moment used are Davenport function and Sears function, respectively.

$$\text{Drag:} \quad |\chi_D(K)|^2 = \left\{ \frac{2}{(cK')^2}[cK' - 1 + \exp(-cK')] \right\} \quad (6.26)$$

$$\text{Lift \& Moment:} \quad |\chi_L(K)|^2 = |\chi_M(K)|^2 = \frac{a + \overline{f}}{a + (\pi a + 1)\overline{f} + 2\pi \overline{f}^2} \quad (6.27)$$

where $K' = DK/2\pi B$, D deck height, a = 0.1811 and $\overline{f} = \pi f B / U$.

PSD functions for S_{uu} and S_{ww} are Hino spectrum and Bush&Panafsky spectrum, respectively.

$$S_{uu}(K) = 0.4751 \frac{u^2}{\beta} \{1 + (f/\beta)^2\}^{-5/6}, \quad \beta = 1.169 \times 10^{-2} \frac{\alpha U_{10}}{\sqrt{K} Z_{10}} \left(\frac{z}{Z_{10}} \right)^{2\alpha - 1} \quad (6.28, 6.29)$$

$$S_{ww}(K) = 0.632 w^2 \frac{z / f_{\max}}{U \left[1 + 1.5 \left(\frac{fZ}{U f_{\max}} \right)^{5/3} \right]} \quad (6.30)$$

where $\alpha (= 0.16)$ is the power, K_r (= 0.005) is the surface friction coefficient and U_{10} = 40 m/s.

Finally, the covariance matrix of the physical displacement is given as

$$\sigma_h^2(x_1, x_2) = \int_0^{\infty} \sum_i \sum_j B^2 h_i(x_1) h_j(x_2) S_{\xi_i \xi_j}(f) df \quad (6.31a)$$

$$\sigma_p^2(x_1,x_2)=\int_0^\infty \sum_i \sum_j B^2 p_i(x_1)p_j(x_2)S_{\xi_i\xi_j}(f)df \qquad (6.31b)$$

$$\sigma_\alpha^2(x_1,x_2)=\int_0^\infty \sum_i \sum_j \alpha_i(x_1)\alpha_j(x_2)S_{\xi_i\xi_j}(f)df \qquad (6.31c)$$

where f is frequency.

Neglecting any coupling terms among modes results in a single-mode buffeting calculation. Based on the formulations developed above, the PSD of the physical displacements at a specific point x, for the single-mode buffeting can be obtained by the same procedures as those in the multi-mode buffeting. For the purpose of evaluating the response in the multi-mode sense from single-mode responses, the square-root of the sum of square (SRSS) of single-mode responses method is used, i.e.:

$$SRSS(x)=\sqrt{\sigma_{q_1}^2(x)+\sigma_{q_2}^2(x)+\cdots\cdots+\sigma_{q_n}^2(x)} \qquad (6.32)$$

where n is the number of modes.

In the design stage, the maximum response is important rather than variance. The maximum response is estimated applying the narrow-band random process as well as the mean response as

$$R_{max}=R_{mean}+\left(\sqrt{2\ln \nu T}+0.5772/\sqrt{2\ln \nu T}\right)\sigma \qquad (6.33)$$

where $\nu=\dfrac{\sqrt{\int_0^\infty f^2 S_z(f)df}}{\sqrt{\int_0^\infty S_z(f)df}}$ and T = 600 sec

6.2 Analytical Conditions

The structural system analyzed in this study is an erection stage of the Can Tho Bridge. The deck erection is panned to extend a deck piece from the tower to the end and finally connect at the span center. Therefore, it is judged that the state just before closing at the center would be the most unstable and yield the largest stress as well as deflection. Buffeting analysis was executed for the state as shown in Figure 6.1.

Eigenvalue analysis was first conducted using a 3D finite element model of the erection stage. Analytical conditions (dimensions) are basically the same as those in the complete stage except unit weight of the deck. The unit weight is by 5 tf/m smaller than that in the complete stage because of no pavement. The results of natural frequencies, generalized inertia and equivalent

masses are shown in Table 6.1, and fundamental vibration mode shapes are shown in Figure 6.2.

Static force coefficients and flutter derivatives were measured with the section model of the deck which was used in the section-model wind-tunnel test. The coefficients are shown in Figures 6.3 and 6.3.

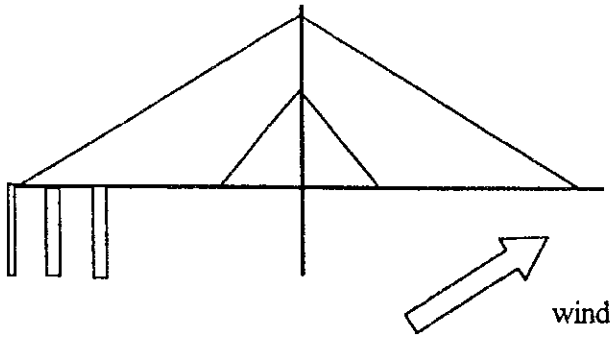

Figure 6.1 Deck Erection Stage of Interest at Buffeting Analysis

Table 6.1 Natural Frequencies, Generalized Masses and Equivalent Masses

No.	Frequency (Hz)	Generalized mass (tf·sec2/m)	Equivalent mass (tf·sec^2/m/m)		
			Lateral	Vertical	Torsion
1	0.2173	1.92E+02	2.15E+00	3.11E+14	2.88E+05
2	0.3690	7.58E+01	5.50E+13	1.80E+00	3.08E+13
3	0.4880	2.44E+02	2.77E+13	3.42E+00	2.49E+12
4	0.7574	2.56E+02	1.64E+12	2.92E+00	6.61E+12
5	0.7636	5.56E+02	1.46E+04	3.04E+08	4.20E+04
6	0.9753	7.48E+02	9.71E+09	7.64E+00	1.40E+10
7	1.0350	1.48E+02	2.63E+00	6.66E+09	3.15E+03
8	1.2110	4.44E+02	2.67E+09	9.95E+00	4.43E+09
9	1.2590	2.17E+02	3.12E+03	7.62E+05	6.24E+03
10	1.2850	2.99E+02	1.26E+08	3.15E+00	1.35E+08
11	1.3660	6.18E+02	6.10E+07	5.38E+00	6.19E+07
12	1.3980	1.57E+02	1.35E+02	1.26E+07	1.32E+02
13	1.5180	5.34E+02	7.49E+08	5.75E+00	6.26E+08
14	1.7120	4.86E+02	7.09E+08	4.42E+00	3.47E+08
15	1.8680	1.16E+02	8.35E+02	1.18E+03	1.89E+02
16	1.9580	7.84E+02	1.65E+10	5.07E+00	3.30E+09
17	2.0230	6.38E+01	3.20E+02	1.13E+08	9.91E+01
18	2.1340	9.28E+02	3.80E+09	4.92E+00	2.95E+09
19	2.2490	1.26E+03	4.53E+09	9.36E+00	6.97E+09
20	2.3750	6.61E+02	1.94E+11	4.92E+00	7.06E+11
21	2.4470	3.95E+02	1.66E+10	1.96E+02	7.70E+10
22	2.6170	3.01E+02	3.23E+00	5.88E+10	3.07E+03
23	2.8390	5.56E+02	6.89E+10	3.60E+00	6.35E+10
24	2.8610	3.52E+02	2.34E+08	7.12E+01	3.19E+08
25	2.8890	1.05E+02	3.71E+02	7.01E+07	2.56E+02
26	2.9180	1.48E+02	6.93E+01	1.02E+10	1.67E+02
27	3.0440	2.67E+02	8.96E+03	2.66E+08	5.17E+03
28	3.0730	2.23E+02	5.24E+12	2.40E+00	1.51E+12
29	3.1690	8.11E+02	7.28E+10	4.11E+00	5.02E+10
30	3.8100	2.32E+02	4.51E+02	2.53E+09	1.68E+02

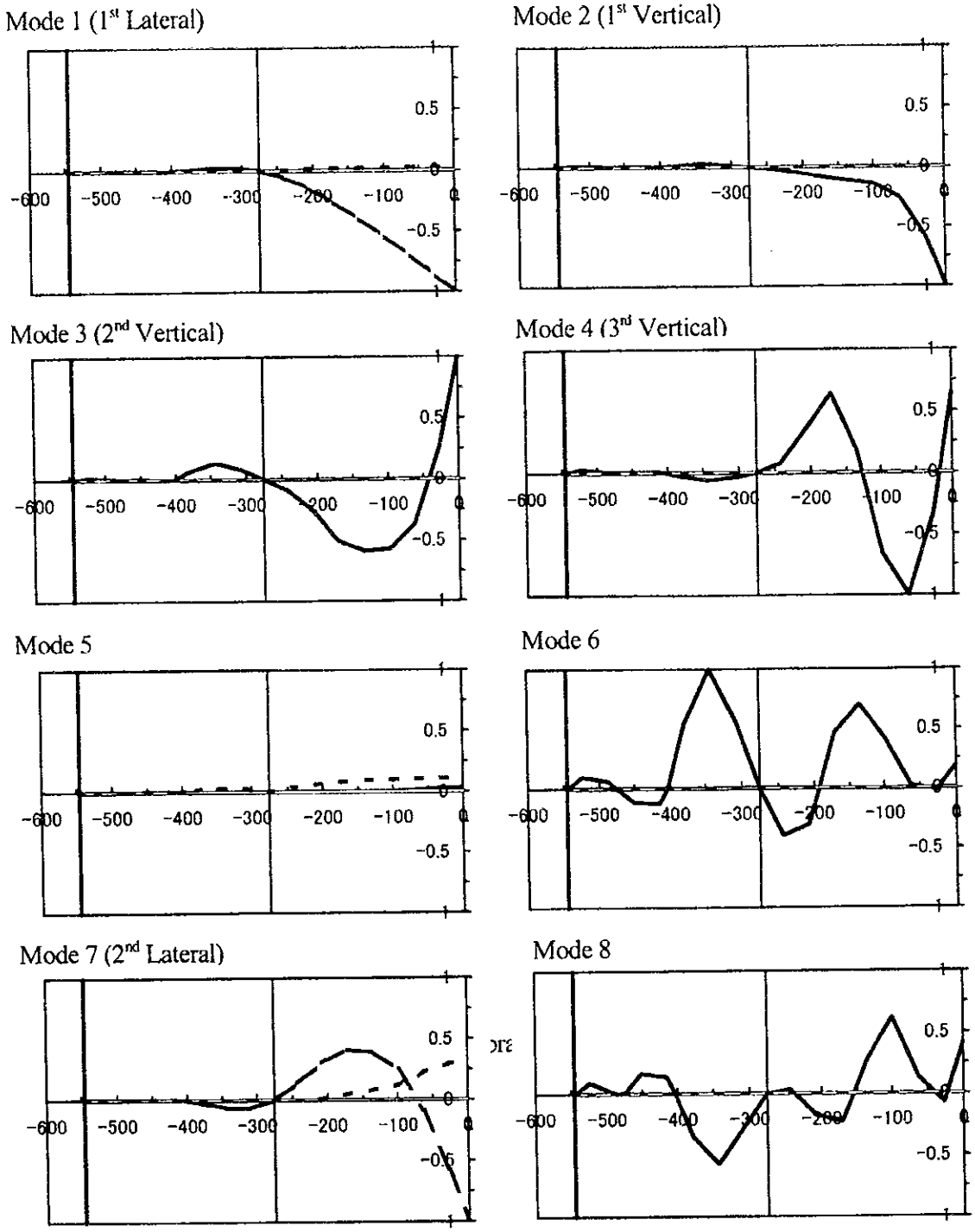

Figure 6.2 (1) Vibration Mode Shapes (1)

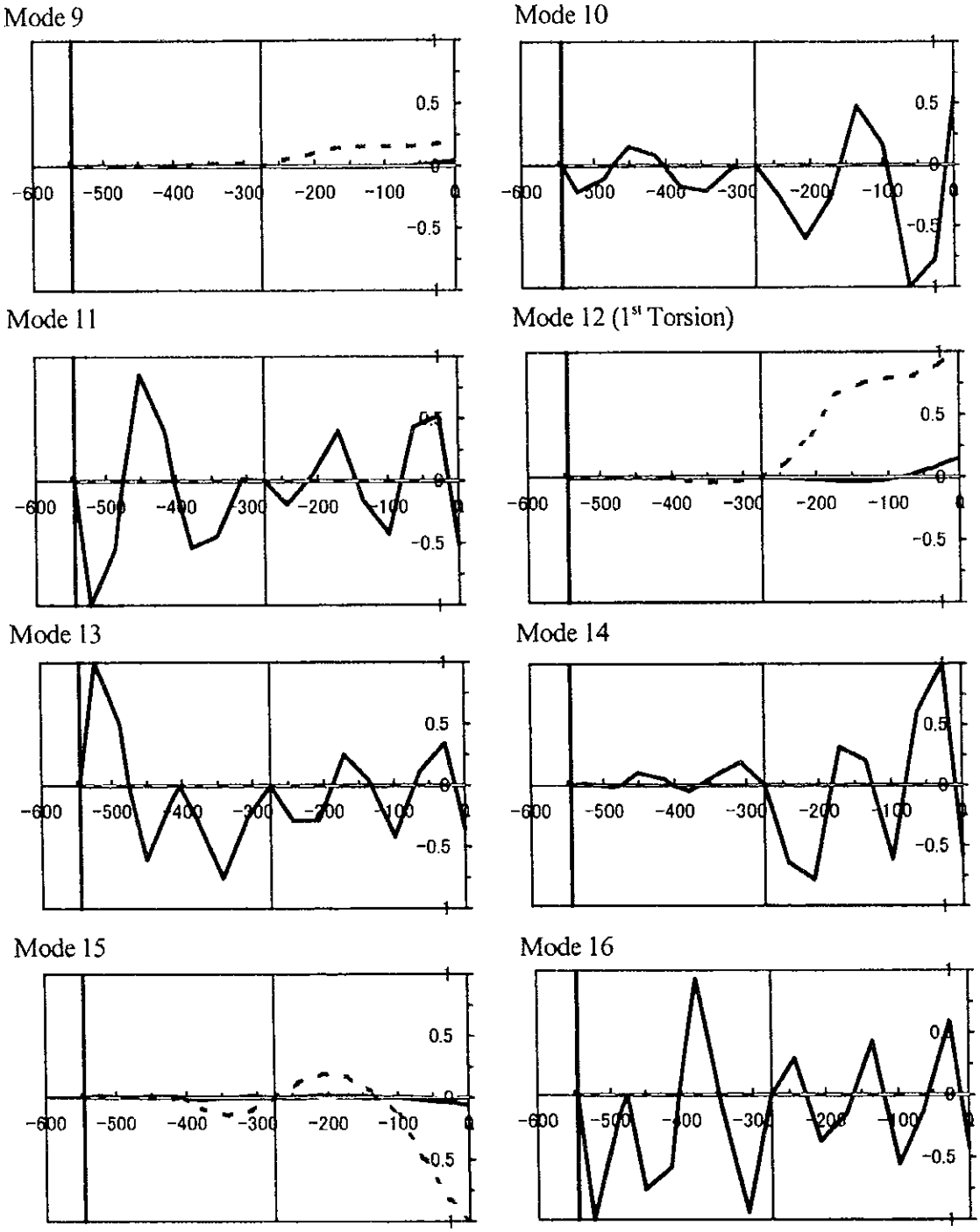

Figure 6.2 (2) Vibration Mode Shapes (2)

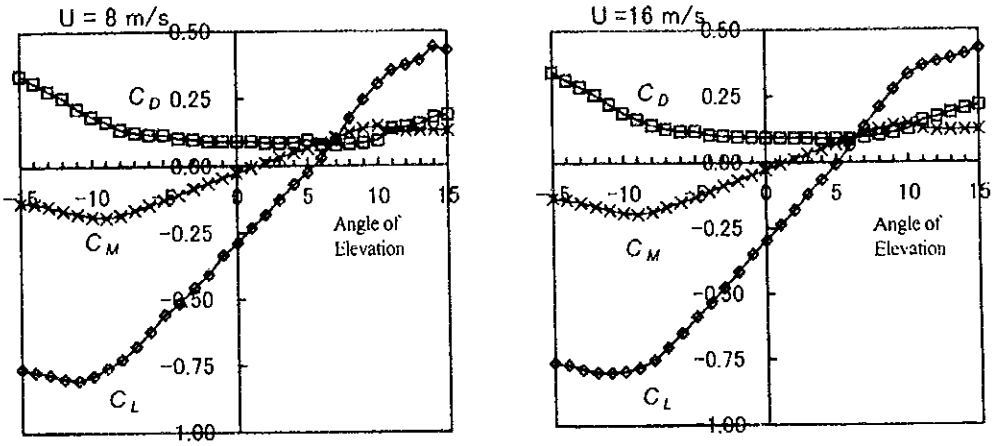

Figure 6.3 Static Force Coefficients

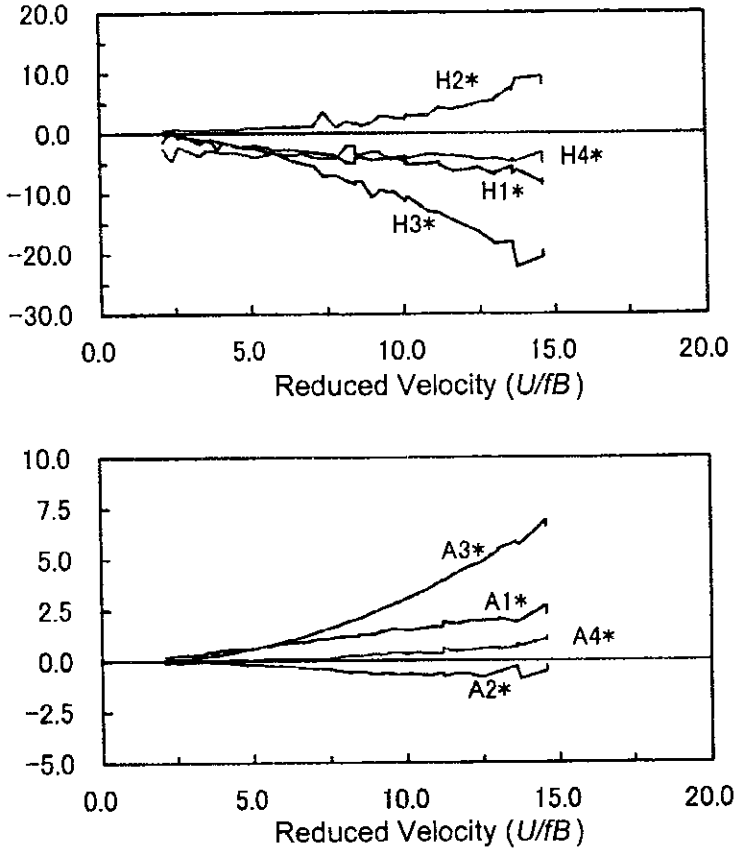

Figure 6.4 Flutter Derivatives

Eight components of flutter derivatives as shown in Figure 6.4 and P_1^* estimated by quasi-steady theory were used in this study. Other components were excluded because of small effects. Other analytical conditions are shown in Table 6.2.

Table 6.2 Analytical Conditions in Buffeting Analysis

	Dimensions
Power in wind profile	0.16
Surface friction coefficient	0.005
Turbulence intensities I_u	0.15
I_w	0.075
PSD of wind speed fluctuations	Along wind: Hino
	Cross wind: Bush & Panofsky
Spatial correlation function	exponential (decay factor 8)
Aerodynamic admittance	Along wind: Davenport
	Cross wind: Sears
Structural damping	0.02 in log decrement
Flutter derivatives	Measurement
Static force coefficient	$C_D = 0.1639$, $C_D' = -0.0388$ $C_L = -0.2884$, $C_L' = 2.883$ $C_M = -0.02669$, $C_M' = 1.059$
Deck height	3.889 m
Deck width	26.0 m
Projection area of cable ($\times$ 1/2)	2.65 m^2/m
Number of modes	17

6.3 Results of Analysis

As described in the previous chapter, the design wind speed at an erection period was decided to be $0.71 \times U_Z$ (design wind speed at a completion stage). Therefore, the design wind speed at an erection period is 35 m/s ($= 0.71 \times 50$). Buffeting analysis was executed at different wind speeds which were 10, 20, 30, 35, 40 and 50 m/s at the deck elevation.

Buffeting responses (static, rms, maximum and total response) analyzed are shown in Figures 6.5 along the bridge axis. In addition, buffeting responses with a function of wind speed and power spectral density at the deck end are shown in Figures 6.6 and 6.7.

$U_Z = 10$ m/s

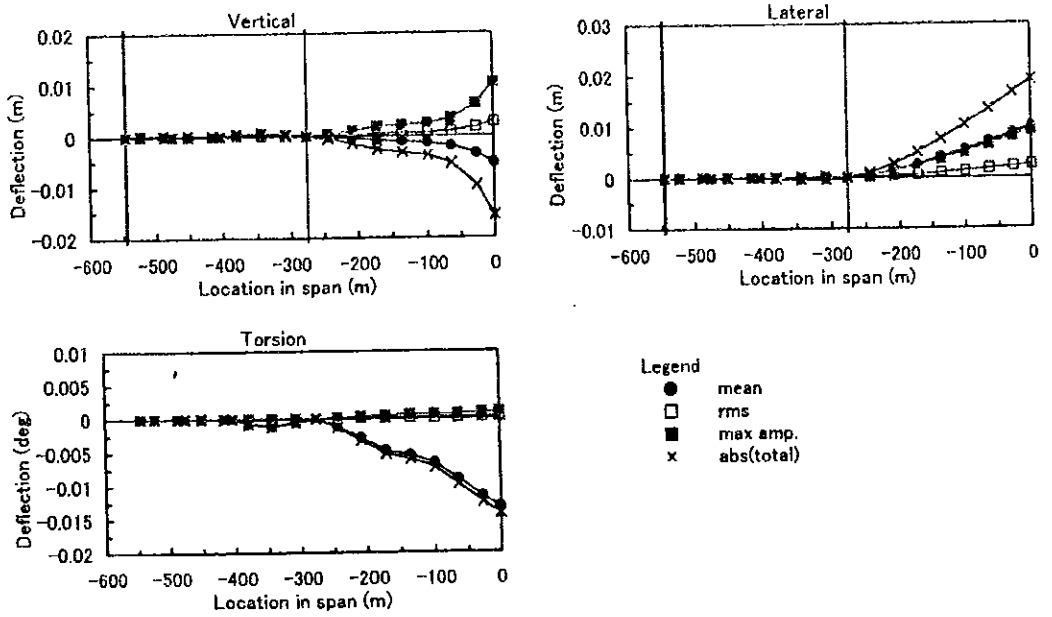

Figure 6.5 (1) Buffeting Responses along Bridge Axis ($U_Z = 10$ m/s)

$U_Z = 20$ m/s

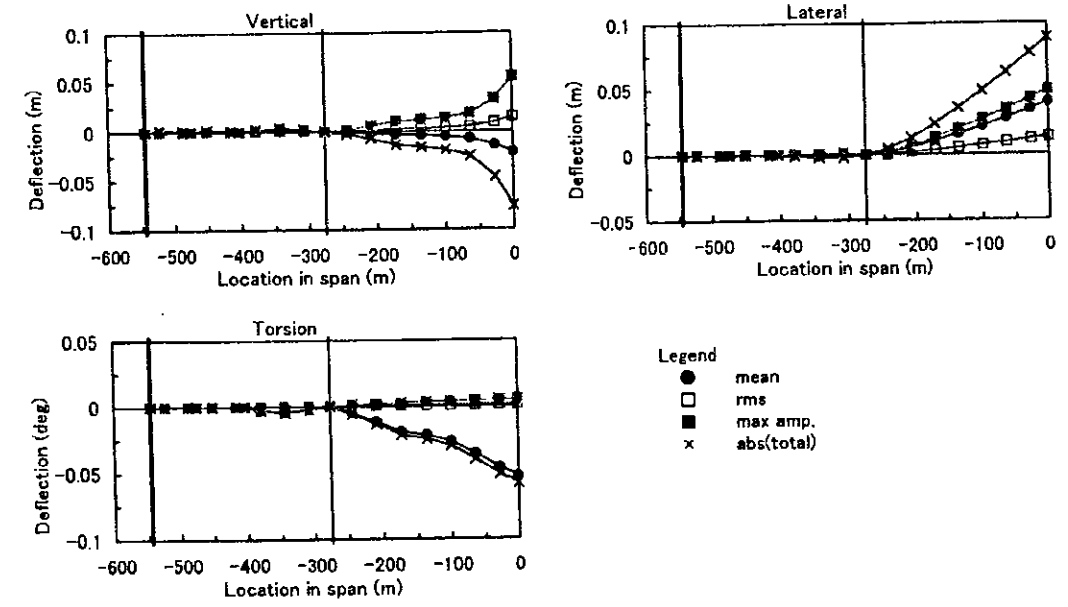

Figure 6.5 (2) Buffeting Responses along Bridge Axis ($U_Z = 20$ m/s)

$U_Z = 30$ m/s

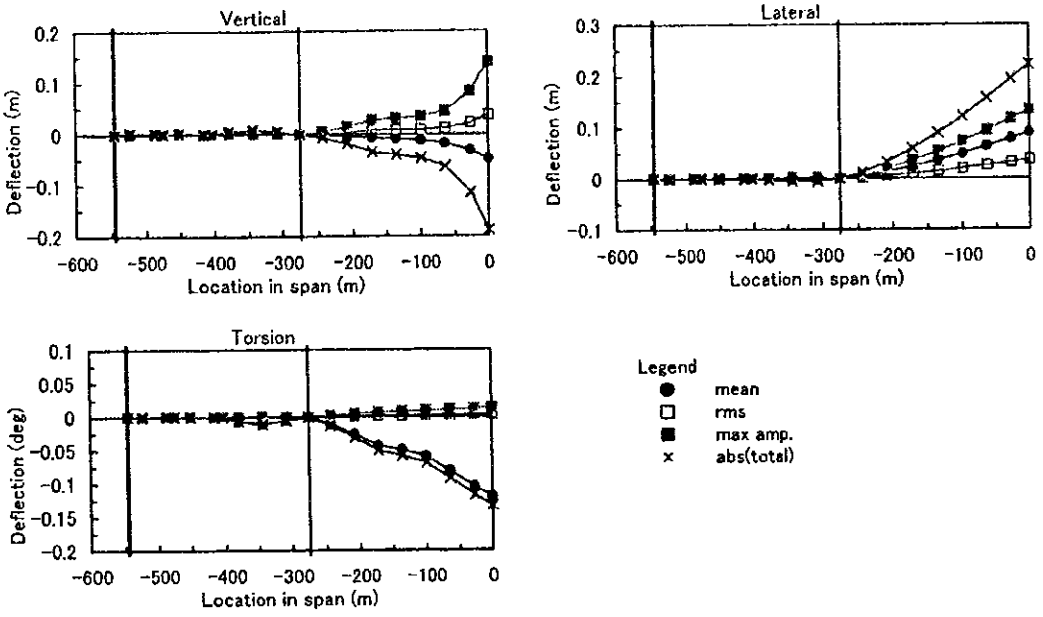

Figure 6.5 (3) Buffeting Responses along Bridge Axis ($U_Z = 30$ m/s)

$U_Z = 35$ m/s

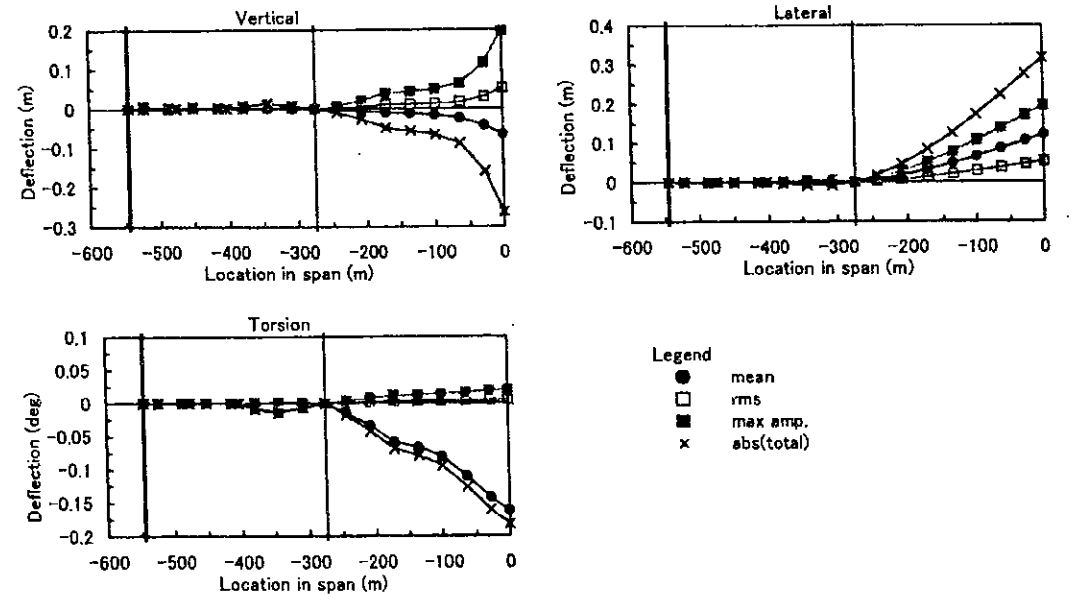

Figure 6.5 (4) Buffeting Responses along Bridge Axis ($U_Z = 35$ m/s)

$U_Z = 40$ m/s

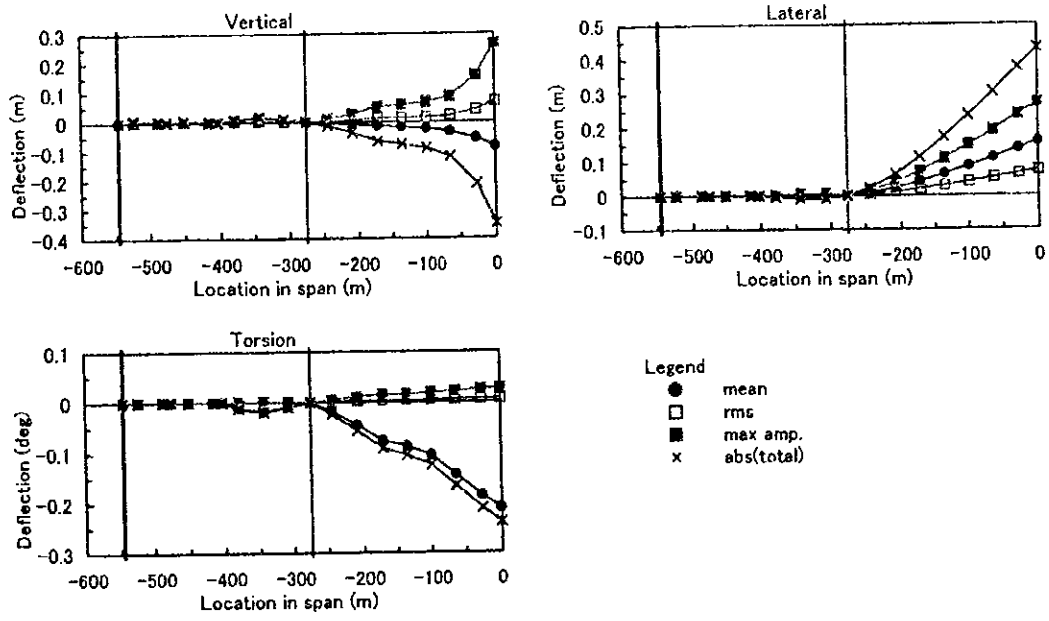

Figure 6.5 (5) Buffeting Responses along Bridge Axis ($U_Z = 40$ m/s)

$U_Z = 50$ m/s

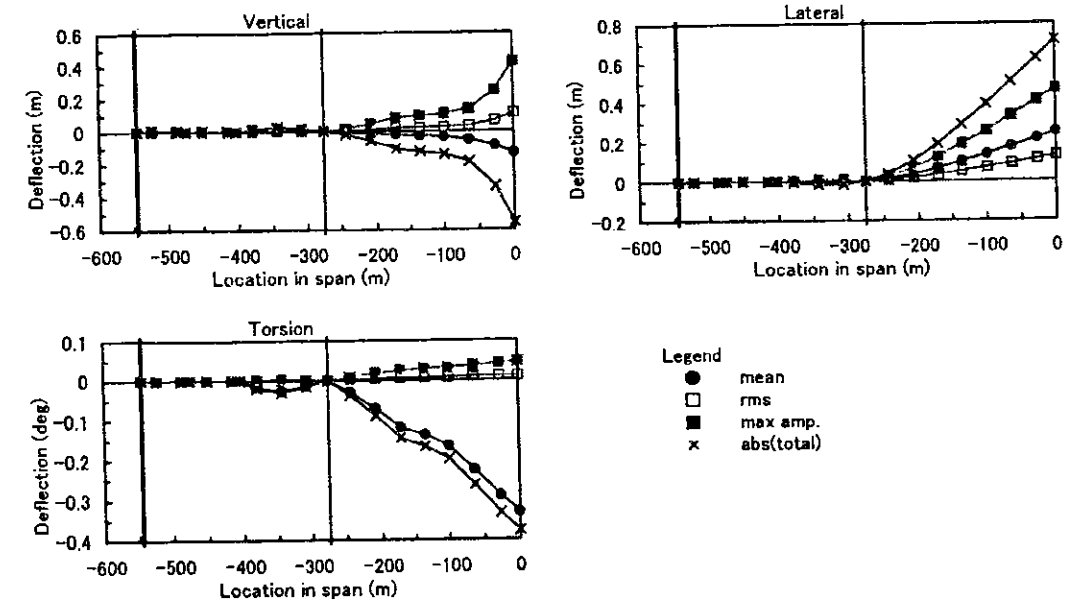

Figure 6.5 (6) Buffeting Responses along Bridge Axis ($U_Z = 50$ m/s)

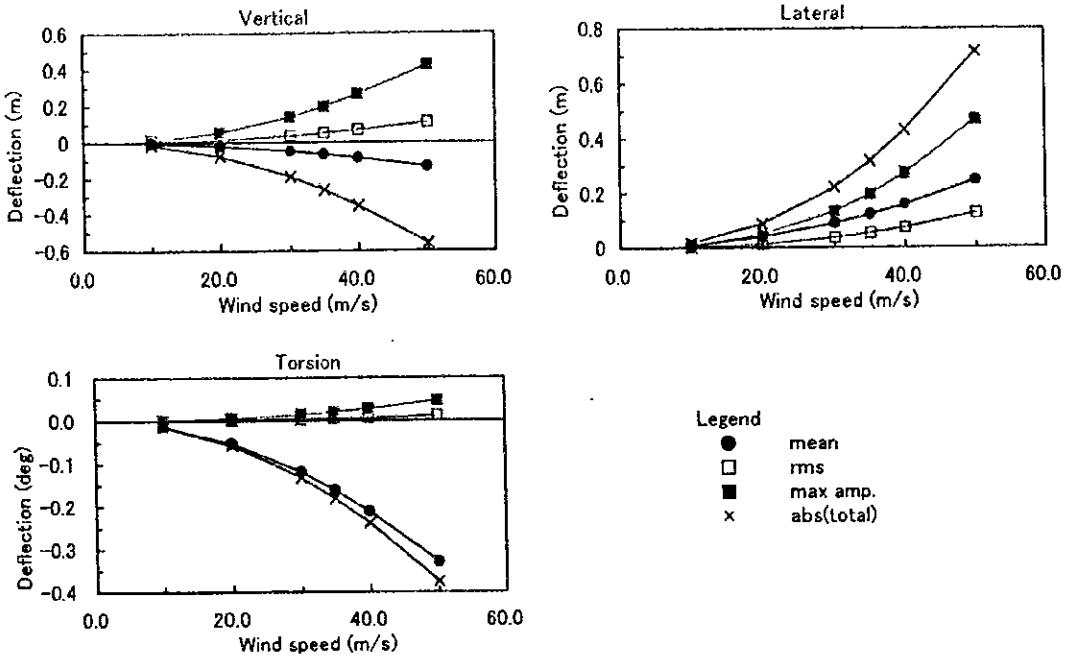

Figure 6.6 Buffeting Responses at Deck End and Wind Speed

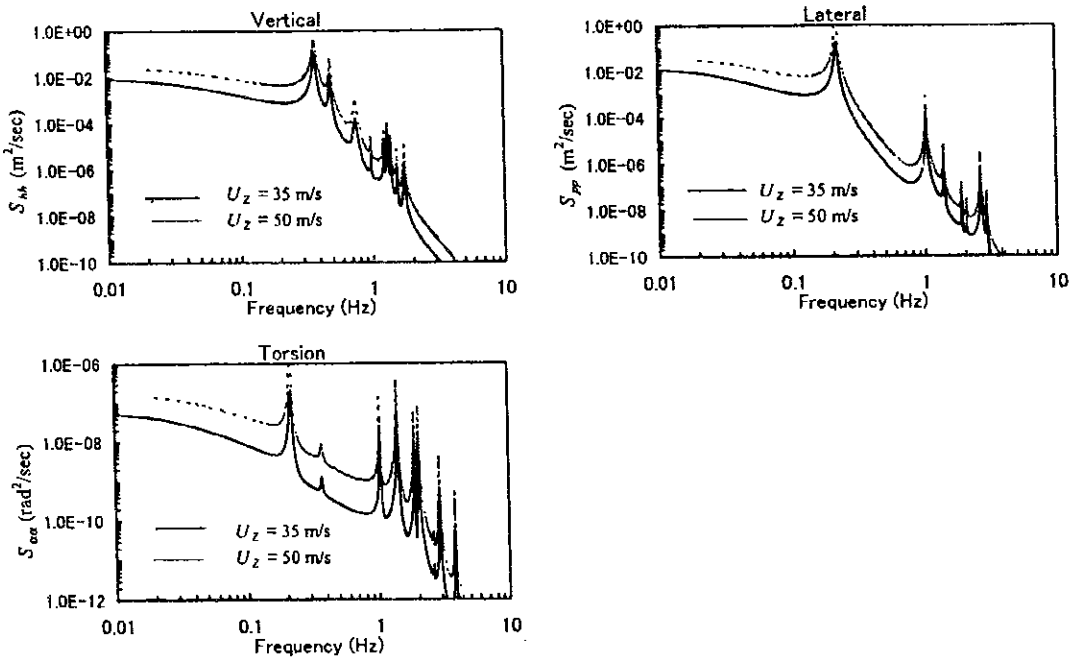

Figure 6.7 Power Spectral Density of Deck-End Deflection

6.4 Evaluation of Buffeting Responses of Deck at Erection Period

In the previous section, deflections of buffeting responses were investigated. For the convenience of design work, section forces or stresses rather than deflection are important. Based on the deflections analyzed, sectional stresses are estimated here.

Lateral bending moment of the deck M is calculated by

$$M = -EI\frac{d^2y}{dx^2} \tag{6.34}$$

where E is the Young modulus, I is the bending stiffness of a cross section, y is the lateral deflection and x is the coordinate along the bridge axis. Once the bending moment is obtained, section stress is evaluated as

$$\sigma = \frac{M}{I}y' \tag{6.35}$$

where y' (= 12.0 m) is the distance from deck center to deck edge in a cross-section plane.

First, lateral deflections obtained by buffeting analysis in Figure 6.5 are regressed with a polynomial function ($y = f(x)$). Then, substituting the function into Eq. (6.34) yields lateral bending moment distribution along the bridge axis. The regression process was made at two wind speeds of 35 and 50 m/s.

Tables 6.3 and 6.4 show the coefficients a and b of the second derivative in Eq. (6.34) (d^2y/dx^2 $ax + b$) and the section stresses by Eq. (6.35). Section stress shows the maximum values at the tower position and transient position between a steel and concrete desk (x = 0 and 176.0 m). The values are 37.75 kgf/cm^2 at x = 0 and 66.55 kgf/cm^2 at x = 176.0 at a wind speed of 35 m/s, and 85.35 kgf/cm^2 at x = 0 and 150.56 kgf/cm^2 at x = 176.0 at a wind speed of 50 m/s. Figure 6.8 shows the distribution of the section stress in the lateral direction along the bridge axis.

Table 6.3 Section Stresses in Lateral Direction (U_Z = 35 m/s)

x (m)	a	b	d^2y/dx^2	I (m^4)	σ (kgf/cm^2)
0.0	8.1090e-08	9.5328e-06	9.5328E-06	978.16	37.75
32.0	-3.4493e-08	9.5328e-06	8.4290E-06	978.16	33.38
68.0	-5.8710e-08	1.0340e-05	6.3477E-06	978.16	25.14
104.0	-5.4072e-08	1.0020e-05	4.3965E-06	978.16	17.41
140.0	-4.7699e-08	9.3618e-06	2.6839E-06	978.16	10.63
176.0	-1.1923e-09	2.8508e-06	2.6410E-06	56.40	66.55
212.0	-1.4381e-08	5.1720e-06	2.1232E-06	56.40	53.51
248.0	-4.3469e-08	1.1339e-05	5.5869E-07	56.40	14.08
275.0	-4.3469e-08	1.1339e-05	-6.1498E-07	56.40	-15.50

Note: a and b are the coefficients of the second derivative ($d^2y/dx^2 = ax + b$).

Table 6.4 Section Stresses in Lateral Direction (U_Z = 50 m/s)

x (m)	a	b	d^2y/dx^2	I (m^4)	σ (kgf/cm^2)
0.0	1.8322e-07	2.1554e-05	2.1554E-05	978.16	85.35
32.0	-7.8168e-08	2.1554e-05	1.9053E-05	978.16	75.45
68.0	-1.3274e-07	2.3374e-05	1.4348E-05	978.16	56.82
104.0	-1.2214e-07	2.2652e-05	9.9494E-06	978.16	39.40
140.0	-1.0778e-07	2.1160e-05	6.0708E-06	978.16	24.04
176.0	-2.6496e-09	6.4408e-06	5.9745E-06	56.40	150.56
212.0	-3.2550e-08	1.1703e-05	4.8024E-06	56.40	121.02
248.0	-9.8202e-08	2.5622e-05	1.2679E-06	56.40	31.95
275.0	-9.8202e-08	2.5622e-05	-1.3836E-06	56.40	-34.87

Note: a and b are the coefficients of the second derivative ($d^2y/dx^2 = ax + b$).

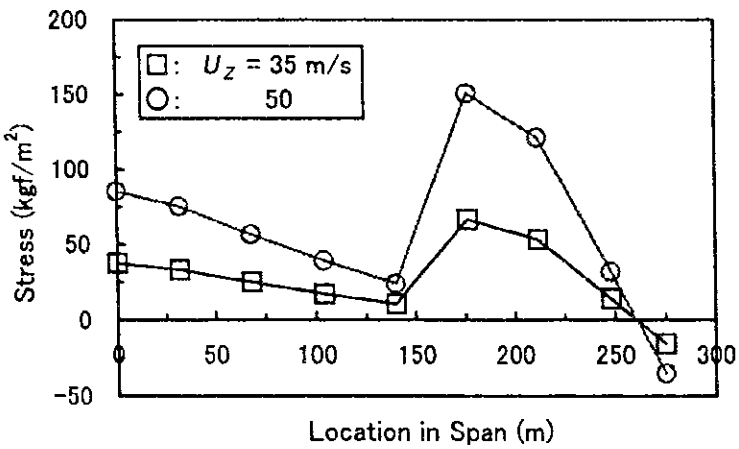

Figure 6.8 Section Stress Distribution along Bridge Axis

7 WIND-INDUCED VIBRATION AND COUNTERMEASURES OF STAY CABLES

7.1 Wind-Induced Vibration of Stay Cables

Wind-induced vibration observed at stay cables of cable-stayed bridges is often classified into

1) Vortex-induced vibration
2) Rain-wind-induced vibration
3) "High-wind-speed-induced vibration"
4) Wake galloping

Vortex-induced vibration is caused by well-known Karman vortices formed after a round-shape cable. It is usually observed at relatively low wind speed and is easily suppressed with small additional damping. Since a buffer rubber for anti angle bend installed at cable fixing points, vortex-induced vibration disappeared in many cases.

Rain-wind-induced vibration is thought to occur with a wind flow and water rivulets on the cable surface which deforms the cable cross section to wind-susceptible. It was pointed out that a relatively strong axial flow along the leeward cable axis plays an important role. Rain-wind-induced vibration with large amplitude has been observed at many cable-stayed bridges. Damping devices such as an oil damper and rubber damper are often used to suppress the vibration.

"High-wind-speed-induced vibration" (name is not formally recognized) has been reported to occur at a relatively high wind speed (30 – 40 m/s) [7.1]. There are many unknown facts to be investigated, however. It is difficult to include the investigation and its countermeasure in this study.

Wake-galloping is observed at parallel cables. The leeward cable vibrates with large amplitude. If the Can Tho Bridge has single-plane cables, this study does not need to deal with wake-galloping.

From the facts above, rain-wind-induced vibration (and wake galloping if necessary) will be the utmost concern in the design stage.

Figure 7.1 shows the wind-tunnel-test results (responses of rain-wind-induced vibration) of stay cables of a cable-stayed bridge with a center span length of about 900 m [7.2]. The test was executed with three conditions of cable frequency. The longer cable is, the lower frequency is. It is seen that the onset wind speed of vibration except for 1st peak with f = 0.45 Hz is about 10 m/s in three cases. This means that cable frequency does not affect the onset wind speed. Since rain-wind-induced vibration is caused by water rivulets on the surface as well as wind, onset wind speed of rain-wind-induced vibration is governed by the change of cross-section shape.

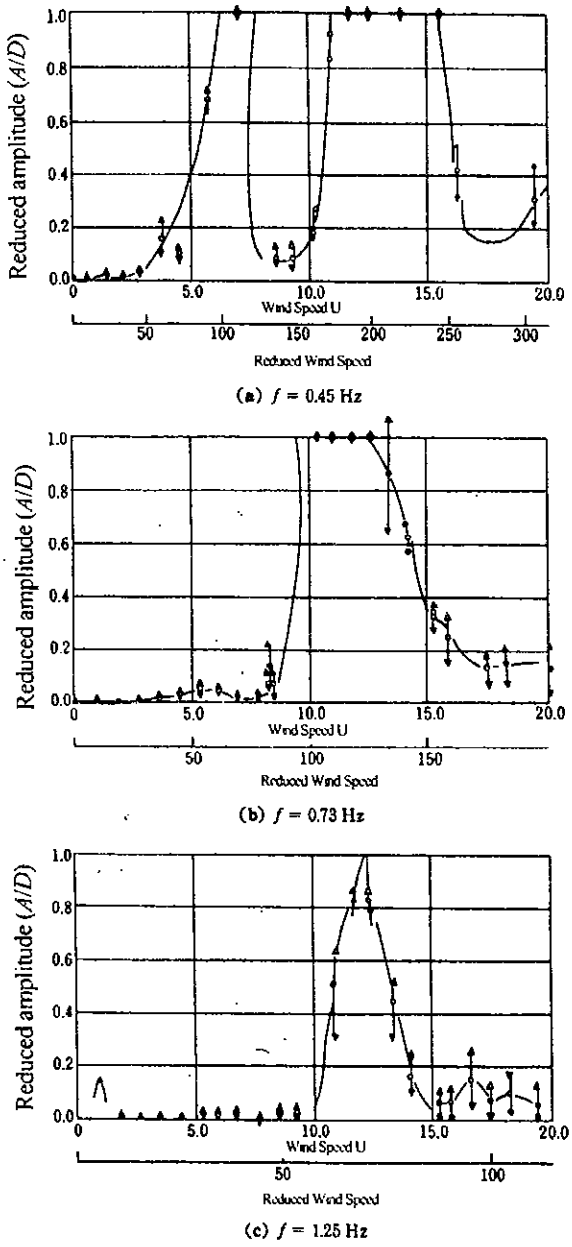

Figure 7.1 Relationship of responses of rain-wind-induced vibration and frequency [7.2]

In fact the response from a wind-tunnel test changes at about 10 m/s, as shown in Figure 7.2,

which corresponds the change of the water rivulet pattern on the cable surface [7.2].

Figure 7.3 shows the relationship between the onset wind speed of rain-wind-induced vibration and Scruton number (S_c) [7.3]. From this result, $S_c = 60$ is the minimum requirement to suppress the vibration. Another report says that cable damping in log decrement of 0.02 (approximately equal to $S_c = 60$) is required to suppress. It can be roughly said that these values are recommended as a reference for the Can Tho Bridge. However, the latest and detailed information is necessary.

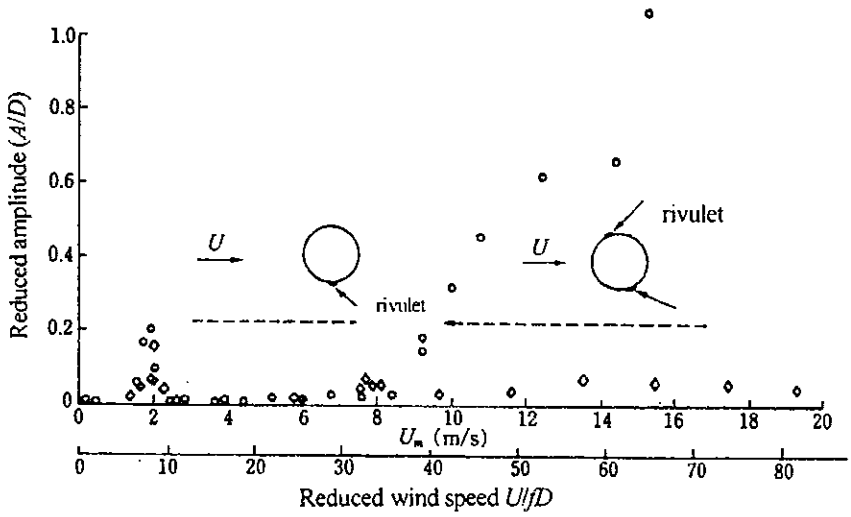

Figure 7.2 Responses of Rain-Wind-Induced Vibration and Position of Water Rivulets against Wind Speed [7.2]

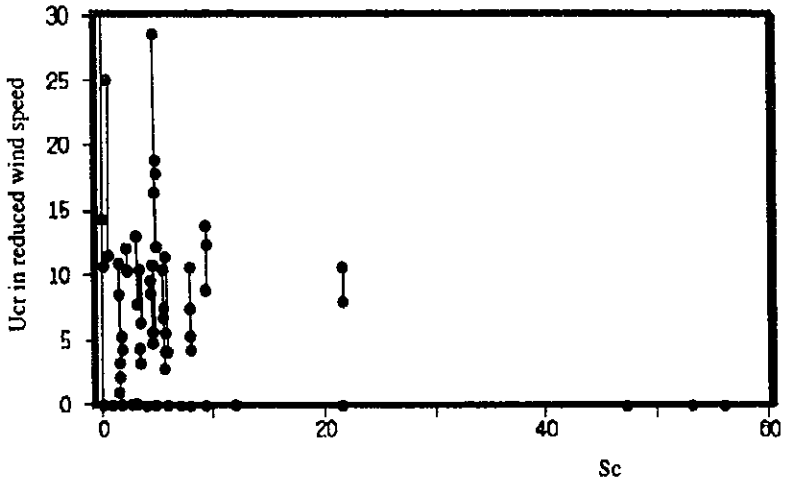

Figure 7.3 Relationship between Onset Wind Speed of Rain-Wind-Induced Vibration and Scruton Number [7.3]

7.2 Countermeasures of Wind-Induced Vibration of Stay Cables

7.2 Countermeasures of Wind-Induced Vibration of Stay Cables

There are three types of countermeasures to suppress wind-induced vibration of stay cables.

1) Connecting cables each other at intermediate position(s)

(This is understood that connecting cables makes natural frequency high and increase the onset wind speed.)

2) Damping devices

3) Change of cable shape or surface

(Making strips, indents on the surface changes aerodynamic characteristics)

Historically, the method of connecting cables has been applied and the effectiveness was recognized to a certain degree. However, mechanical problem at connecting points such as breaking connecting wire has often been reported.

Second method with dampers is the most commonly used these days. But disadvantage of this method is that dampers are expensive and needs regular maintenance.

Recently a new idea of the third method has developed. There are three types of the change of cable surface. First [7.4] is to make indents on the cable surface randomly and applied at the Tatara Bridge as shown in Figure 7.4. Usually, making patterns on a round shape cable increases roughness and drag. However, adjusting patterns such as one of the Tatara Bridge keeps drag as low as that of a round cable. Second [7.5] is to change the cable cross section as shown in Figure 7.5. This idea is base on the prevention of forming water rivulets on the surface. This cable was applied at the Higashi Kobe Bridge. However, the cable yield large drag coefficient of 1.2. The last [7.6] is to make U-shape strips on the surface as shown in Figure 7.6. This cable was applied at the Yuge Bridge.

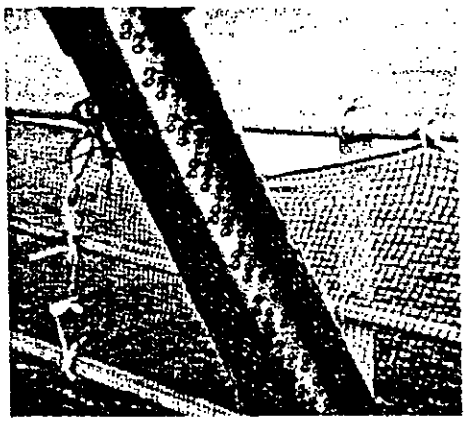

Figure 7.4 Indent Cable of Tatara Bridge

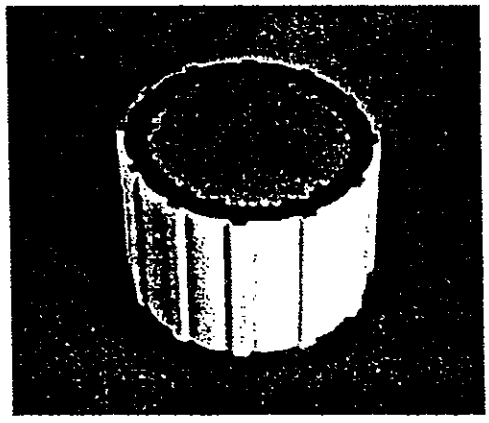

Figure 7.5 Protuberance Cable of Higashi Kobe Bridge

Figure 7.6 U-Shape Stripe Cable of Yuge Bridge

7.3 Recommendation for Cable Vibration of Can Tho Bridge

Vortex-induced vibration is anticipated to occur, however installing anti-angle-bend rubber buffers at cable fixing points (commonly used in large cable-stayed bridges) will suppress the vibration.

If the bridge adopts parallel or multi cables in one plane, wake galloping will inevitably occur without appropriate cable distance. In this case, appropriate cable distance or allocation is the most important.

It is not easy to judge in advance whether rain-wind-induced vibration would occur or not at the bridge site. Recommendations for rain-wind-induced vibration of the Can Tho Bridge will be as follows:

1) After cable erection without any countermeasures, vibration monitoring is to be carried out.

2) In case that the vibration would occur during the monitoring, countermeasure(s) is to be taken. If no vibration is observed, judgment that rain-wind-induced vibration would not occur at the Can Tho Bridge is to be made. (Since the vibration is relatively easy to occur with conditions of a wind speed of about 10 m/s and rain, the vibration is likely to be observed in a short period.)

3) Even in case that the vibration would occur, there is one solution that no countermeasure is taken. However, the vibration is often accompanied by quite large amplitude ($\geq$ 1 m). It will be proper to take some countermeasures.

Since countermeasures are taken after cable erection, damping devices will be only option to be left.

4) Specifications of damping devices such as required damping level can be referred to the description in this Chapter. The Central Miko Bridge with a center span length of 590 m, which is the same level as that in this bridge, installed damping devices to suppress cable vibration. It will be a reference to the countermeasure of cable vibration of the Can Tho Bridge

REFERENCES

2.1 Honshu-Shikoku Bridge Authority, Wind-Resistant Design Code for Onomichi-Imabari route, 1994.1. (in Japanese)

2.2 Yamada, H., Approach to Wind Engineering, Kensetsu Tosho Publisher, 1995. (in Japanese)

2.3 Simiu, E. and Scanlan R. H., Wind Effects on Structures, Wiley, 1996.

3.1 Japan Society of Civil Engineers, Report on Suppression of Wind-Induced Vibration of Bridges, subcommittee on Aeroelastic Phenomena of Structures and Turbulence Effects on Them, 1999.12. (in Japanese)

4.1 Japan Road Association, Wind-Resistant Design Manual for Road Bridges, 1991. (in Japanese)

6.1 Katsuchi, H., Jones, N. P., Scanlan, H. R. and Akiyama, H. : A Study of Mode Coupling in Flutter and Buffeting of the Akashi-Kaikyo Bridge, *Structural Eng./Earthquake Eng.*, JSCE, Vol.15, No.2, pp.175s-190s, 1998.

6.2 Katsuchi, H., Jones, P. N. and Scanlan, H. R. : Multi-Mode Coupled Flutter and Buffeting Analysis of the Akashi-Kaikyo Bridge, *J. of Struct. Engrg.*, ASCE, Vol.125, No.1, pp60-70, 1999.

7.1 Matsumoto, M., Hikami, Y. and Kitazawa, M., Cable Vibration and Its Aerodynamic/Mechanical Control, Cable-stayed and Suspension Bridge, Deauville, France, 1994.

7.2 Tokyo Denki University Press, Wind Engineering of Structures, 1997. (in Japanese)

7.3 Public Works Research Center, Investigation on Wind-Induced Vibrations of Stay Cables of Cable-Stayed Bridges, 1994. (in Japanese)

7.4 Miyata, T., Yamada, H. and Hojo, T., Aerodynamic Reponses of PE Stay Cables with Pattern-Indented Surface, Cable-Stayed and Suspension Bridges, Deauville, France, 1994.

7.5 Matsumoto, M., Kitazawa, M., Ishizaki, H., Ogawa, K., Saito, T. and Shimodoi, H, Wind-Resistant Design of Higashi Kobe Bridge, Bridge and Foundation, Kensetsu Tosho Publissher, 1991. (in Japanese)

7.6 Miyazaki, M., Wind-Induced Vibration of Stay Cables and Its Countermeasures, Proc. of 10th Wind Engineering Symposium, 1988. (in Japanese)